NORTHWESTERN UNIVERSITY

# Wireless Sensor Networks for Crack Displacement Measurement

A Thesis

Submitted to the Graduate School In Partial Fulfillment of the Requirements

For the Degree

MASTER OF SCIENCE

Field of Civil Engineering

By
Hasan Ozer

EVANSTON, IL

July 2005

ACKNOWLEDGEMENTS ..... III

ABSTRACT ..... V

INDEX OF FIGURES ..... VII

INDEX OF TABLES ..... XI

1 INTRODUCTION ..... 1

2 CRACK DISPLACEMENT MEASUREMENTS WITH WIRELESS SENSOR NETWORK ..... 4

2.1 Introduction ..... 4

2.2 Wireless Communication Basics ..... 5

2.3 Components of the Wireless System Network ..... 8
2.3.1 Hardware ..... 8
2.3.2 Software Protocol: TinyOS (Tiny Operating System) ..... 12

2.4 Benefits of the wireless system ..... 15

2.5 Installation of the system ..... 23
2.5.1 Description of the installed system and operation basics ..... 23
2.5.2 Analysis of the results ..... 28
2.5.2.1 Measurement of crack response (Single-hop customization) ..... 32
2.5.2.2 Roof test (Multi-hop customization) ..... 39

2.6 Conclusion ..... 42

3 QUALIFICATION OF POTENTIOMETER ..... 45

3.1 Introduction ..... 45

3.2 Experimental Setup ..... 47
3.2.1 Long-Term Qualification ..... 47
3.2.1.1 Test Description and Configuration ..... 47
3.2.1.2 Instruments and Hardware ..... 49
3.2.2 Transient Response ..... 53
3.2.2.1 Test Description and Configuration ..... 53
3.2.2.2 Instruments and Hardware ..... 55

3.3 Interpretation of Data ..... 56
3.3.1 Long-Term Test ..... 56

3.3.1.1 Sensor Displacement and Temperature Variations with time..... 57
3.3.1.2 Comparison of sensor response with theoretical displacement ..... 59
3.3.1.3 Comparison of performance of Potentiometer to LVDT in the plate and donut tests ..... 62
3.3.1.4 Discussion of the results ..... 67
3.3.2 Transient Response ..... 69
3.3.2.1 Combination of Potentiometer and the other sensors ..... 69
3.3.2.2 Discussion of the results ..... 73

3.4 Conclusion ..... 79

4 CONCLUSION..... 81

REFERENCES ..... 85

A. APPENDIX NOISE LEVEL IN POTENTIOMETER OUTPUT ..... 86

B. APPENDIX DYNAMIC TEST-IMPACT DISPLACEMENT TIME HISTORIES AND FFT ANALYSIS ..... 92

C. APPENDIX COMPARISON OF BLAST INDUCED CRACK RESPONSES MEASURED BY POTENTIOMETER AND LVDT..... 107

D. APPENDIX RELATIVE TEMPERATURE CORRECTIONS IN PLATE AND DONUT TESTS…..... 114

# ACKNOWLEDGEMENTS

This thesis is a collaboration of many people who deserve much more than a simple acknowledgement. Firstly I would like to thank to Professor Charles Dowding for his guidance, motivation, expertise, and foresight without which this thesis would certainly not have been possible. I am very grateful to Professor Dowding for the opportunity to pursue my graduate work at Northwestern University. Professor Richard J. Finno is sincerely thanked for his invaluable teaching and unconditional support he gave me whenever I needed it. I am grateful to all of my professors for giving me this unforgettable and precious experience.

I would like to gratefully acknowledge Mat Kotowsky's extensive programming that was a critical component of this work. The success described herein would not have been possible without his intensive labor. Thanks are also extended to Dan Marron, Dave Kosnik and Dan Hogan for their assistance, advices and patience to my endless questions and requests.

I would also thank to my fellow graduate students Wan-Jei Cho, Cecilia Rechea, Xuxin Tu and Tanner Blackburn for their friendship and sharing this sometimes fun but mostly exhausting voyage.

Heartfelt appreciation goes to my parents Nahide and Vahap Ozer for their unconditional love, endless support and patience without which I would not have reached out to this degree. I shouldn't forget my father's insistent inspiration to pursuing higher education.

Finally, I would like to dedicate this work to my precious wife Deniz who never withheld her support and help. I would not have made it through without her love.

# ABSTRACT

Miniaturized, wireless instrumentation is now a reality and this thesis describes development of such a system to monitor crack response. Comparison of environmental (long-term) and blast-induced (dynamic) crack width changes in residential structures has lead to a new approach to monitoring and controlling construction vibrations.

In wireless systems transducer power requirements and continuous surveillance challenge available battery power, which declines with decreasing size of the system. Combining low power consumption potentiometer displacement transducers with a short communication duty cycle allow the system described herein to operate for many months with changing its AA size batteries. The system described won third place honors in the 2005 Crossbow Smart Dust Challenge, which represented the best executable ideas for wireless sensor networks that demonstrate how it is used, programmed and deployed to positively impact society.

Wireless communication basics are introduced along with operational principles and necessary components. Two different configurations were investigated and produced based on the communication between the remote nodes; single-hop and multi-hop customizations. Battery lifetime, and wireless communication were enhanced by adoption

of the multi-hop protocol. Both of the systems were field tested to evaluate the long-term performance of the software and the hardware components.

This thesis also describes the qualification process of the potentiometer through several tests. Potentiometers were chosen for use with the wireless sensor network because of their extremely low power consumption (0.5 mA), which is crucial for the long-term, uninterrupted operation of wireless system relying on only 2 AA batteries. Three different test mechanisms were established to quantify the consistency of the potentiometer response against the hysteresis, drift, noise and transient displacements.

## INDEX OF FIGURES

2.1: Sensor nodes scattered in the sensor field and the base station ..... 7
2.2: Radio communication channel model..... 8
2.3: A "sensor node" that consists of remote node and the displacement sensor (mica2 that will be attached to the MDA300 is not shown) ..... 9
2.4: MOXA NPort (left) and MIB510 with mote running TOSBase (right) ..... 10
2.5: The components of the wireless sensor network ..... 11
2.6: Plastic Ivy used to hide wires and sensor (bottom right) and the wireless remote node on the ceiling..... 16
2.7: Mote battery voltage decline during the field test (with 5 minute duty cycle)..... 18
2.8: Power consumption profile of single-hop application (15 minutes duty cycles) ..... 19
2.9: Power consumption profile of one of the low power modes in Xmesh. (This sampling window is the oval in Figure 2.10, which shows its duration compared to ongoing operation) ..... 21
2.10: Power consumption profile of Xmesh protocol showing the two consecutive sampling intervals (details of history in ellipse is shown in Figure 2.9) ..... 22
2.11: A potentiometer attached to a “remote node” and LVDT displacement sensors across the same ceiling crack (bottom right) and picture of the instrumented house (top left) ..... 25
2.12: Remote nodes deployed on the roof of a downtown building ..... 27
2.13: Long-term crack displacements and weather changes (McKenna, 2002) ..... 29
2.14: Level 2 comparison of crack response (Kentucky, 2005) ..... 31
2.15: Temperature and crack displacement measurements by wireless and wired data acquisition system in Milwaukee test house during November 18, 2004 to January 16, 2005..... 34
2.16: Crack displacement measurements by wireless system with blast events annotated . 37
2.17: Close-up view to the long-term data during blast events..... 38
2.18: Temperature and displacement variation measured by the wireless remote nodes on the roof..... 40
2.19: Humidity variations with the expansion/contraction of the aluminum plate measured by mote ID2 with the potentiometer on the plate. ..... 41
2.20: Battery voltage fluctuations of the motes during the roof test..... 42
3.1: Experimental setup from the test on the aluminum plate ..... 48
3.2: Experimental setup from donut test..... 49
3.3: Close-up view of the potentiometer across a crack on the ceiling of the test house in Milwaukee..... 50

3.4: A test mechanism to measure the transient response with LVDT and potentiometer sensors ..... 54
3.5: Eddy current sensor-potentiometer (on the left) and LVDT-potentiometer (on the right) attached on the dynamic test setup ..... 54
3.6: Potentiometer and LVDT glued on the ceiling crack of the test house in Milwaukee . 55
3.7: Sensor displacements with temperature variation during the plate and donut tests ..... 59
3.8: Comparison of measured and calculated potentiometer sensor displacements induced by cyclically varying temperatures ..... 61
3.9: Comparison of LVDT and potentiometer displacements induced by cyclically varying temperatures ..... 63
3.10: Residual, largest cumulative displacements on a sketch ..... 64
3.11: A potentiometer displacement sensor used in qualification tests showing the irregularities in the cable ..... 67
3.12: Comparison of potentiometer and Kaman (eddy current) sensors to dynamic events produced by the same drop weight impacts ..... 69
3.13: Comparison of various sensors to the same impact produced by the laboratory device ..... 70
3.14: Responses of low-tension potentiometer and eddy current sensor to the same three impacts ..... 72
3.15: Same comparisons as in Figure 3.14 only with high-tension potentiometer ..... 72
3.16: Responses of high-tension potentiometer (top) and LVDT sensors to the same impact displacement (bottom) ..... 74
3.17: FFT analysis of the response of the high-tension potentiometer (top) and LVDT (bottom) to impact loading shown in the previous figure. ..... 74
3.18: Potentiometers and LVDT displacement time history recorded during a blast event at the Milwaukee test house ..... 75
3.19: Potentiometer output measured by wireless (top) and wired SOMAT (bottom) system at 10 Hz ..... 78

A- 1: Noise level in the potentiometer and LVDT output during the donut tests ..... 86
A- 2: Noise level in the potentiometer and LVDT output during the plate test ..... 87
A- 3: Noise level and frequency content of noise with SOMAT and external power supply (1000 HZ sampling) ..... 87
A- 4: Noise level and frequency content of noise with SOMAT and internal power supply (1000 HZ sampling) ..... 88
A- 5: Noise level and frequency content of noise with SOMAT and external power supply (10 HZ sampling) ..... 89
A- 6: Noise level and frequency content of noise with SOMAT and internal power supply (10 HZ sampling) ..... 89
A- 7: Noise level during the dynamic test (1000 HZ sampling) ..... 90
A- 8: Noise level during the field test (1000 HZ sampling) ..... 91

B- 1: Dynamic test impact displacements of high-tension potentiometer (top) and Kaman (bottom) ..... 92

B- 2: Dynamic test impact displacements of low-tension potentiometer (top) and Kaman (bottom)..... 92
B- 3: Dynamic test impact displacements of high-tension potentiometer (top) and LVDT (bottom)..... 93
B- 4: Dynamic test impact displacements of low-tension potentiometer (top) and LVDT (bottom)..... 93
B- 5: Dynamic test impact displacements of LVDT (top) and Kaman (bottom)..... 94
B- 6: One impact loading from dynamic test with high-tension potentiometer and Kaman 95
B- 7: FFT of the impact loading. High-tension potentiometer (top) and Kaman (bottom) . 95
B- 8: One impact loading from dynamic test with high-tension potentiometer and Kaman 96
B- 9: FFT of the impact loading. High-tension potentiometer (top) and Kaman (bottom) . 96
B- 10: One impact loading from dynamic test with high-tension potentiometer and Kaman ..... 97
B- 11: FFT of the impact loading. High-tension potentiometer (top) and Kaman (bottom) 97
B- 12: One impact loading from dynamic test with high-tension potentiometer and LVDT ..... 98
B- 13: FFT of the impact loading. High-tension potentiometer (top) and LVDT (bottom) 98
B- 14: One impact loading from dynamic test with high-tension potentiometer and LVDT ..... 99
B- 15: FFT of the impact loading. High-tension potentiometer (top) and LVDT (bottom) 99
B- 16: One impact loading from dynamic test with high-tension potentiometer and LVDT ..... 100
B- 17: FFT of the impact loading. High-tension potentiometer (top) and LVDT (bottom) ..... 100
B- 18: One impact loading from dynamic test with low-tension potentiometer and Kaman ..... 101
B- 19: FFT of the impact loading. Low-tension potentiometer (top) and Kaman (bottom) ..... 101
B- 20: One impact loading from dynamic test with low-tension potentiometer and Kaman ..... 102
B- 21: FFT of the impact loading. Low-tension potentiometer (top) and Kaman (bottom) ..... 102
B- 22: One impact loading from dynamic test with low-tension potentiometer and Kaman ..... 103
B- 23: FFT of the impact loading. Low-tension potentiometer (top) and Kaman (bottom) ..... 103
B- 24: One impact loading from dynamic test with low-tension potentiometer and LVDT ..... 104
B- 25: FFT of the impact loading. Low-tension potentiometer (top) and LVDT (bottom)104
B- 26: One impact loading from dynamic test with low-tension potentiometer and LVDT ..... 105
B- 27: FFT of the impact loading. Low-tension potentiometer (top) and LVDT (bottom)105
B- 28: One impact loading from dynamic test with low-tension potentiometer and LVDT ..... 106
B- 29: FFT of the impact loading. Low-tension potentiometer (top) and LVDT (bottom)106

C- 1: Displacement time history and FFT of the high-tension potentiometer response to blast event (April 18, 2005) ..... 107
C- 2: Original displacement time history (top) and filtered displacement time history of high tension potentiometer..... 108
C- 3: Displacement time history and FFT of the low-tension potentiometer response to blast event (April 18, 2005)..... 108
C- 4: Displacement time history and FFT of the low-tension potentiometer response to blast event (April 18, 2005)..... 109
C- 5: Displacement time history and FFT of the LVDT response to blast event (April 18, 2005) ..... 109
C- 6: Original displacement time history (top) and filtered displacement time history of LVDT..... 110
C- 7: Displacement time history and FFT of the high-tension potentiometer response to blast event (May 5, 2005) ..... 110
C- 8: Original displacement time history (top) and filtered displacement time history of high-tension potentiometer ..... 111
C- 9: Displacement time history and FFT of the low-tension potentiometer response to blast event (May 5, 2005)..... 111
C- 10: Original displacement time history (top) and filtered displacement time history of low-tension potentiometer ..... 112
C- 11: Displacement time history and FFT of the LVDT response to blast event (May 5, 2005) ..... 112
C- 12: Original displacement time history (top) and filtered displacement time history of LVDT..... 113

D- 1: Schematic of the plate test showing the importance of fixity length of the sensor to the plate and relative expansion/contraction..... 114
D- 2: Comparison of temperature corrected potentiometer and LVDT response to cyclically changing temperature variations..... 115

## INDEX OF TABLES

2-1: Summary of the properties of single-hop and multi-hop applications ..... 15
2-2: Summary of the current consumed in different modes of single-hop and multi-hop applications ..... 20
2-3: Computed long term crack displacements due to weather effect (The values in parenthesis are from the wired benchmark system)..... 35
3-1: Resolution of measurement systems employed in qualification ..... 52
3-2: Configuration of the EDAQ measurement system employed for dynamic qualification ..... 56
3-3: Some statistical measures of plate and donut tests..... 64
3-4: Normalized displacements of the sensors from plate and donut tests..... 66
3-5: Summary of the peak-to-peak noise level with varying excitation voltages, sampling rates and monitoring equipment..... 77

D- 1: Statistical measures of plate and donut tests with the corrected results ..... 115
D- 2: Temperature normalized displacements from plate and donut tests with corrected results ..... 116

# CHAPTER 1

# 1 INTRODUCTION

Miniaturized, wireless instrumentation is now a reality and this thesis describes development of such a system to monitor crack response. Wireless sensor networks consist of distributed self-powered, tiny, sensor nodes (called motes) capable of wireless communication between each other and/or to a base station, sensing, signal processing and computation. Low power consumption, adaptability to various applications, cost effectiveness and non-obtrusiveness of the wireless sensor nodes are some of the prominent features that make them attractive for structural health monitoring. All such computer-like devices require an operating system one of which, TinyOS, is employed in this study. These operating systems include sensor drivers, data acquisition tools and network communication protocols all of which can be modified for custom applications. The communication tools differ significantly from typical operating systems as they provide for self assembly and configuration of communication pathways to facilitate low power radio transfer of data.

The overall objective of this research is to develop a wireless system capable of executing all of the tasks now accomplished by the wired Autonomous Crack Monitoring (ACM systems). ACM has been developed to simultaneously measure crack response from long-term environmental effects as well as the transient response to blast induced

ground vibrations. As ACM has evolved, two levels of surveillance have developed. In Level-I surveillance only long-term crack response to environmental effects is measured. This type of surveillance is adapted to the low power consumption environment of wireless sensors necessary to maintain multi months of deployment without changing the batteries. To do so it was necessary to adopt a low power communication protocol and choosing low power consuming outboard devices, such as the potentiometer displacement transducer described herein. Level-II surveillance involves measurement of both long-term and dynamic crack response. It requires a high sampling rate, continual operation and a triggering mechanism, all of which consume power and are not provided in current operating systems. More research is necessary to develop a wireless, Level-II ACM system.

This thesis, which describes the development of the Level-I, ACM wireless sensor network, is divided into two major chapters. Chapter 2 begins with a description of wireless communication basics and introduces the components of the wireless system as well as some operational details of the system. The main thrust of the chapter is evaluation of two field installations of two versions of the system. Finally the chapter compares the wired and wireless system in terms of robustness, accuracy of the results and physical appearance.

Chapter 3 presents the studies necessary to qualify the low power consumption potentiometer displacement transducer. Two different laboratory test mechanisms were designed to determine the accuracy and robustness of the potentiometer when subjected to long term cyclically changing temperatures and impact loadings similar to those induced by vibratory crack response. The response of the potentiometer was also

compared to the benchmark sensors such as LVDT and eddy current sensors, which are the sensors that have been traditionally employed with ACM systems.

# CHAPTER 2

# 2 CRACK DISPLACEMENT MEASUREMENTS WITH WIRELESS SENSOR NETWORK

## 2.1 Introduction

A wireless data acquisition system is an extension of ongoing projects in Internet-enabled remote monitoring of critical infrastructure at the Infrastructure Technology Institute and the Department of Civil and Environmental Engineering at Northwestern University. The overall objective of Internet-enabled remote monitoring is to provide timely information to parties interested in the structural health of critical infrastructure components such as cracks in the bridges or houses nearby a quarry. Sensors on a structure are polled regularly so that responses may be compared graphically with past readings to identify trends and automatically alert authorities of impending problems. The natural extension of past wired systems is a wireless system that drastically reduces the cost of installation and eliminates the impact of the sensor network on the day-to-day use of a structure.

A wired predecessor has operated since 1996 and provided graphical comparison of crack displacements produced by environmental factors such as temperature, humidity and wind etc. as well as transient events such as blast induced ground motion and some

household activities. The main drawback of such a system of sensors is the cost in labor and materials for installation, wiring, and maintenance of this system. Siebert (2000) and Louis (2000) describe the development of this system in detail.

Rapid developments in wireless communications and electronics have enabled the development of low-cost wireless sensor networks that makes them attractive for various applications in structural health, military surveillance and civil engineering. Complexity of the network deployment and maintenance is considerably reduced when system are wireless, which in return reduces the cost of instrumentation.

Adapting wireless sensing technology to ongoing Internet-enabled remote monitoring projects required development a system that would:

- Eliminate hard-wired connections to each sensor
- Operate for at least a year without human intervention
- Record response data at least one per hour, including sensor output voltage, temperature, humidity and mote battery voltage
- Reduce cost, installation effort, and intrusion.

Features of the resulting wireless sensor networks that will be discussed in this chapter include communication architecture, sensor network protocols, power management and noise issues along with a case study conducted via a customized application of the wireless sensor network.

## 2.2 Wireless Communication Basics

In a wireless sensor network, communicating nodes are linked by a wireless medium such as radio, infrared or optical media. The transmission medium options for radio links are the ISM (Industrial, Scientific and Medical) bands, which is available for

license free communication. The Federal Communication Commission allocated frequencies between 420-450 MHz for radiolocation and amateur applications, which are also available for wireless sensor radio communication. This is a relatively low-level frequency band and is suitable for low power sensing devices since it decreases the power usage when compared to ultra-high frequency bands allocated for some other applications.

A typical wireless mesh network is shown in Figure 2.1 with its components; a sensor mesh of a multi-hop network where each of the sensor nodes is capable of collecting the data and routing it back to the base station. An off-site PC polls the data autonomously via Internet. It is not only the sensor data that is transmitted between the nodes but sensor nodes also route necessary information to form the network initially and re-organize the network in case one of the nodes is dysfunctional. This rearrangement in communication is a self-healing process where a continuous flow of data is maintained even if some of nodes are blocked due to lack of power, physical damage or interference. Multi-hop networks also increase the total spatial coverage and also maintain low energy requirements.

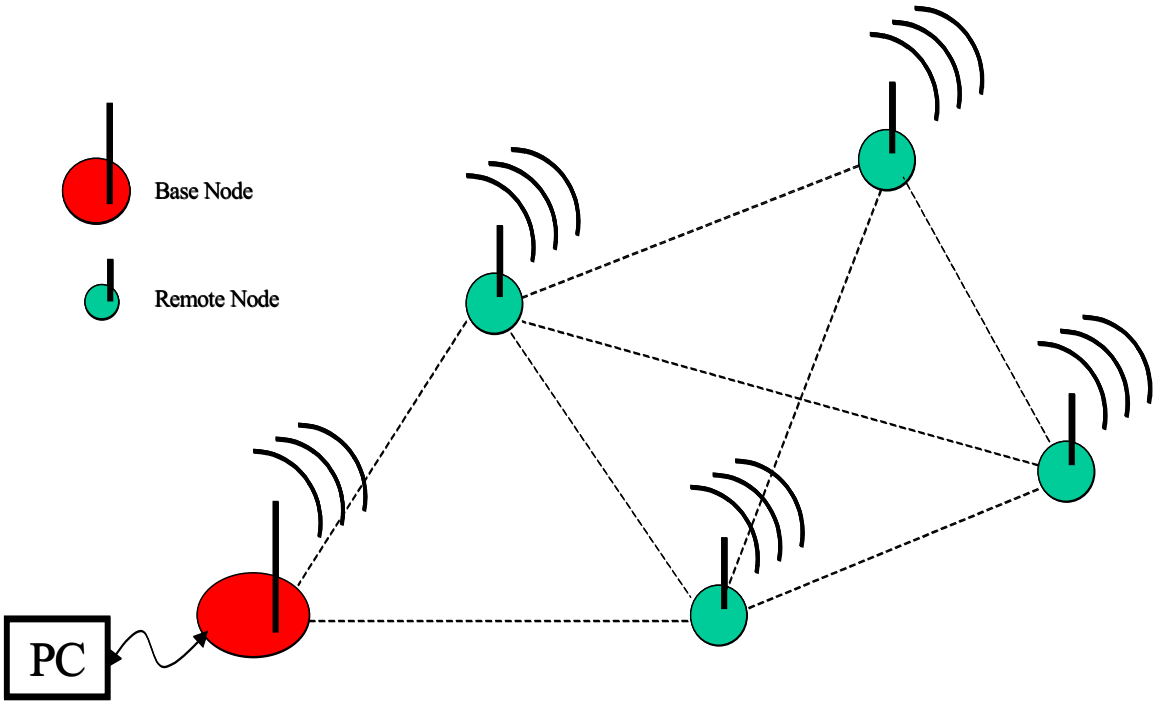


**Figure 2.1: Sensor nodes scattered in the sensor field and the base station**

A sensor node is the key element of the network. It is comprised of four major components: a sensing unit, a processing unit, a transceiver and a power unit. Sensing units are also composed of two subunits: analog-to-digital converters (ADC) and sensors. Analog signals produced by a physical phenomenon are converted to digital signals by ADC's and sent to the processing unit of the sensor node. The processing unit manages the procedures that alert the sensor node to respond and perform assigned sensing tasks, and collaborate with the other nodes. These units are responsible for pre-processing (encoding, decoding etc.) the data for transmission. The transceiver unit connects the node to the sensor network via a wireless link such as a radio module. And lastly, the power unit is the source of power for the node, which powers all activities on a sensor node including communication, data processing and sensing etc. Figure 2.2 summarizes the tasks processed by those units on a sensorboard.

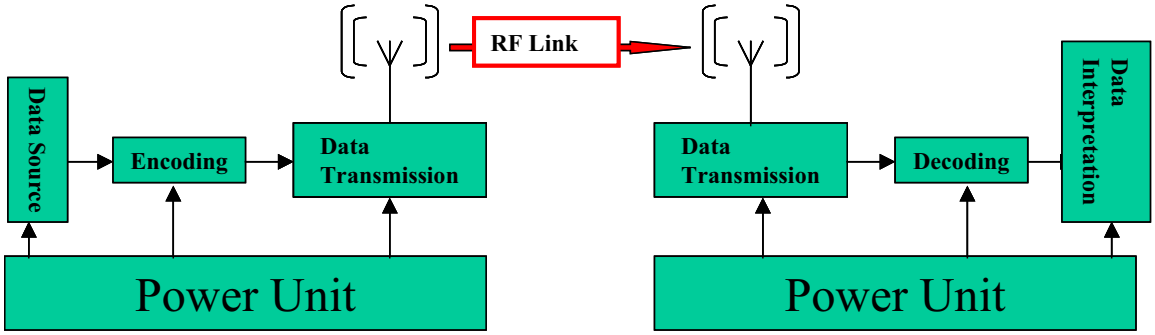


**Figure 2.2: Radio communication channel model**

Further information on miniaturized wireless systems can be found in the literature and product manual of Crossbow Incorporation (Crossbow, 2005) and TinyOS tutorials (TinyOS, 2005). Culler (2002) introduces the mica platforms for embedded network especially for habitat monitoring. Glaser (2004) presents some real-world applications of the wireless networks.

## 2.3 Components of the Wireless System Network

### 2.3.1 Hardware

A wireless data acquisition system consists of a network comprised of one "base node" and any number of "sensor nodes." As shown in Figure 2.3, each sensor node consists of one Mica2 mote, one MDA300 sensor board, and one ratiometric string displacement potentiometer connected to the screw terminals of the MDA300.The mote with its attached sensor board is mounted a few inches away from the sensor. Though only one "sensor node" is pictured, any number of "sensor nodes" may be attached within radio range of the any of the motes in multi-hop communication.

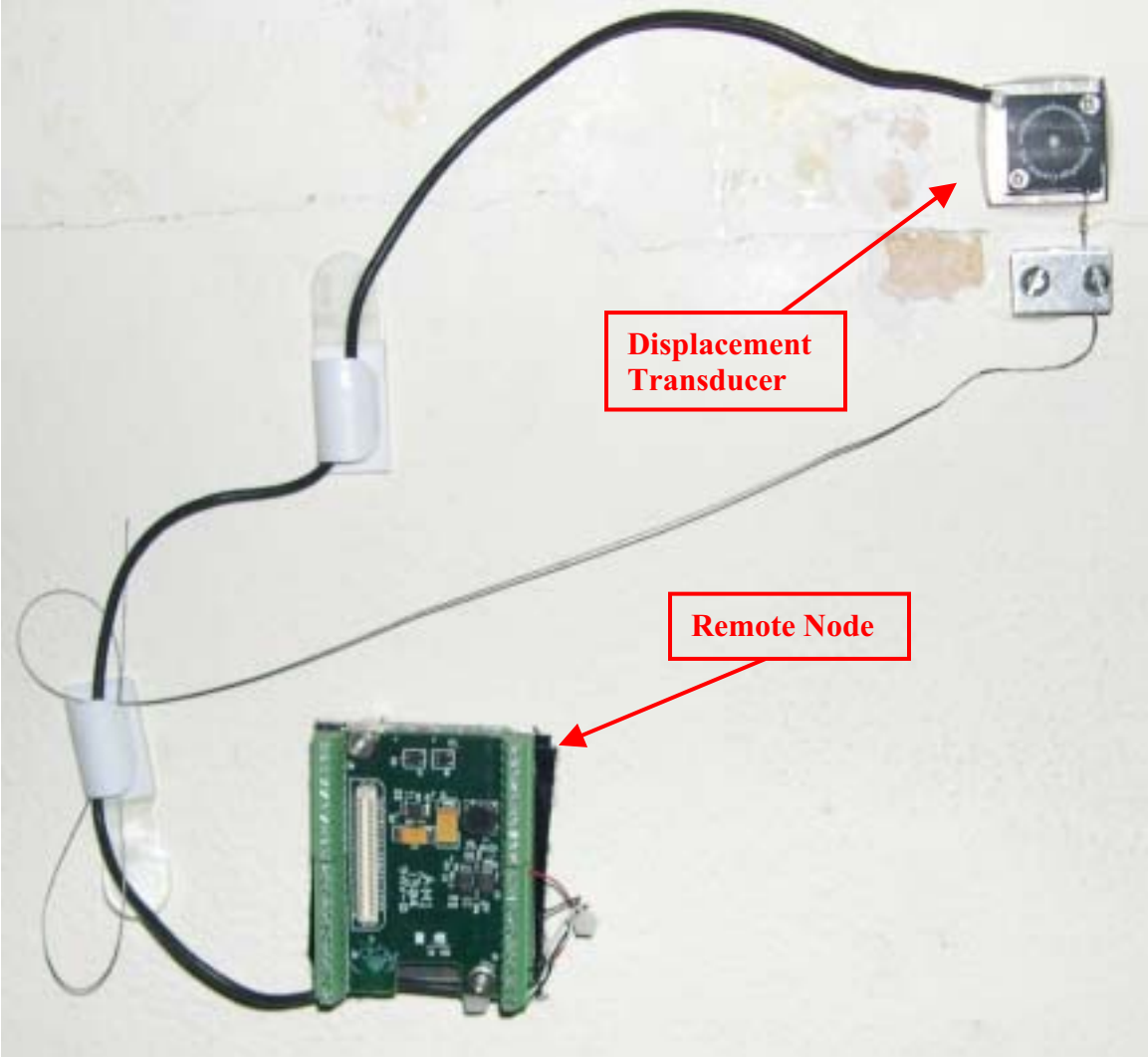


**Figure 2.3: A "sensor node" that consists of remote node and the displacement sensor (mica2 that will be attached to the MDA300 is not shown)**

As shown in Figure 2.4, the “base node” consists of a mica2 mote mounted on an MIB510 interface board. The interface board is connected via a serial cable to a MOXA NPort device that allows remote access to the system via variable communication paths. A cable modem connection was employed in this case to facilitate high rate of data transmission. This “base node” requires AC power, which normally is available since this node supplies backcasting communication to the Internet and it can be placed

anywhere within radio range of the “sensor nodes”, which reportedly can be separated up to 300 m (1000 ft) in outdoor applications.

**Figure 2.4: MOXA NPort (left) and MIB510 with mote running TOSBase (right)**

*Processor/Radio modules*

Mica2 motes are even smaller than the a deck of playing cards (2.25 x 1.25 by 0.25 inches or 5.7 x 3.18 x 0.64 centimeters), which fit on top of two AA batteries that provide power as shown in Figure 2.5. It is built around a 4 MHz Atmel Atmega 128L, a low power microcontroller, which operates the necessary software from its 512 Kbytes of flash memory. This memory stores both the operating system as well as the data. To operate the outboard sensors the mica2 must be combined with the MDA300 sensor board shown in Figure 2.5 or other compatible sensorboards. The mica2 motes also house a Chipcon model CC1000 single chip radio transceiver that operates at 433 MHz RF frequency band. It has 1000 ft outdoor range and transmits 40,000 bits per second, but consumes approximately 8 miliamps during transmission. In sleep mode, power

consumption is reduced to about 40 microamps as will be discussed later under power the consumption profile of the sensor network.

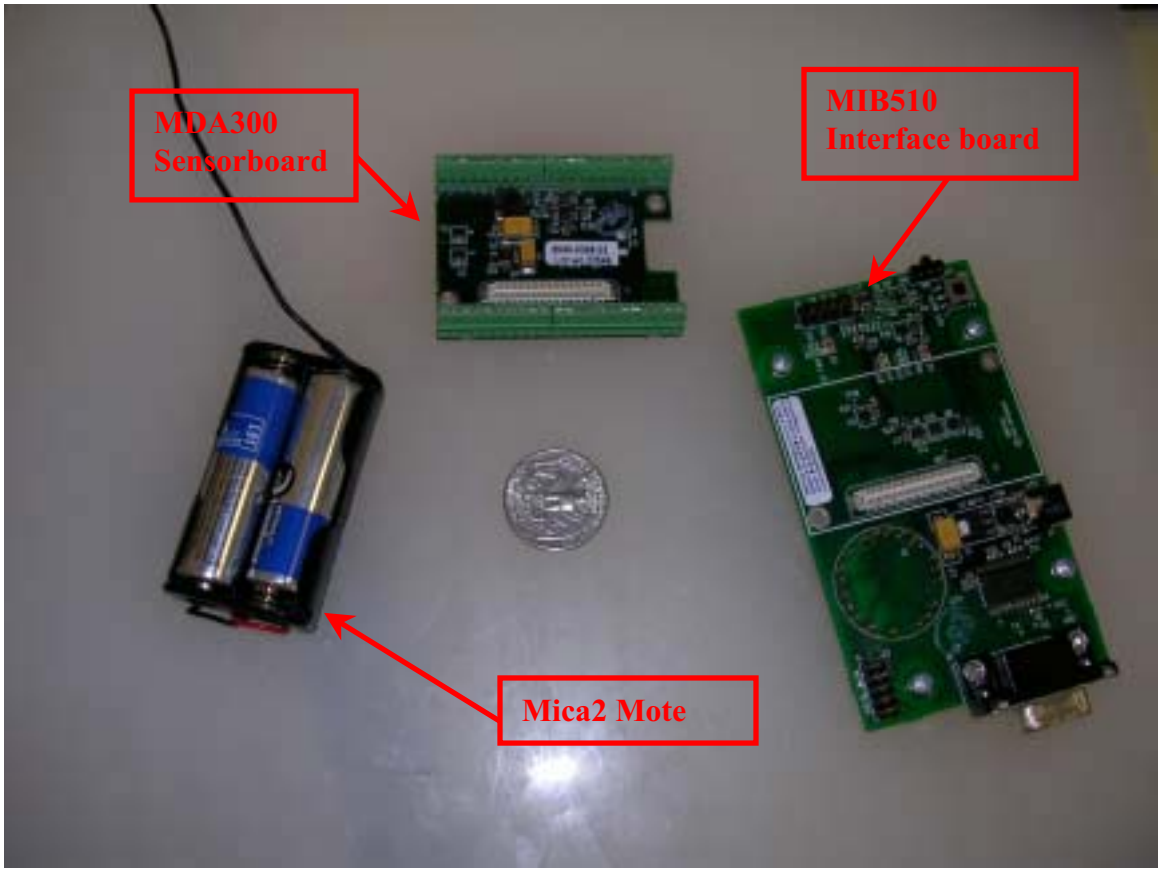


**Figure 2.5: The components of the wireless sensor network**

*Sensorboard*

MDA300 is a general measurement platform for the mica2. It is primarily designed to gather slowly varying (e.g. once measurement per hour) data such as temperature, humidity, light intensity etc. Up to 8 outboard analog and digital sensors can be connected through its screw terminals. It provides 12 bits analog-to-digital conversion for analog external sensors. Three excitation voltages (2.5, 3.3 and 5.0 V) are available for exciting those outboard sensors. Temperature and humidity sensors are provided onboard.

*Base Station*

The MIB510 (Mica2 Interface Board) shown in Figure 2.5 is a multi-purpose interface board that allows a Mica2 to act as a base receiving station. This base station is connected by an RS 232 serial port to the Moxa Nport, as shown in Figure 2.4, to backcast the wireless collected data over external communication links. The MIB510 has on-board in-system processor, An Atmega 16L, to program the motes attached on the connectors, but does not store the data. The board's power is supplied through an external power adapter.

During this project Stargate is also used as the base station. Stargate processor platform is an alternative to the MIB510. It is a powerful single board computer with enhanced communications and sensor signal processing capabilities. It has onboard Intel PXA 255 (400 MHz) processor, 64 MB SdRam and 32 MB flash memory. USB port, RS-232 serial port and Ethernet ports maintain communication. Those attributes make Stargate function not only as an interface to the motes but also as a computer to store the data. Whereas reliable and constant Internet connection was indispensable for MIB510 communication, this dependency is weakened in the case of Stargate. Because, the stored data will not be lost even if the connection failed.

### 2.3.2 Software Protocol: TinyOS (Tiny Operating System)

TinyOS is an open-source operating system designed for wireless embedded sensor networks. This operating system is designed in such a way that it can meet the requirements of a self-assembling sensor network. First of those requirements that shapes the design of the software protocol are the low power consumption and small size. As technology evolves, there will always be a tendency to reduce size of hardware, which

constrains the power and storage facilities. Therefore software must efficiently use the processor and memory. Second prominent feature of the sensor networks is the diversity in design and usage. Associated software protocol must be flexible enough for customizing applications according to the necessities. Third is the suitability of the operating system for concurrent-intensive operations. The operating system must allow for the flow of data from one place to another with minimum amount of processing. This becomes crucial in multi-hop networks where information from either the nodes own sensors or that from the other nodes needs to be captured, manipulated and streamed onto the network simultaneously. Lastly, the operating system should allow for the robust and reliable operation of the sensor network. Further information about the operating system can be found in the literature. (Lewis, Madden, Gay, Polastre, Szewczyk, Woo, Brewer, and Culler, 2004)

Two different applications of TinyOS were customized in order to measure crack displacements from environmental factors. The first of those applications, a single-hop wireless communication, was customized from a "SenseLightToLog" application. The second was a multi-hop application that provides a more power efficient operation and thus a more robust long-term operation of the sensor network.

*Single-hop customization*

The MDA300logger single-hop customization is based on SenseLightToLog application, which is essentially designed to obtain photo readings from a sensor. This application basically causes the mote to collect readings at predetermined intervals, write them to the EEPROM, and transmit the sensor readings over the radio. In this customized

application, a potentiometer ratiometric analog sensor is attached to the MDA300 sensorboard.

The interface from the off-site central PC to the wireless data acquisition system is provided through the command-line java application BcastInject. The customized application is initiated by two commands given by the central PC:

- START_SENSING: This command invokes the Sensing interface to collect a specified number of samples at a specified sampling rate, and to store these samples in mote's EEPROM.
- READ_LOG: This command will retrieve a line of data from the EEPROM and broadcast it in a radio packet.

This application functions as a single hop network. The wireless remote nodes are individual data loggers and they only transmit their data to the base station when READ_LOG command is given. In this application, MIB510 and Moxa Nport form the base station and served as an interface between the motes and an off-site PC. Battery lifetime is between 27 to 50 days in this configuration and mode of operation.

*Multi-hop Customization*

This configuration provides a sophisticated method of multi-hop data propagation. The XMesh software protocol is the routing layer for this application. It is an open-architecture, flexible, and powerful embedded wireless networking and control platform built on top of the TinyOS operating system. Some of the features of Xmesh include: 1.) True mesh (Self-forming and self-healing in the case of loss of communication between the motes) 2.) Coverage area is extended as the motes are added to the mesh 3.) Low

power listening (wake up several times per second to listen to RF if there is any data ready to be transmitted). 4.)Can achieve more than year of battery life with reporting intervals of 60 minutes.

In this configuration, even if the motes are out of the range of the base station, they can form their own coverage area and communicate via multi-hop networking. As opposed to the single-hop configuration, multihopping employs remote motes only as sensing units. There is only one data logger, which is the base station. Stargate stores the data and communicates with an off-site PC. Table 2-1 summarizes the properties of the two applications in a comparative way.

**Table 2-1. Summary of the properties of single-hop and multi-hop applications**

| *Single-hop Application* | *Multi-hop Application* |
|---|---|
| Wireless network of sensor data loggers | Wireless network of sensors |
| Each remote node acts as a data logger | Only base station acts as a data logger |
| MIB510+Moxa Nport base station acts as a gateway only | Stargate is the base station as a gateway and data storing unit |
| Limited battery lifetime (~ month) | Enhanced battery lifetime (~ year) |

## 2.4 Benefits of the wireless system

*Physical Appearance*

As described in previous sections, miniaturized wireless system saves time and money in installation. Additionally, it significantly reduces the risk of disruption associated with running cables through a structure that is in use. It also reduces significantly the visual intrusion when employed within occupied structures.

As shown by the insert in Figure 2.6, wires are an attractive nuisance. This photo was taken after the tenant of the test house decided to “hide” the wires and transducers. The plastic ivy across the transducers rendered them completely inoperable and the system had to be moved out of the living room. For comparison, the center picture in Figure 2.6 from the same house shows both wireless remote node with attached potentiometer and wired sensors, which are connected by wires to the data acquisition system. This picture demonstrates the contrast between wired and wireless systems from the aspect of obtrusive appearance.

**Figure 2.6: Plastic Ivy used to hide wires and sensor (bottom right) and the wireless remote node on the ceiling**

*Power Consumption*

Long-term power requirements of the wireless system were overcome by taking advantage of the Crossbow hardware's low-power sleep mode in both applications. Since environmental surveillance applications should operate for months or years, it must operate at low power consumption without maintenance. A node spends most of its time asleep, and then periodically wakes up to sample, communicate and compute. The percentage of time that a node is awake is simply known as node's duty cycle. There are varieties of approaches to achieve low power duty cycles; these applications described herein are just two of them. Figure 2.7 shows battery voltage decline during the test performed with the single-hop application and 5 minutes duty cycles, from December 20, 2004 to 2004 to January 16, 2005. It is not possible to validate directly the battery lifetime with those field measurements because the test was stopped when the motes were removed for further development in the laboratory. However, if the battery decline curve is projected to the future, the lifetime is estimated to be 40-42 days, which is very close to the estimated lifetime calculated with 5 minutes duty cycles.

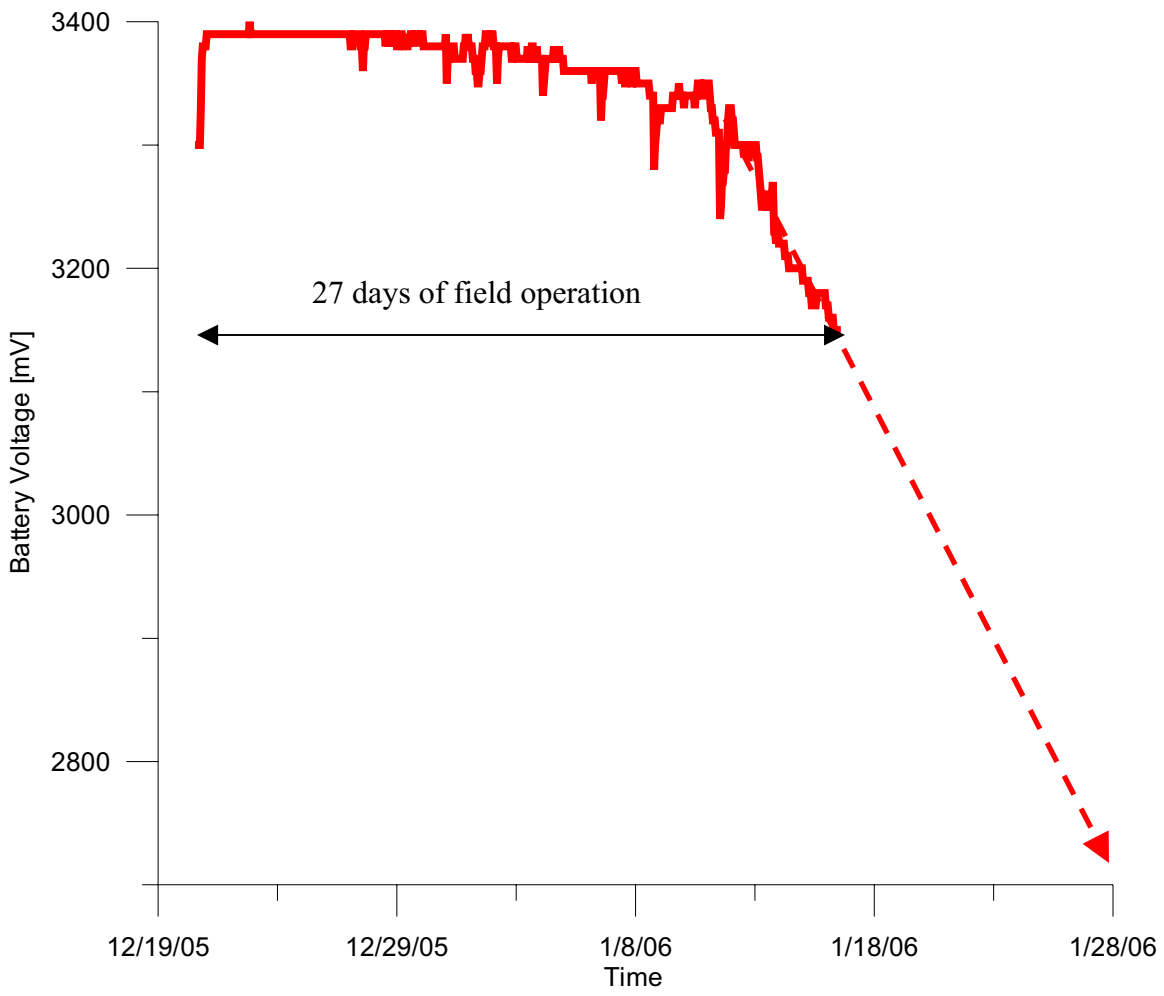


**Figure 2.7: Mote battery voltage decline during the field test (with 5 minute duty cycle)**

In the single-hop mode, motes wake up for certain intervals of time to execute sampling and to communicate with the base. At the end of this interval, they go to sleep until the start of the new cycle. The power consumption profile during sleeping and operating is shown in Figure 2.8. The spikes denoted by (a) represent sampling off the potentiometer, which lasts in about 0.3 seconds and consumes 20-30 miliamps. Interval (b) is the time span when the mote is awake for communication. This interval is totally dependent on the choice of convenience for communication. The shorter it is, the longer the battery life. But then access to the system becomes available only at shorter intervals per hour. Finally (c) denotes the sleep interval when the radio is turned off. The system,

with radio communication allowed for 15 minutes per hour, operated for about 27 days with 2 AA lithium ion batteries. If the radio access period is reduced to 5 minutes, the battery life will extend to 45 days with the same batteries. Use of higher density power cells might prolong the battery life up to a year.

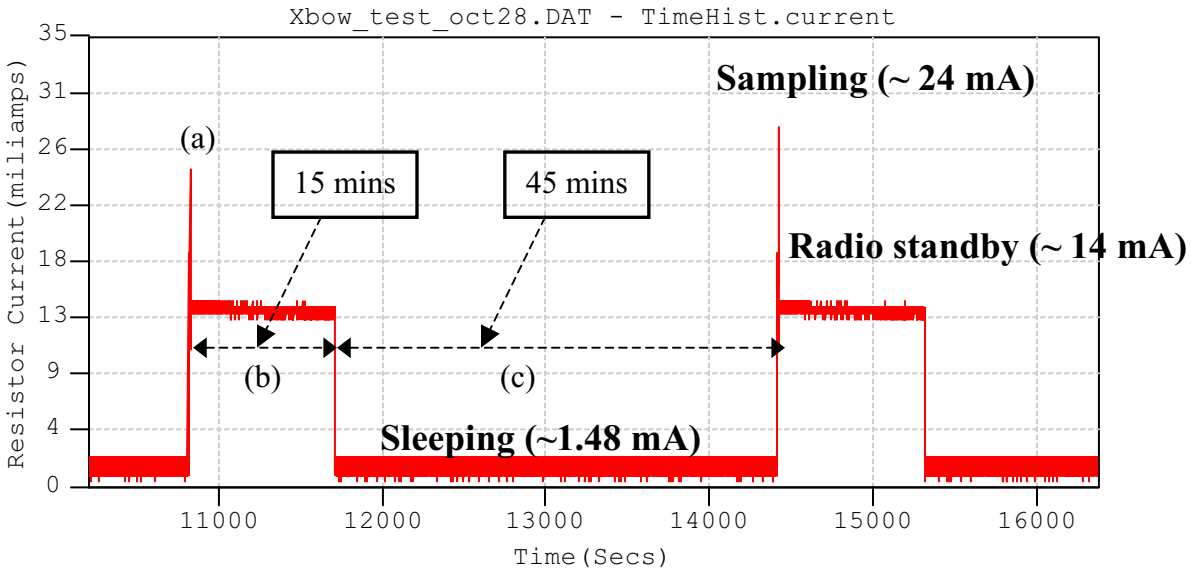


**Figure 2.8: Power consumption profile of single-hop application (15 minutes duty cycles)**

The Xmesh multi-hop protocol with the Stargate base provides more efficient and built-in power saving model, which allows mote operation for about a year with two AA batteries. Figure 2.9 and Figure 2.10 illustrates the power consumption profile obtained by one of the low power modes available in multi-hop customization. According to this protocol, as shown by the spikes in the figure, the motes wake up several times in one second for listening to RF and for transmission. But in this case transmission does not necessarily mean that the motes are transmitting the analog sensor data. Those transmitted packets shown with spikes several seconds apart from each and magnitudes of 8-10 miliamps include the routing information between the motes in order to locate the sensor in the network or re-form the network. In this manner, the motes can calculate the

propagation path that will minimize the cost of transmission. During the first 3600 seconds in the timeline, data packets were sampled more frequently (1 minute apart from each other) to form the topology and allow the motes recognize their neighbors. It was experimentally proven that, for a mesh of 3 to 4 remote nodes, 20 to 30 packets would be sufficient to initiate a reliable and robust wireless network. In case of field deployment, it is desirable to form the network quickly for the sake of installation time. Therefore, sampling interval was chosen to be 1 minute for the first 60 packets. After that, 18 minutes passes between each sent packet.

Table 2-2 summarizes the current consumed in sleeping, transmission and listening modes. Significant improvement from single-hop to multi-hop application is apparent. Average current consumed during sampling and sleeping+listening modes are about 4.20 and 0.31 miliamps respectively. Considering sampling intervals of 5 to 60 minutes, sampling clearly will not have a significant effect on the average power consumption. In this situation, the overall hourly average current draw is approximately 0.31 miliamps and battery lifetime is estimated to be about 380 days.

| ***Type of mode*** | ***Single-hop application*** | ***Multi-hop application*** |
|---|---|---|
| Sleeping [mA] | 1.48 | 0.04 |
| Transmission [mA] | 20-30 | 8-10 |
| Listening [mA] | NA | 2-4 |

**Table 2-2. Summary of the current consumed in different modes of single-hop and multi-hop applications**

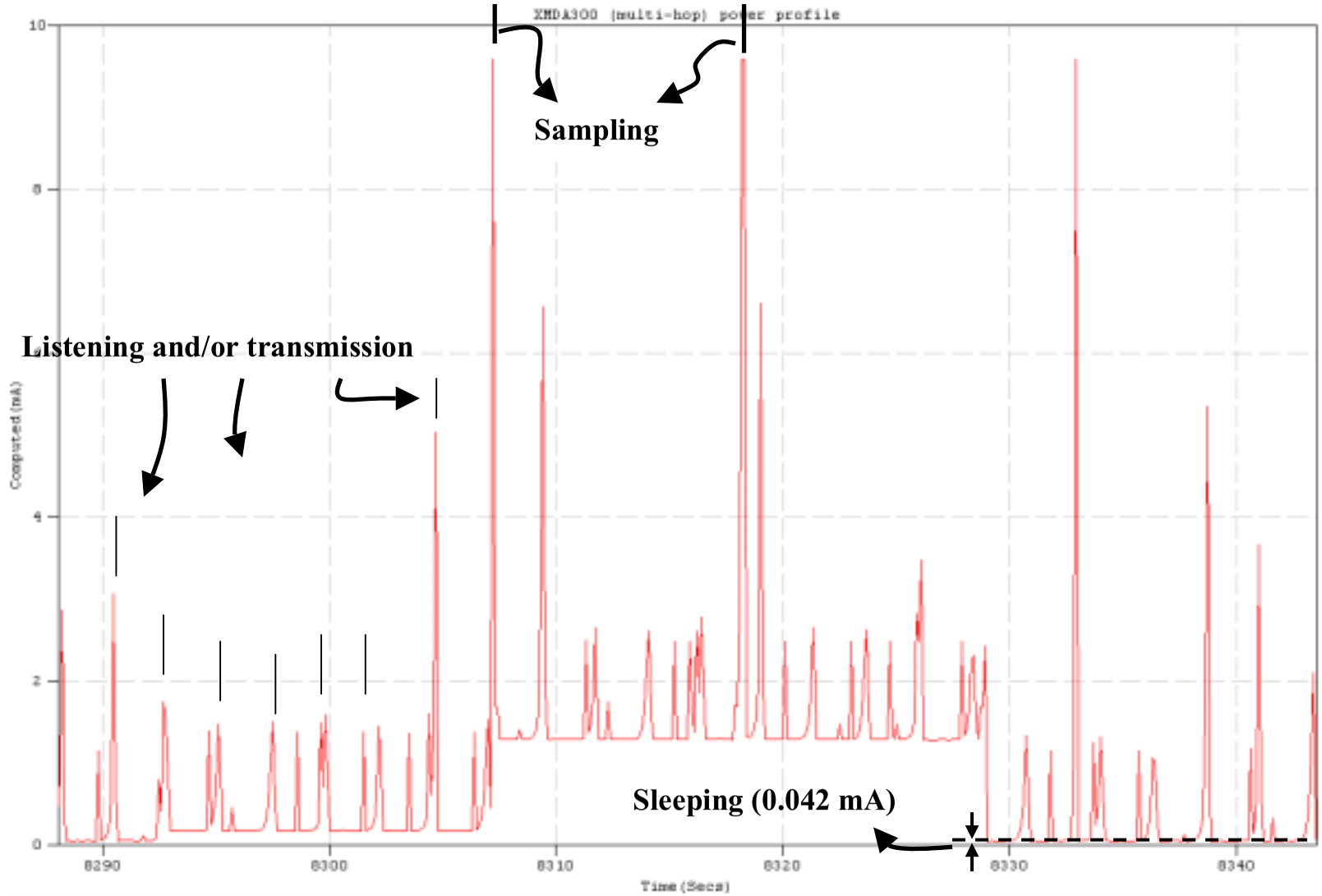


**Figure 2.9: Power consumption profile of one of the low power modes in Xmesh. (This sampling window is the oval in Figure 2.10, which shows its duration compared to ongoing operation)**

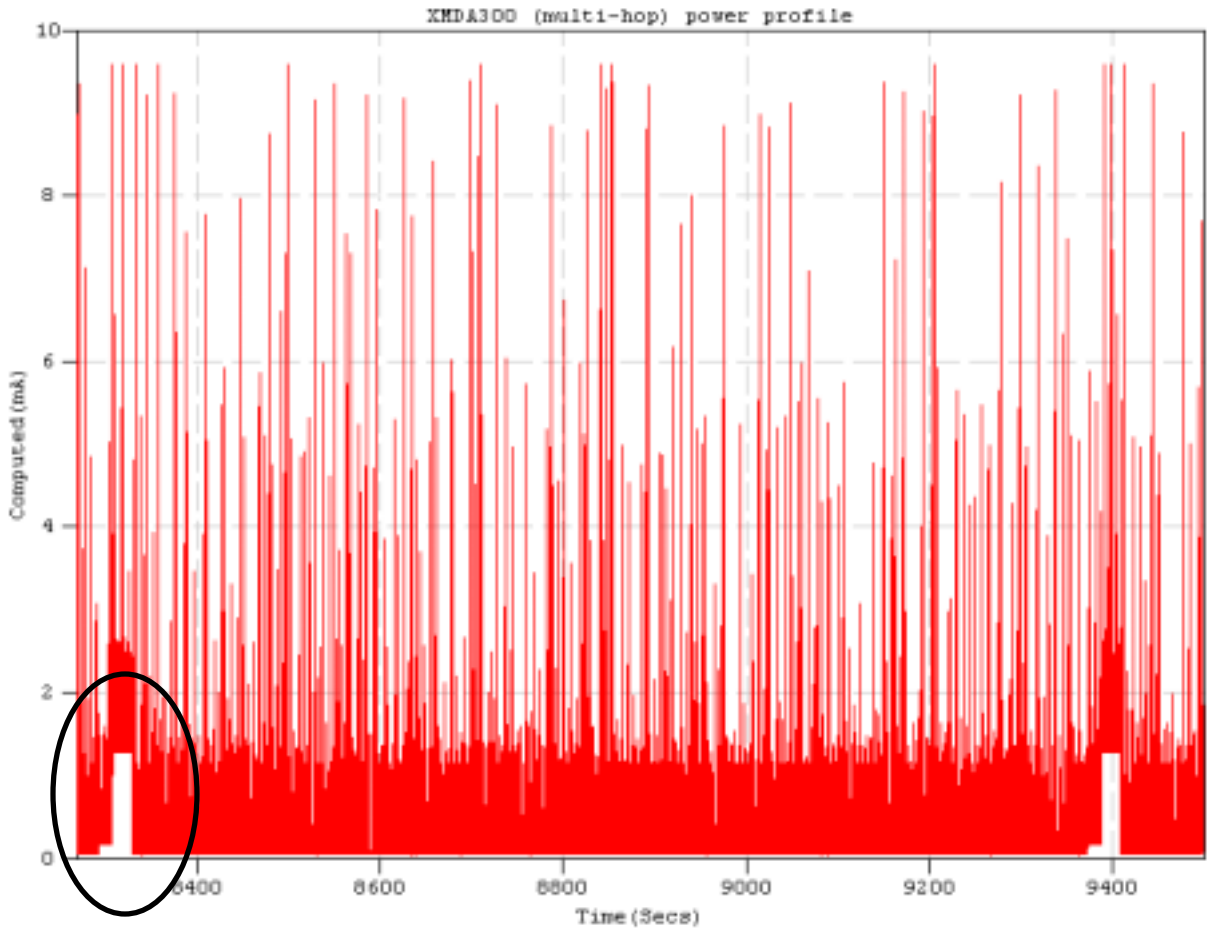


**Figure 2.10: Power consumption profile of Xmesh protocol showing the two consecutive sampling intervals (details of history in ellipse is shown in Figure 2.9)**

As mentioned before, the profile shown in Figure 2.9 and Figure 2.10 is just one of the low power models available in Xmesh protocol. However, there are different power consumption model that can decrease the average power consumption considerably. Therefore battery lifetime can be prolonged to even more than two years with adaptation of yet lower power modes.

On the other hand, power limitations complicate the issue of high-frequency sampling triggered by outside phenomenon, since the motes must be sleeping most of the time in order to conserve power. Even though power limitations are overcome and system is triggered somehow, high frequency sampling still remains as an issue due to inadaptability of current software that

runs with the motes. Therefore the system described in the scope of this research is only capable of acquiring long-term continuous measurements whose data rate is slower than 1 minute. Future Wireless Data Acquisition systems could rely on solar cells for energy scavenging or a device such as a geophone that produces a voltage pulse to wake up the mote.

*Noise Level*

Wireless systems are less noisy than the wired counterparts. The length of the wire connecting the potentiometer to the MDA300 is only about 1 foot long and this is the only wire that can affect the output of the sensor. Wired systems on the other hand require much longer wires in order to connect the sensors to the data acquisition system usually located far from the sensors, which causes intrusion of noise to the sensor outputs through ground loops etc.

Since high frequency sampling cannot be implemented in the wireless system so far, it is difficult to have a meaningful comparison of wired and wireless systems in terms of noise levels. The highest sampling rate that is achieved by the wireless system is 10 Hz and the data swing in the potentiometer output at this level is about 0.5 to 0.6 micrometers. On the other hand, as will be discussed in Chapter 3, wired system yielded 10 to 15 micrometers of data swings in the potentiometer output at 10 Hz sampling.

## 2.5 Installation of the system

### 2.5.1 Description of the installed system and operation basics

*Single-hop Configuration*

This system is designed to record the response of any infrastructure component where the rate of change is slower than 1 unit per minute. Proof of this system was established by measuring the response of cosmetic cracks in a house subjected to blasting at a nearby quarry.

The structure, shown in Figure 2.11, is a concrete block house and blasting operations are conducted 1500 to 2000 feet away from the structure. Data have been collected in this house on experimental basis since August 2000. (Louis 2000 and McKenna 2002)

As shown in Figure 2.11, sensors are attached across cracks to monitor long-term changes in crack width induced by environmental conditions and/or blasting activity. As discussed in the previous sections, the wireless system is designed for measuring data whose rate of change is less than 1 minute. The sampling rate was set to be 1 sample per hour in order to match that of the wired data acquisition system in the house. Data presented in this section were collected from November 18, 2004 to January 16, 2005. During this monitoring period, internal temperature and humidity varied between 16 to 24 Celsius and 21 to 47 % respectively. Since measurement of dynamic events requires high frequency sampling (1000 Hz in this case), crack displacements from ground motion induced by the blast events were not measured. However, any long-term effect of blast events on the general trend of crack displacement can be detected with the long-term data.

The system excites and records the voltage output of the ratiometric string potentiometer, shown in Figure 2.11, which measures micrometer changes in crack width. As will be described in Chapter 3, the potentiometer is optimal because of its high sensitivity, low power draw, and instantaneous response time. Such devices that operate with low power draws are essential to the success of any wireless sensor system. As the width of the crack changes, so will the resistance of the potentiometer. The change in crack width is then a linear function of the output voltage of the potentiometer given a known input voltage.

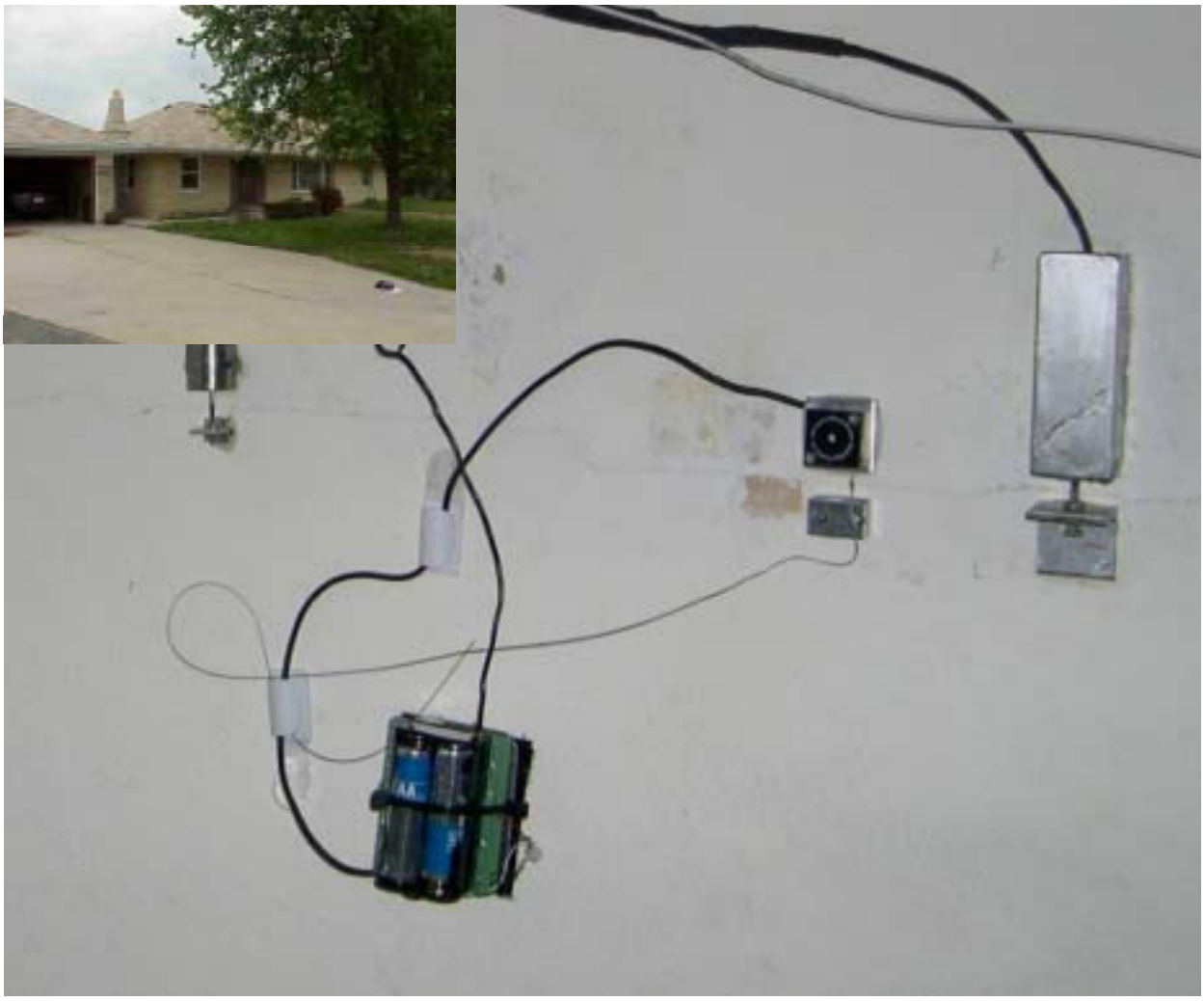

**Figure 2.11. A potentiometer attached to a "remote node" and LVDT displacement sensors across the same ceiling crack (bottom right) and picture of the instrumented house (top left)**

At each sampling time (every hour in this test case), the Mica2 activates the MDA300's 2.5 Volt excitation voltage to power the potentiometer. The voltage output of the potentiometer along with temperature, humidity, and battery voltage are stored locally on the "sensor node" mote's onboard non-volatile memory. It is necessary to utilize the precision input channels on the MDA300, which have 12-bit resolution over the approximately 0.4mm (0.016 in) full-scale travel length of the string potentiometer to achieve a resolution of about 0.1 μm (3.9 μin).

Whenever data retrieval is required from the remote site (every day at 11:00 PM in this test case) the central PC autonomously communicates with the wireless system via the Internet via a modified version of BcastInject to broadcast a "read_log" command and a mote address across the mote network. The mote in question will then transmit all of its data back to the off-site PC where it is recorded to the hard disk. This process is repeated for each mote address in the network. Once all motes have sent their data, a "start_sensing" command is issued which tells all motes in the network to clear their memory and resume scheduled sampling. This process is easily automated to acquire the data and display it on the Internet.

The interface from the off-site central PC to the Wireless Data Acquisition system is provided through the command-line java application BcastInject. Since single-hop application is based on SenseLightToLog, BcastInject requires only slight modification to interact properly with the current configuration.

*Multi-hop Configuration*

Like single-hop configuration, this protocol is also designed for long-term measurements of data whose rate of change is relatively slow. As discussed before, this system allows multi-hop networking between the remote nodes and the base station, Stargate, which functions as a gateway and a storage unit in the field. This configuration utilizes much more sophisticated methods of data logging and power consumption in terms of wireless communication as discussed earlier

The multi-hop system has been field tested on the roof of the building housing the Infrastructure Institute of Technology laboratories as shown in Figure 2.12. This test was performed in order to validate the field performance of the wireless motes operating in a multi-hop mode. The motes were exposed to the harshest environment on the roof of a downtown

building in terms of wireless communication. Two potentiometers were attached to two different remote nodes. Each outside remote node, which consists of sensorboard (MDA300), radio module (mica2) and an outboard sensor (potentiometer), sampled the temperature, humidity, battery voltage and displacement sensor data every 18 minutes. One remote inside the elevator penthouse measured only temperature, humidity and battery voltage.

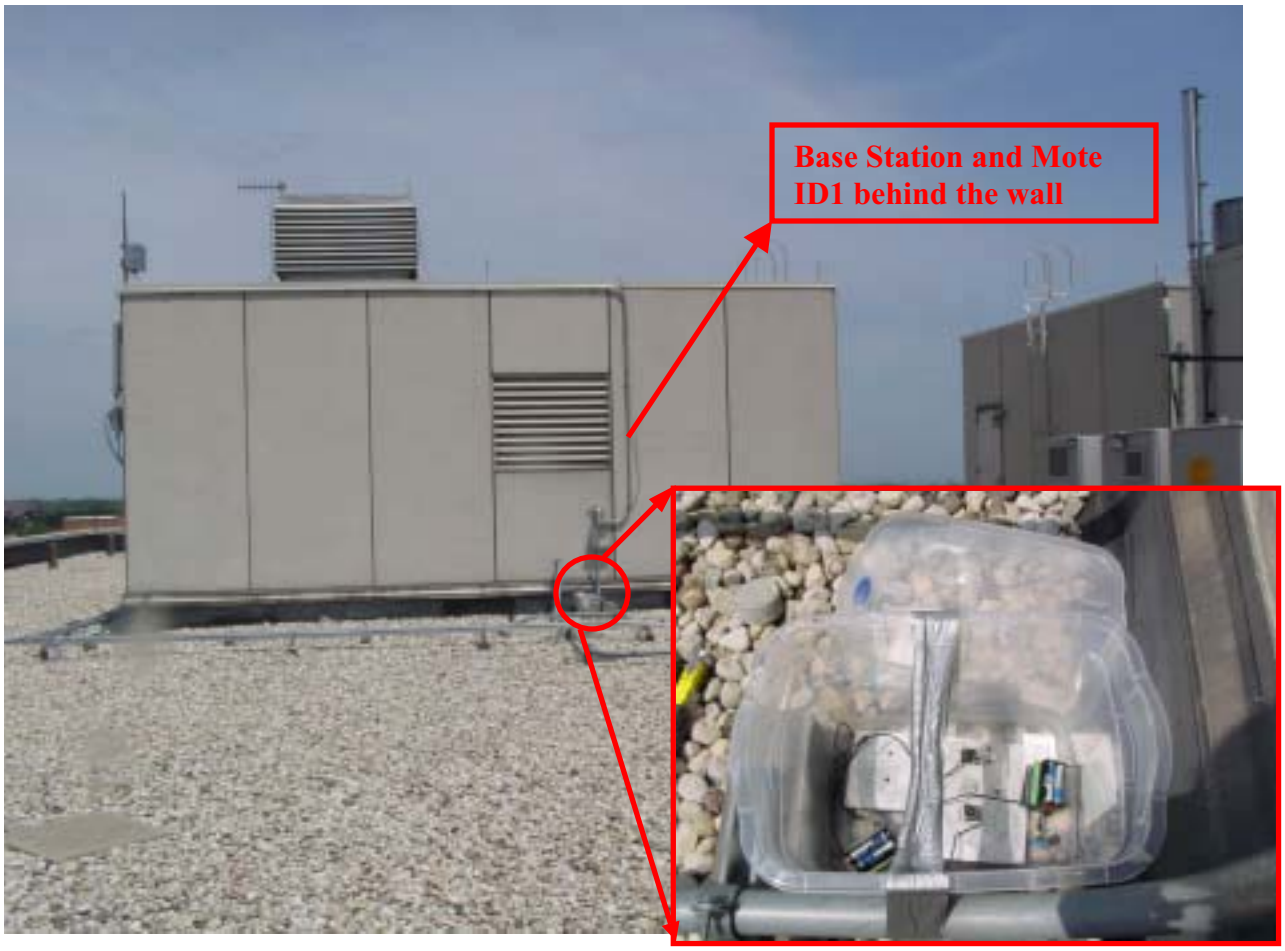


**Figure 2.12: Remote nodes deployed on the roof of a downtown building**

Those samples were propagated to the base through the most efficient path network. Efficiency (cost) is a measure of distance and is calculated by wireless routing algorithms, which will not be discussed in detail. Data sampled every 18 minutes were stored in the base (Stargate) and retrieved via Internet autonomously every night.

### 2.5.2 Analysis of the results

*Crack response to environmental effects*

Two strategies are emerging for measuring crack response to determine the effect of vibratory motions: 1.) Long-term measurement or Level 1 2.) Dynamic as well as long-term measurement or Level 2. Level 1 approaches answer the question: Did the ground motion change the long-term pattern of crack response? Long-term in this case is that response that occurs on a daily, weekly or yearly basis. Figure 2.13 presents such a change in long-term response observed with Level 1 surveillance. (McKenna, 2002) Rain in New Mexico on July 11$^{th}$ (high humidity on the lower graph) produced the permanent offset in the response pattern. The average daily crack response (shown on the middle graph) was shifted 20 μm (800 μin). The cyclic daily changes are heavily influenced by the large temperature changes shown in the upper graph.

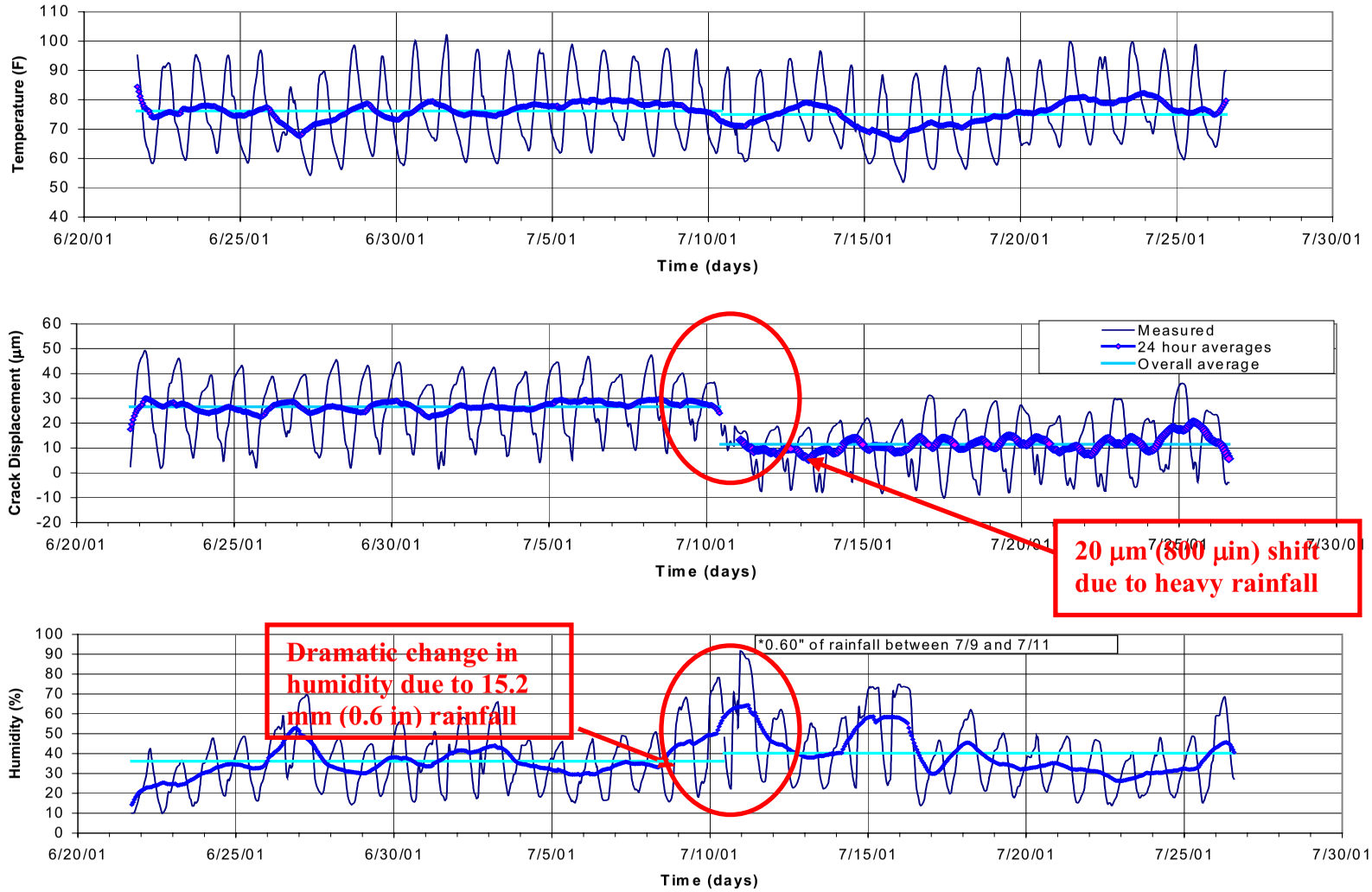


**Figure 2.13. Long-term crack displacements and weather changes (McKenna, 2002)**

Level 2 comparison is shown in Figure 2.14. Level 2 surveillance involves measurement of both long term and dynamic crack response with the same gauge. The dynamic, 4.83 μm (190 μin) peak to peak crack response to the 9 May 2.03 mm/s (0.08 ips) blast induced ground motion is shown on the bottom right. This dynamic crack response (shown by red dots in the bottom left) is compared to the long-term crack response in the bottom left. In this case the dynamic response is only 1/100 that of the average daily, zero to peak, response of the crack induced by the temperature changes.

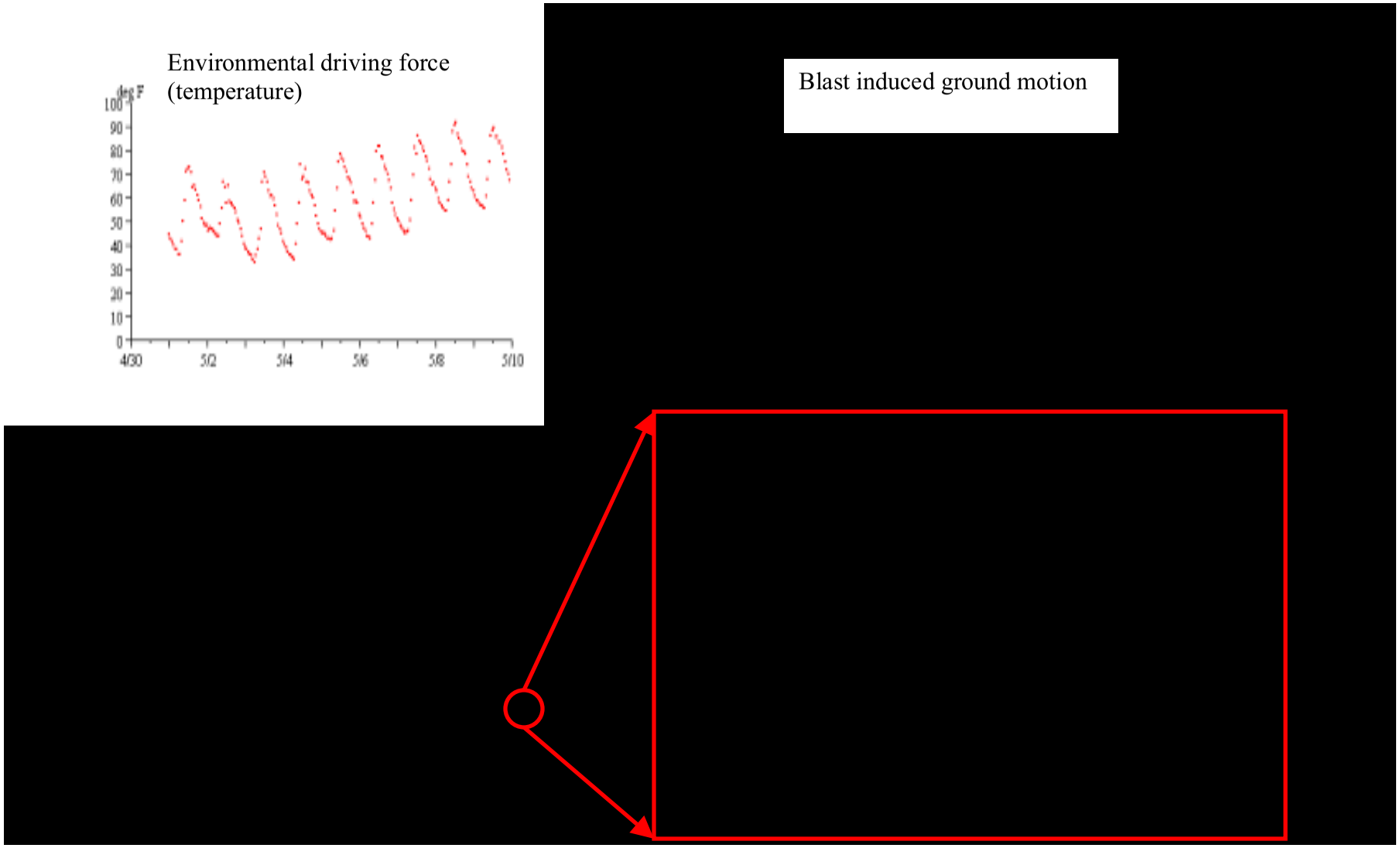


**Figure 2.14. Level 2 comparison of crack response (Kentucky, 2005)**

Level 1 monitoring is simpler than Level 2 for at least three reasons: lower sampling rate, single mode of operation, and less required precision. First, measurement of long-term or Level 1 response only requires measurements of change in crack response once an hour (or one sample per hour), the timing at which can be predetermined. Level 2 requires measurement at 1000 samples per second during dynamic excitation, which can occur at any time and thus ordinarily requires constant sampling and power draw. Second, measurement of dynamic response requires switching between the 1000 samples per second mode of operation upon dynamic excitation and the one sample per hour mode for long-term. A complex triggering code is needed to facilitate this change "on the fly". Third, crack response to typical vibratory excitation tends to be much smaller than that to weather induced responses. As can be seen from the above examples, long-term response only requires accuracy to say 1 μm (40 μin) to capture the long-term, 20 to 200+ zero to peak μm, daily and longer-term changes.

Since the wireless system developed in the scope of this research is only capable of performing long-term measurements, crack response analysis must be conducted on the basis of Level-I monitoring.

#### *2.5.2.1 Measurement of crack response (Single-hop customization)*

*Comparison of the measurements with the wired benchmark system*

Data obtained from the wireless system were validated by comparison with a wired benchmark system that had been used in the test house for some five years. The benchmark system employs two types of position sensors to measure micrometer changes in crack width – an LVDT displacement sensor and an eddy current proximity sensor. The LVDT was the only sensor operable with the wired benchmark system during the wireless monitoring period. Figure 2.15 compares the long-term crack displacements measured by wired and wireless systems

along with the associated temperature changes. In addition to the raw crack displacements, 24-point moving averages are also plotted in Figure 2.15. As can be seen, the long-term response measured by the two data acquisition systems is remarkably similar.

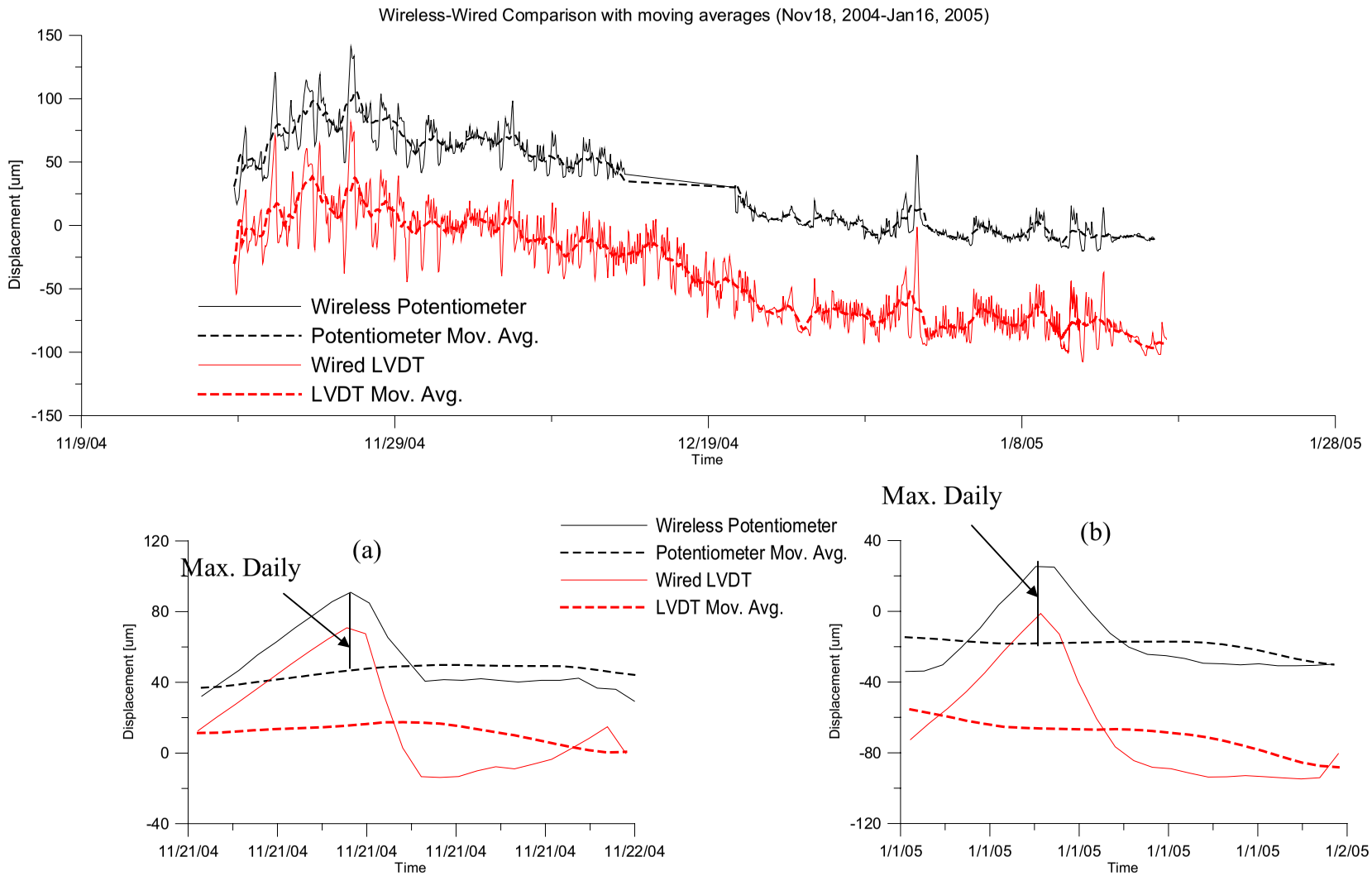


**Figure 2.15: Temperature and crack displacement measurements by wireless and wired data acquisition system in Milwaukee test house during November 18, 2004 to January 16, 2005.**

The actual measurements, 24-hour averages, and overall averages were used to determine crack response to weather effects. Weather effects have three distinct contributors:1) frontal movements that change overall temperature and humidity for periods of several days to several weeks, 2) daily responses to changes in average temperature and 3) events that contain extremes of unusual weather or other environmental effects. Table 2-3 lists all of the average and maximum values for the frontal, daily, and weather effects. As seen from the values in the table, temperature measurements obtained by the wireless system agree with those obtained by wired benchmark system. On the other hand, humidity results indicate a mismatch either caused by the inaccuracy of the MDA300's onboard humidity sensor or incorrect conversion of the analog voltage data to physical data within the software protocol of wireless hardware.

**Table 2-3: Computed long term crack displacements due to weather effect (The values in parenthesis are from the wired benchmark system)**

| | Temperature [Celsius] | Humidity [%] | Crack Displacement [μm] |
|---|---|---|---|
| Frontal Effect | | | |
| Average deviation of 24 pt. average from overall average | 1.85 (1.72) | 12.46 (16.01) | 76.20 (76.0) |
| Max. Deviation of 24 pt. average from overall average | 0.39 (0.36) | 4.06 (5.12) | 33.70 (34.6) |
| Daily Effect | | | |
| Average deviation of actual data from 24 pt. average | 3.36 (3.14) | 8.00 (8.87) | 44.20 (64.98) |
| Max. Deviation of actual data from 24 pt. average | 0.65 (0.55) | 1.15 (0.98) | 6.40 (10.56) |
| Weather Effect | | | |
| Average deviation of actual data from overall average | 4.00 (3.52) | 14.81(17.15) | 111.60 (118.9) |
| Max. Deviation of actual data from overall average | 0.75 (0.66) | 4.29 (5.25) | 34.00 (35.2) |

Crack displacements associated with the weather effects are also listed in Table 2-3. According to the results listed in the table and plotted in the (a) and (b) figures of Figure 2.15, displacements obtained by the wireless system are in a reasonable agreement with those

obtained by the wired benchmark. Data exhibit very similar patterns but with slightly different magnitudes. Inaccuracy in the output of the potentiometer, as will be discussed in Chapter 3, might contribute to the differences in the magnitude of the displacements.

*Effects of blast events on long-term crack displacements (with Single-hop customization)*

As discussed before, this is a Level 1 wireless system. Since it is not designed for high frequency sampling, crack displacements induced by ground motion cannot be measured. Instead, the effect of blast events on the overall response pattern will be analyzed during the monitoring period. Blast events during the monitoring period are listed below.

1- November 19, 2004 9:04, 9:08, 9:13 blasts
2- November 23, 2004 9:47, 9:52, 9:56 and 10:00 blasts
3- November 30, 2004 10:47, 10:51, 10:56, 11:00, 11:05 and 13:42 blasts
4- December 2, 2004 15:44 blast
5- December 6, 2004 12:30 blast
6- December 21, 2004 11:53 blast
7- January 4, 2005 11:03, 11:08, 11:11, 13:00 and 13:05 blasts

Those blast events are annotated in Figure 2.16. Measurements during the entire monitoring period are separated into two plots for the purpose of clarity. Temperature variations are included in the charts to provide a reference for “other” drivers of crack response.

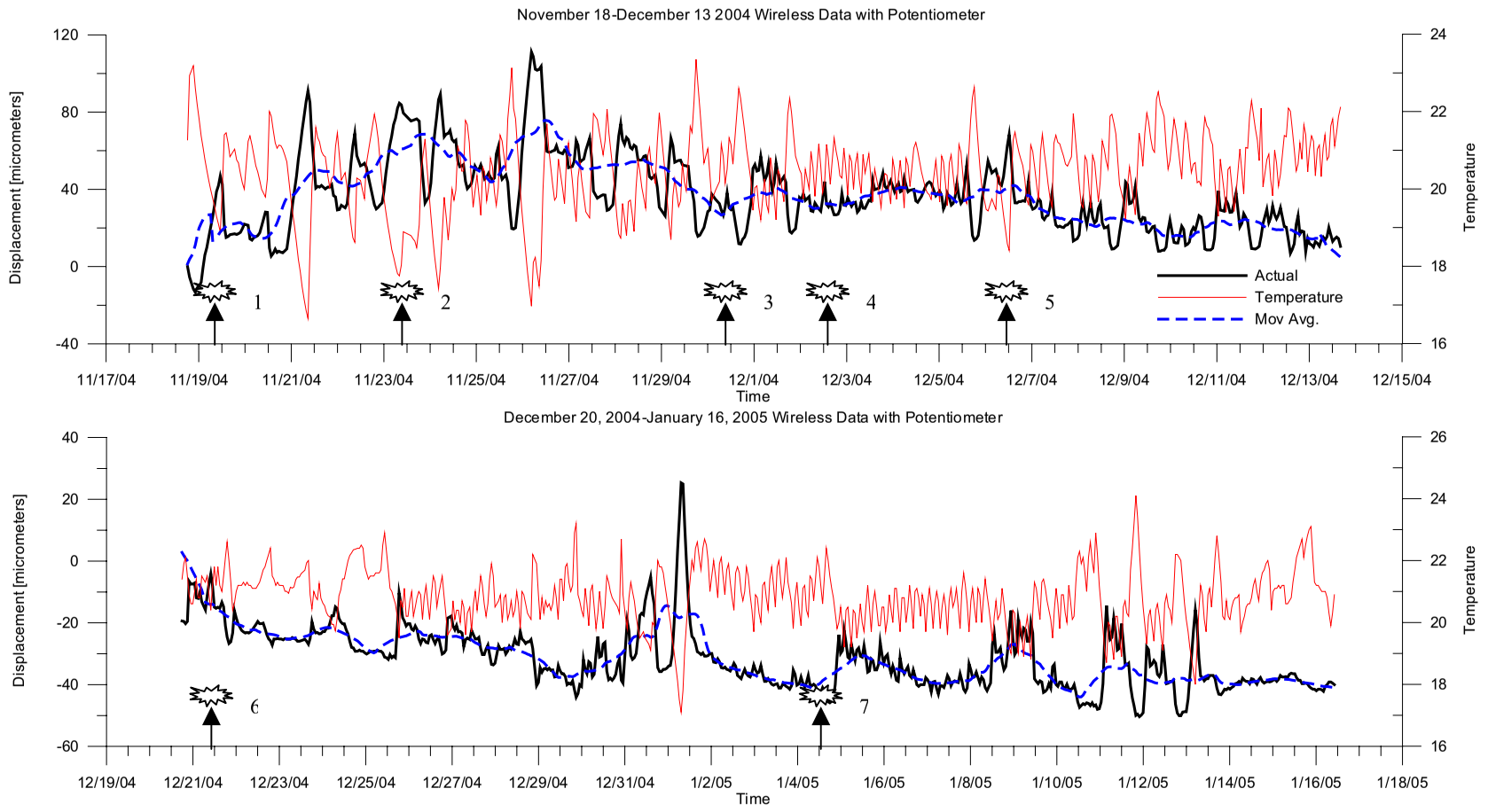


**Figure 2.16: Crack displacement measurements by wireless system with blast events annotated**

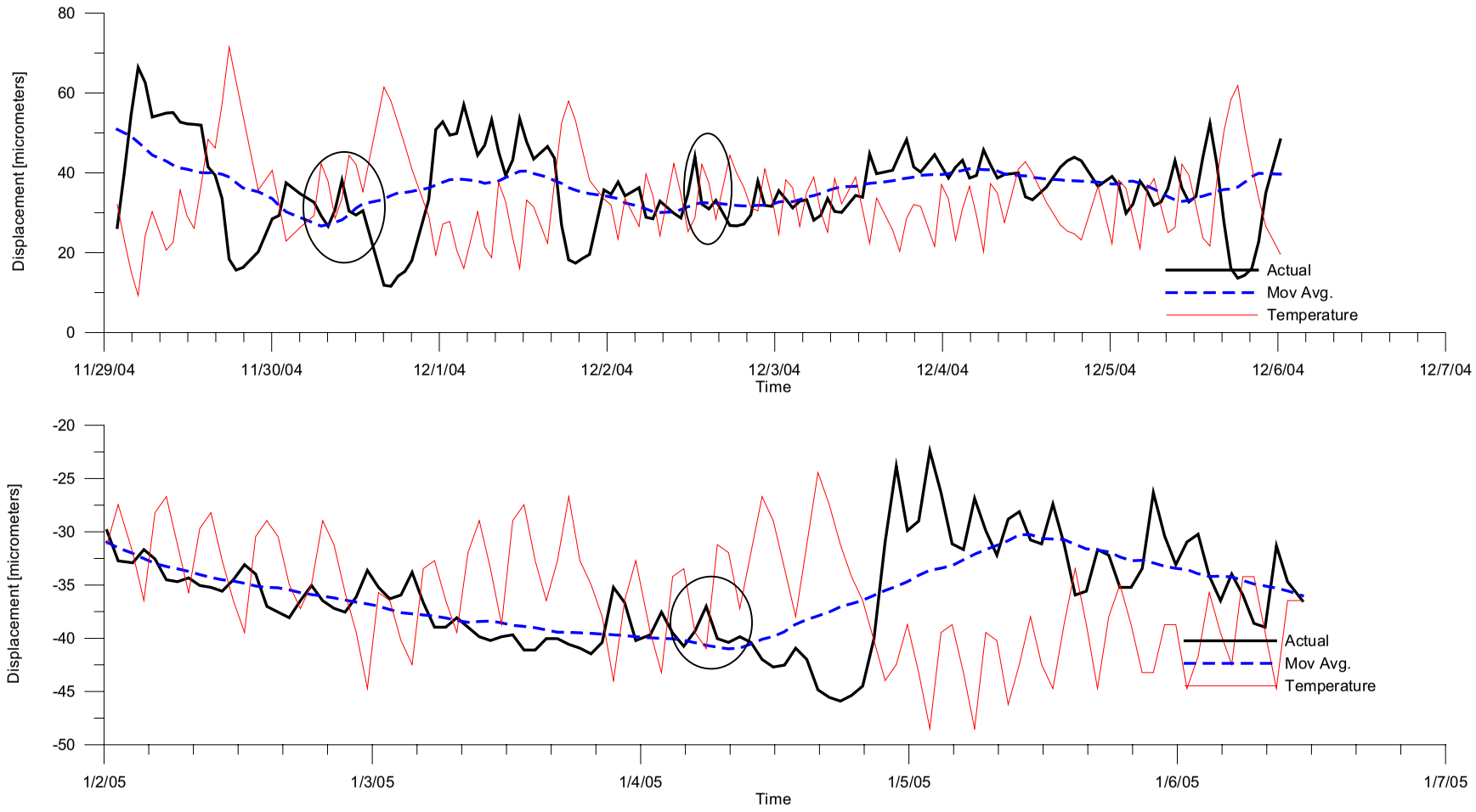


**Figure 2.17: Close-up view to the long-term data during blast events**

Enlarged displacement profiles for time periods surrounding some of the blast events are presented in Figure 2.17. As shown, crack displacements did not exhibit any different behavior than during non-blasting periods, where environmental factors are the only the driving force inducing crack opening and closing. Several blast events occurred during this monitoring period, within a range of 1.27 to 3.05 mm/s (0.05 to 0.12 ips) peak particle velocity, but none of them influenced the long-term crack displacement behavior triggered by environmental effects, mainly temperature.

#### *2.5.2.2 Roof test (Multi-hop customization)*

As discussed in previous sections, multi-hop mesh network application allows the network operates for about a year on one pair of batteries. As opposed to the single-hop configuration, this customization is a very sophisticated method of forming a wireless network in terms of power saving and data transmission efficiency. Figure 2.18 shows the results obtained from the test performed to validate the performance of the motes programmed with multi-hop configuration. Two remote nodes measured the expansion and contraction of aluminum and plastic donut respectively via potentiometer. The mote ID2 and ID3 denote the nodes with the potentiometers on the aluminum plate and with the plastic donut respectively. Remote node ID1, inside the elevator penthouse, measured only temperature, humidity and battery voltage. The reason for using another remote node was to make sure the mesh network could operate with multiple motes. Therefore, mote ID1 results will not be shown due to insignificance of its data. Although the temperature was not directly measured on the plate or donut, the cyclic temperature variations in the box clearly reflect the daily expansion and contraction cycles of aluminum plate and plastic donut.

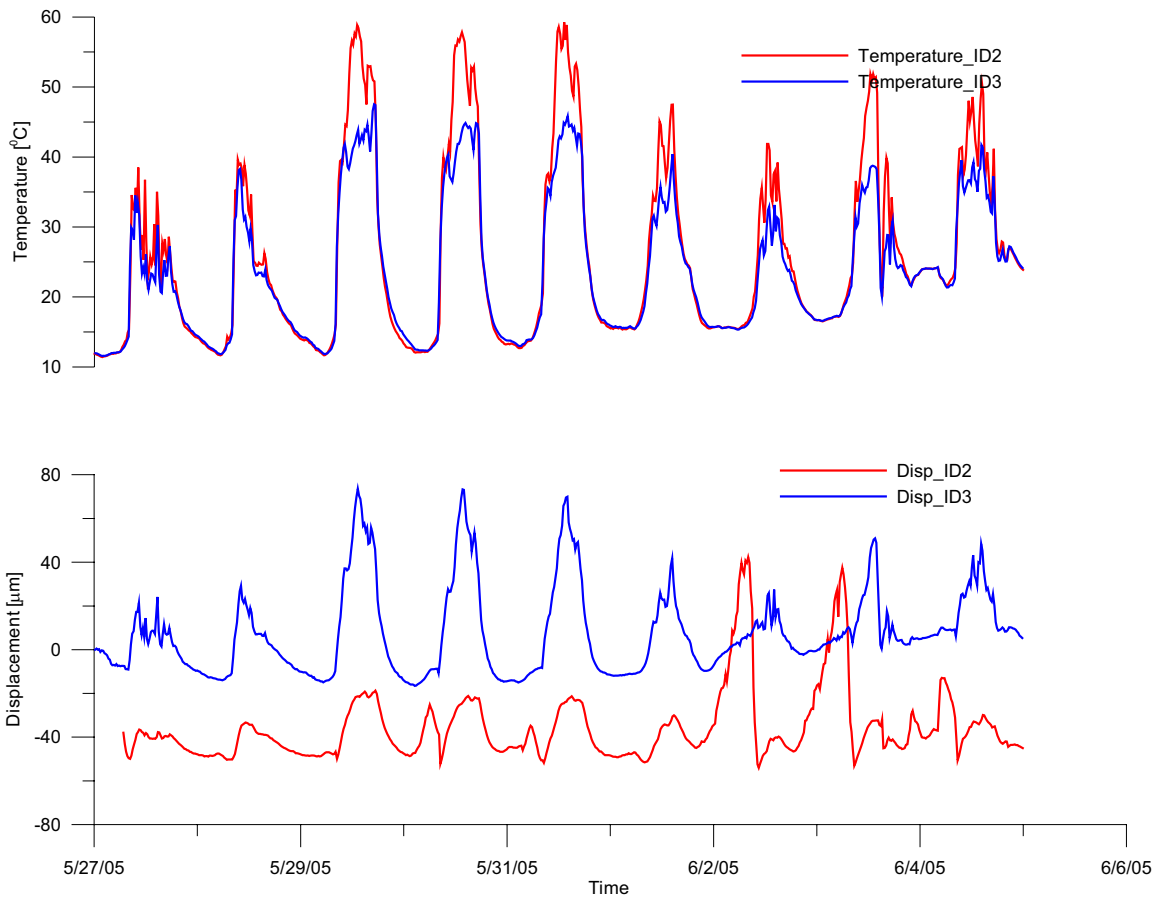


**Figure 2.18. Temperature and displacement variation measured by the wireless remote nodes on the roof**

Dominant and secondary peaks of ID2 (measured by the potentiometer on the aluminum plate) follow the daily humidity changes as well as they do the daily temperature changes as shown in Figure 2.19. Humidity dependency is apparent on June 3 and 4 at around 5:00 AM when the humidity level reached 89 %.

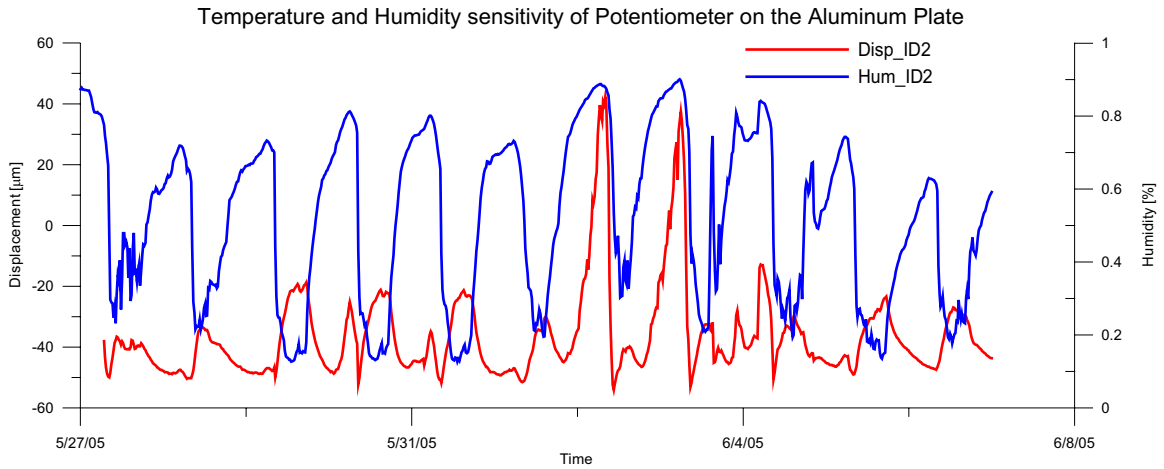


**Figure 2.19: Humidity variations with the expansion/contraction of the aluminum plate measured by mote ID2 with the potentiometer on the plate.**

The motes were located on the roof and they were separated from the base station by the wall of equipment house. Existence of numerous antennas on the roof complicated the wireless communication for the motes. Even so, the motes worked well under these conditions. During the monitoring period, no data were lost in transmission and the mesh operated without any stoppage. Based on the algorithm written for dynamic mesh networks, the motes searched continuously for the most convenient path of propagation to the base. For example, the mote denoted by ID2 used two different paths during the monitoring period. First path was the direct path from itself and the other is the path to the base through the mote denoted by ID3 and ID1. This is an outcome of dynamic process of motes listening to the environment. They find the path that will yield minimum cost of transmission and this path changes dynamically according to the environment. This feature of multi-hop operation makes the motes aware of their mesh environment and allows for quick adaptation without losing any data during transmission.

Plotted in Figure 2.20 is the battery voltage status of the motes during the roof test. The fluctuations in battery voltage indicate the sensitivity of the AA batteries to the temperature of

the environment. But the overall average voltage of the batteries does not exhibit any decline during the monitoring period.

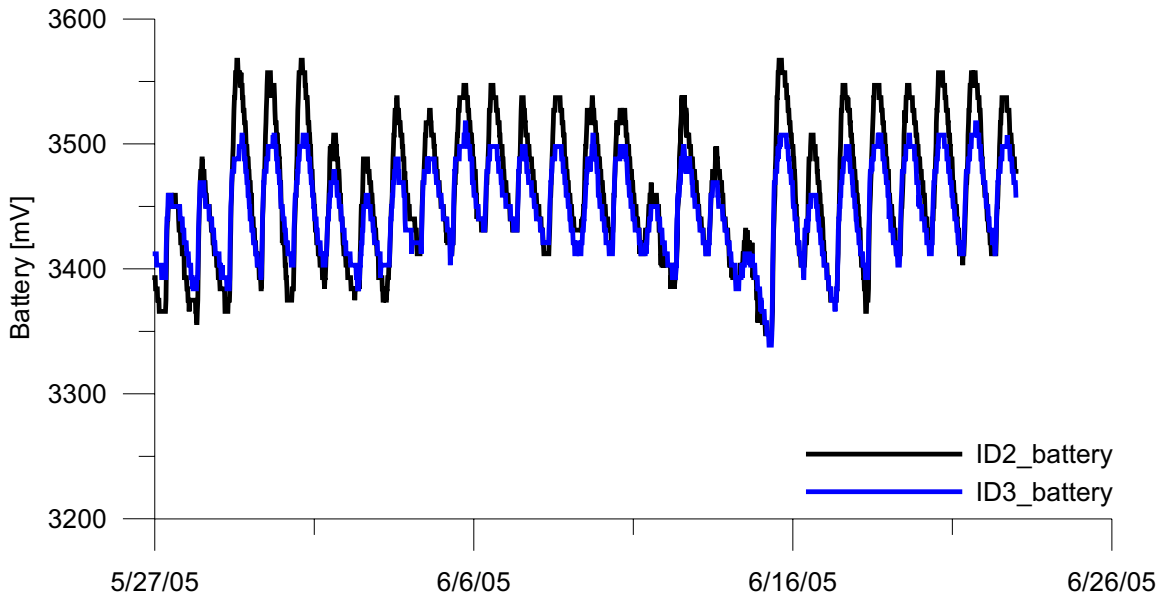


**Figure 2.20. Battery voltage fluctuations of the motes during the roof test**

## 2.6 Conclusion

Recent advances in electronics and wireless communication have accelerated development of low cost wireless sensor networks that can be employed to monitor structural health. While these wireless mesh networks are promising for wireless technology for numerous applications, much research remains to deploy a wide variety of sensor instruments and data collection protocols.

Performance of the wireless network for monitoring long-term crack response described herein is promising when compared to results obtained by a wired system at its peak development level. Crack displacements produced from environmental effects such as temperature and humidity were measured during a two-month period and the data were autonomously displayed on the Internet successfully. This is a Level-I of the Autonomous Crack Monitoring (ACM) systems, which includes installing an operable remote controlled data

acquisition system, measuring and collecting data (temperature, humidity and displacement or velocity) at regular intervals. Level-II, which requires sampling at high data rates for random events via a triggering mechanism, requires more research and development for wireless deployment.

Major issues that complicate deployment of Level-II systems include high frequency sampling, triggering, low power consumption and efficiency of data transmission, all of which can induce high levels of power consumption. Power management is crucial for low power wireless sensor nodes and uninterrupted measurements. Wireless sensor node can only be equipped with small batteries, which limit power and operational life. Thus power management and conservation gains additional importance and all external devices connected to the sensor node, such as potentiometer displacement transducer in this case, must be selected to consume the least energy possible. Sensor nodes rely on two lithium ion AA batteries and battery lifetime can vary between 27 days to a year depending on the sampling interval and the selected power management model provided by the software protocol. Higher density batteries or solar cells could be adapted to the sensor node to scavenge energy.

Two specific operational modes were designed for Level-I measurements and deployed in the field to test wireless system performance. The single-hop system was deployed in a test house to measure crack displacements. Results obtained by this system were compared to those obtained by the wired benchmark system operating at the same time. The wireless system measured inside temperature, inside humidity, battery voltage and displacement. According to the results and comparisons presented in the previous sections, the outcome is promising in terms of measurement of general trend of crack displacement from environmental factors such as temperature and humidity. Battery lifetime of this application is expected to be 27 to 47 days.

Reliable and constant Internet connection was essential in this operation to retrieve data stored in the remote nodes. This indispensable dependency sometimes resulted in poor data transmission efficiency.

The multi-hop configuration is a much more sophisticated wireless mesh network. It provides for extended spatial coverage and expands the battery lifetime to a year. Sampled data was stored in the Stargate, a more powerful and versatile base station. Since data are stored in the base, dependency on the Internet for connection communication is decreased. This application also eliminated the transmission efficiency problem in long-term measurements. The wireless system with multi-hop configuration was deployed on the roof of a downtown building where the motes were exposed to a very harsh environment in terms of wireless communication. Surveillance continued for about 1 month and the system functioned continuously without any loss of data.

Current operational protocol with its power management module prevented high frequency measurement of randomly timed events via a triggering mechanism. According to the current protocol, the motes only wake up about 1 to 2 times per second for listening to the other motes, transmitting routing information several times per second and transmitting the actual data at pre-determined intervals. Randomly timed events may be measured by triggering with a hardware interrupt. Work has already begun to create a circuit to compare a threshold voltage with the signal coming from an outboard geophone, which produces a voltage without requiring an excitation voltage. If the threshold level is exceeded, the output signal will trigger the mote to begin high frequency sampling of the potentiometer output for a fixed time interval. This application requires construction and adaptation of the analog comparameter circuit to the mote as well as modification of high frequency sampling module.

# CHAPTER 3

# 3 QUALIFICATION OF POTENTIOMETER

## 3.1 Introduction

This chapter summarizes qualification testing of string potentiometers for measuring sub micro-meter changes in crack width or displacement. Potentiometer displacement sensors do not require a warm-up interval and thus draw little power. As a result, they are attractive for wireless measurement, which is important as future autonomous crack displacement measurements almost certainly will be wireless. Potentiometers measure displacement through rotation of a spring-loaded drum. While this system is thought to have little influence on the long term, quasi-static changes in crack width, it has its own dynamic response. Thus in addition to the usual qualification tests needed to ensure low noise, drift, and hysteresis during long-term surveillance, potentiometers also required development of a qualification method to determine their dynamic response characteristics. Procedures to qualify potentiometer performance should be similar to those for the more traditional, high power drawing LVDT and eddy current sensors.

Any instrument that must endure cyclic temperature and humidity over long periods of time must maintain a constant relation between its output and the parameter being measured. Thus it cannot drift or have a large hysteretic response. Furthermore its noise level must be less

than typical variations of the parameter being measured. Before proceeding it is important to define these three parameters with respect to measurement of micro inch crack displacement.

Linearity of the sensor output with respect to cyclic variations in displacements is one of the major factors that determine the accuracy of that sensor output. The ideal transducer is one that has an output exactly proportional to the variable it measures within the sensor's quoted range. Linearity of the sensors can be defined by the hysteretic bandwidth of the displacement during the expansion-contraction cycle of the material to which sensors are attached. Hysterisis is the difference in the output of the sensor at the same temperature during one cycle. Obviously, the sensors that have smaller hysteretic bandwidths are more reliable. Importance of hysterisis is amplified by cyclic temperature environment that accompanies and induces the change in sensor displacement.

In addition to hysteresis, electronic drift is another challenge posed by the cyclic variable temperature environment. It is important that there be no to little instrument drift during crack response to cyclic environmental change over long period of time. Drift can be explained as major changes or shifts in the sensor output over time. The only change in output of with time should be caused by the displacements of the crack.

It is also important that the instrument noise level be smaller than the particular physical quantity measured by the sensors. Otherwise the actual quantity will be buried in the noise and will not be detected by the sensors.

Three different test mechanisms were established to quantify the consistency of the potentiometer response against the hysteresis, drift, noise and transient displacements. Two of the tests were designed to evaluate the response of the potentiometer to the long-term variations in temperature while measuring long term changes in displacement. The other mechanism was

designed to analyze the response of the potentiometer to transient displacements. The overall purpose of these tests was to mimic the effects of cyclic temperature variations and blast induced ground motion in a controlled test environment so that the results can be compared to the other sensors whose response has already been qualified in similar tests and field conditions.

In addition to the laboratory measurements, responses of the potentiometer and LVDT mounted across the same crack in a test house were compared. This field test was devised to assess the performance of the potentiometer in field conditions that included in blast events.

## 3.2 Experimental Setup

Two different mechanisms were designed in such a way that they can simulate the effect of field conditions that are responsible for crack width change, which in turn produce sensor displacements. Several field conditions were simulated. First, the system was subjected cyclic temperature variations, which cause crack opening and closing due to expansion and contraction of the walls. Long-term qualification tests involve sensor measurements of temperature induced cyclic expansion and contraction of two types of expandable materials. Second, the system was subjected to dynamic displacements. This transient displacement qualification test involved sensor measurements of change in separation of two aluminum blocks subjected to impact loadings.

### 3.2.1 Long-Term Qualification

#### *3.2.1.1 Test Description and Configuration*

Long-term response of the potentiometer to cyclical temperature variations was monitored on two different types of plates of known coefficient of thermal expansion and with a hollow cylinder of PE-UHMW (Polyethylene -Ultra High Molecular Weight) glued between the

sensor and its target. All sensors in these tests were subjected to temperatures that cyclically changed between 15 and 30 degrees Celsius.

Figure 3.1 shows the one of the plate tests. The potentiometer and a comparative DC 750-050 LVDT were glued close together on the surface of aluminum and PE-UHMW plates to respond to similar thermal expansion and contraction of the plates due to cyclically changing temperature. Temperature on the plate was measured with a thermocouple between the sensors. SOMAT 2100 stacks whose details will be given in the succeeding section collected sensor and thermocouple measurements. The traction on the boundaries of the plates was minimized in order to have homogeneous thermal strains on the plate surface.

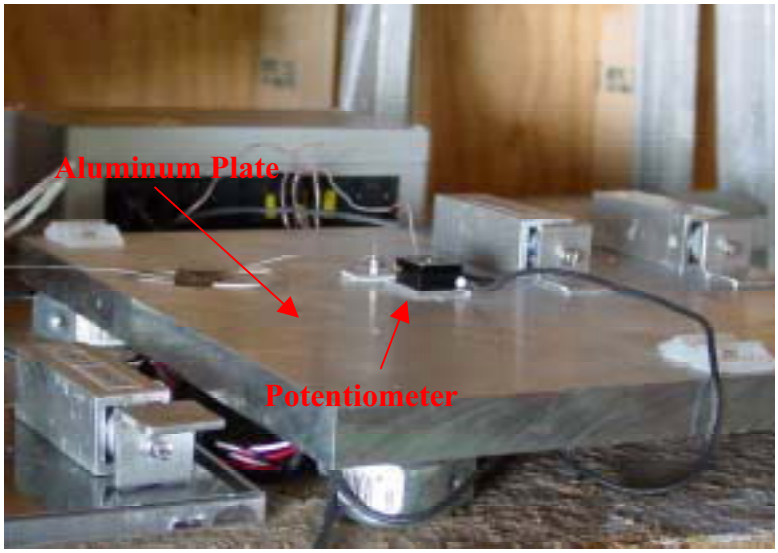


**Figure 3.1 Experimental setup from the test on the aluminum plate**

Figure 3.2 shows the configuration of another long-term test, which will be referred as "donut" test. Same types of sensors used in plate test directly measure displacements in a material of known coefficient of thermal expansion. In this case the hollow cylindrical material, which is a PE-UHMW, was glued between each of the sensors and their targets. Thermal expansion and contraction of the donut directly changed the opening and closing of the gap

between the sensor and target. Thermocouples taped on the donut measured the cyclically changed temperatures of the polyethylene.

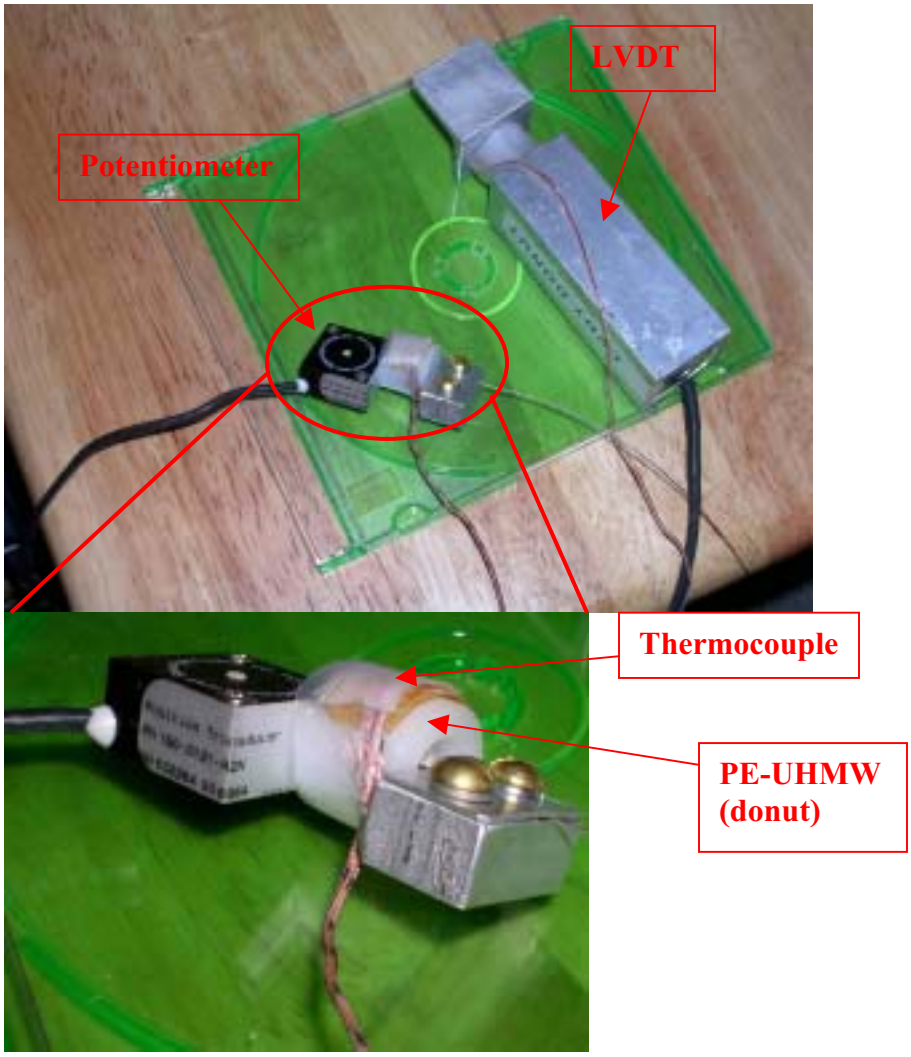


**Figure 3.2: Experimental setup from donut test**

### *3.2.1.2 Instruments and Hardware*

The potentiometer and comparative LVDT measured the expansion and contraction of the material to which they were glued during the plate test and that between the sensor body and its target during the donut test. LVDT sensors have been used in crack monitoring projects for many years and they are accepted as reliable enough to validate the output of the potentiometer.

A SpaceAgeControl type 150 potentiometer (SpaceAgeControl, 2005) was chosen for evaluation because of its small size, low energy consumption and no warm-up time, which is advantageous in the wireless sensor network projects. Figure 3.3 shows a close-up view of one of potentiometers utilized during the qualification tests. A potentiometer sensor consists of a stainless steel extension cable wound on a threaded drum that is coupled to a precision rotary sensor. Operationally, the position transducer is mounted in a fixed position and the extension cable is attached to a moving object. The axes of linear movement for the extension cable and moving object are aligned with each other.

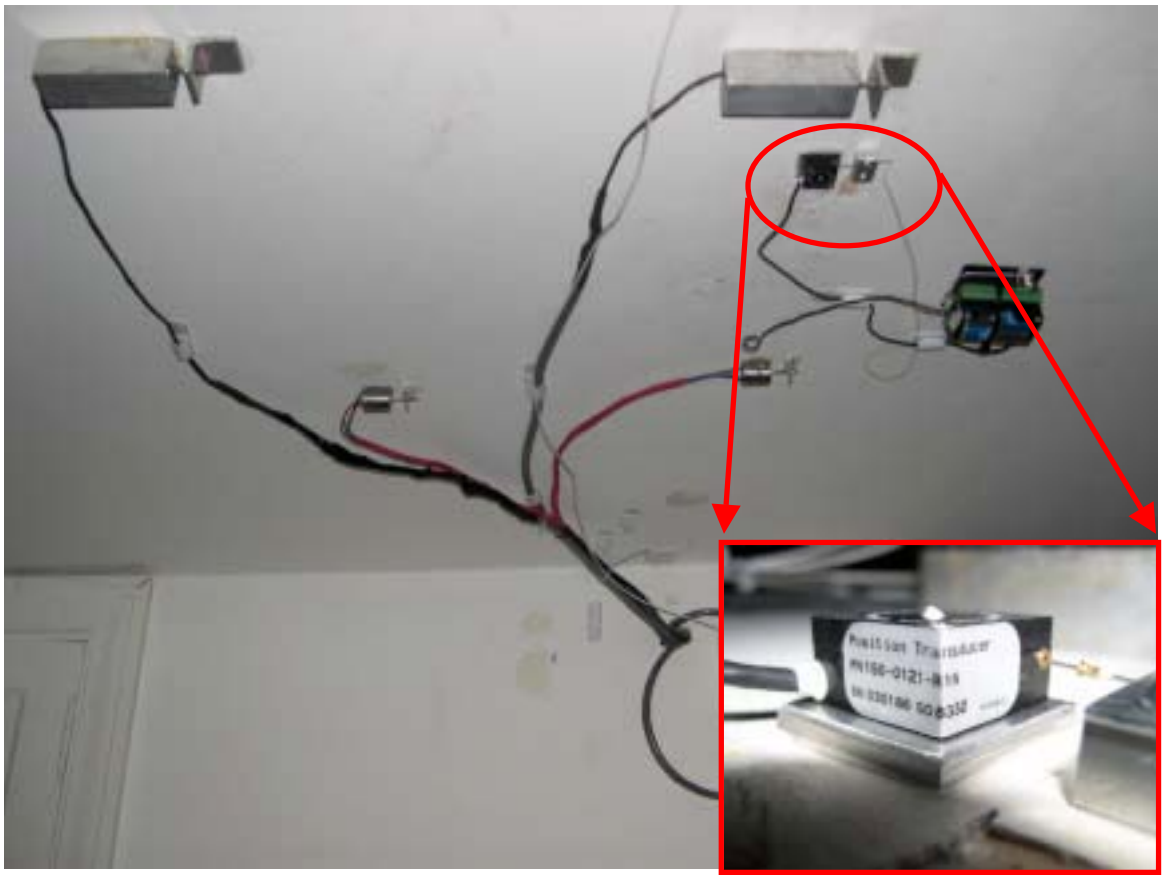

**Figure 3.3 Close-up view of the potentiometer across a crack on the ceiling of the test house in Milwaukee**

As movement occurs, the cable extends and retracts from an internal spring that maintains tension on the cable. The threaded drum rotates a precision rotary sensor that produces an

electrical output proportional to the cable travel. Potentiometers were excited with a linear 2.5 Volts supplied by the data logger whose details will be given in following sections.

For both experiments, a Macrosensors DC-750-050 “infinite resolution” LVDT served as the benchmark sensor. They were powered with a regulated, linear –15 to +15 volts DC power supply.

All sensors deployed in plate and donut test were wired to SOMAT 2100 data logger system. Resolutions of measurement systems employed in qualification testing shown in Table 3-1 were similar to the protocol of the all other ACM projects. During the monitoring period, the SOMAT would record a single point (duration of less than 1/1000$^{th}$ of a second) sample every hour. As a result single displacement measurements from these hourly readings generated long-term displacement time histories. To download the recorded data, a laptop computer with the Somat Test Control Software for Windows (WinTCS v2.0.1 software), was connected to the SOMAT and data was retrieved either daily or at an interval of several days during the monitoring period. WinTCS output files were converted to ascii text format by means of SOMAT Ease Version 3.0 in order to process the data in Matlab and Excel.

**Table 3-1: Resolution of measurement systems employed in qualification**

| Layers | Full Scale Range | Nominal Range | Actual Range | A/D steps[1] | Conversion factor (mV/υm) | Resolution |
|---|---|---|---|---|---|---|
| **LVDT_1** | -10 to 10 V | 1.25 mm | -0.5 to 0.5 V | 0.244 mV/step | 7.874 | 0.031 (μm) |
| **LVDT_2** | -10 to 10 V | 1.25 mm | -0.75 to 0.75 V | 0.366 mV/step | 7.874 | 0.046 (μm) |
| **LVDT_3** | -10 to 10 V | 1.25 mm | -0.5 to 0.5 V | 0.244 mV/step | 7.874 | 0.031 (μm) |
| **Potentiometer** | 0 to 2.5 V | 38.1 mm | -12.5 to 12.5 mV | 0.0061 mV/step | 0.057 | 0.105 (μm) |

| Layers | ADC conversion (bits) | Actual Range | Resolution | Sampling rate |
|---|---|---|---|---|
| **Temperature 1** | 8 | -100 $^{o}$ –300 $^{o}$ F | 0.2$^{o}$ C | 1000 samples @ 1000 Hz |
| **Temperature 2** | 8 | -100 $^{o}$ –300 $^{o}$ F | 0.2$^{o}$ C | 1000 samples @ 1000 Hz |

[1]A/D steps = Actual Range / $2^{\text{ADC bits}}$

The actual range of the sensors was set to a certain fraction of the output that can be read off the sensor in order to maintain an appropriate resolution. The resolution of a sensor is directly a function of this range divided by the number of A/D steps, assuming that the sensor response is linear within the full output range. The number of bits provided by the SOMAT stacks for all displacement sensors and thermocouples are 12 and 8 respectively. Displacement resolution is 0.1 μm (3.9 μin), which is acceptable as determined from past experience. (Dowding and Siebert, 2000)

Thermocouple sensors were employed to measure the temperature of the material subjected to expansion and contraction cycles during plate and donut tests. Thermocouple voltage signal is converted to logger format in a 2100-compatible SOMAT Multiplexer. As shown in Table 3-1, the resolution of those sensors is 0.2$^{o}$C, which is sufficient enough to capture the fluctuations of the temperature.

### 3.2.2 Transient Response

#### *3.2.2.1 Test Description and Configuration*

Vibration induced transient crack opening and closing was simulated by applying impact loads on the top of aluminum two blocks shown in Figure 3.4 that sandwich thin rubber sheet. Concern about the effect of vibration of the string cable on the potentiometer measurement lead to development of this device, which was subsequently employed to compare responses of LVDT and eddy current devices as well.

Figure 3.4 shows the test configuration to compare potentiometer and eddy current sensor response. The same test procedure was repeated with eddy current sensor and potentiometer sensor couples as shown in Figure 3.5. In each test both sensor bodies were glued on the bottom plate at an equal distance from the centerline of the block whose displacements were restricted in the horizontal and vertical directions. Sensor targets were glued on the upper plate that should ideally move only in vertical direction. A thin rubber sheet was placed in between the aluminum blocks. Small dynamic vertical displacements of the upper block relative to the lower were produced by dropping a small weight on the upper block. Therefore the drop weight mechanism as shown in Figure 3.4 was designed not only to have an adjustable drop height of the weight but also to allow loading at the center of the top face of the upper block. A weight of 0.1 kg (0.22 lbs) was dropped through the pipe at various heights to generate impact loading in the upper block. Although uniform displacements of the upper block was anticipated, either lack of horizontal support or difficulty of aligning the load with the center of gravity of the upper block caused a slight non-uniform displacement at the face of upper block. This slight deviation affected the magnitudes of the displacements measured by the sensors and caused an unknown variation of sensor outputs.

**Figure 3.4: A test mechanism to measure the transient response with LVDT and potentiometer sensors**

**Figure 3.5: Eddy current sensor-potentiometer (on the left) and LVDT-potentiometer (on the right) attached on the dynamic test setup**

In addition to the laboratory experiments, two potentiometer sensors were integrated with an ongoing project in a test house in Milwaukee to compare laboratory and field

performance. As it is shown in Figure 3.6, the potentiometer sensors are next to a LVDT sensor across the same ceiling crack. This house was subjected to ground vibrations from blasting in an adjacent quarry. The purpose of these measurements is to compare displacements measured by the potentiometer and the benchmark LVDT sensor to the same dynamic crack responses.

**Figure 3.6: Potentiometer and LVDT glued on the ceiling crack of the test house in Milwaukee**

*3.2.2.2 Instruments and Hardware*

An EDAQ Data Acquisition System polled all the sensors and stored and transmitted data when it was called. The EDAQ was configured to record sensor output continuously during the impact loadings by a protocol whose details are shown very briefly in Table 3-2. Voltage outputs from the sensors were automatically converted to the displacement units in this protocol. EDAQ analog channels provide 16 bit A/D conversion steps, which results in greater resolution than that of SOMAT 2100 used in plate and donut tests.

**Table 3-2: Configuration of the EDAQ measurement system employed for dynamic qualification**

| Channel Type | Sampling Rate [hZ] | Output Range [mV] | Resolution [mV] (Range/$2^{16}$) | Conversion factor (mV/υm) |
|---|---|---|---|---|
| **LVDT** | 1000 | -1,000 to 1,000 | 0.03 | 7.874 |
| **Potentiometer-I** | 1000 | -1,000 to 1,000 | 0.03 | 0.68 |
| **Potentiometer-II** | 1000 | -1,000 to 1,000 | 0.03 | 0.69 |
| **Eddy Current Sensor** | 1000 | 0 to 5,000 | 0.076 | Determined by a polynomial. |

A DC750-050 LVDT and a Kaman SMU-9000 SU (eddy current) sensor were also employed in the transient testing protocol. The Kaman gauge senses the changes in the magnetic field induced by changes in the distance between the sensor and the target. Eddy current sensors have been utilized in crack monitoring projects for years and are accepted to be the most reliable and sensitive sensor. The operational principal of the LVDT has been described in earlier sections.

All the sensors were connected to EDAQ but powered by a linear external power supply. The excitation range for the sensors was –15V to 15VDC for the LVDT and potentiometer and 0-15VDC for the eddy current sensor. Implications of the higher excitation voltages employed for the potentiometer with EDAQ than with the wireless data acquisition system will be discussed in the following chapter.

## 3.3 Interpretation of Data

### 3.3.1 Long-Term Test

Data retrieved from SOMAT 2100 data acquisition system was converted to ASCII text format with available versions of Ease or Infield software so that Excel and Matlab could be

employed to process the output files. This file contains the displacement and temperature sensor data in volts. The procedure can simply be explained in steps as follows:

- Calculate the average of 1000 data sampled at the end of each hour to represent the hourly data,
- Convert the electrical units to displacement with the conversion factors given in Table 3-2,
- Calculate the displacements relative to the initial position of the sensors
- Calculate the theoretical displacements by using the coefficient of thermal expansion of the material on which the sensor were glued,
- Generate the necessary plots to analyze the behavior of the potentiometer and compare it to the benchmark sensor

In the following sections, response of the potentiometer will be discussed in detail by presenting comparative and trend plots along with some statistical measures.

#### *3.3.1.1 Sensor Displacement and Temperature Variations with time*

Figure 3.7 shows the measured displacements and temperature variations during the two plate and donut tests. As it can be seen from those trend figures, cyclic temperature variations causes the plates and donut expand and contract. Temperature varied from 15 to 32 and 10 to 30 degrees of Celsius during the plate and donut tests respectively. However the donut that was glued in between LVDT sensor body and its target was subjected to temperatures approximately 5 degrees of Celsius higher than the potentiometer donut. The heat generated by the LVDT coil and absorption of this heat by the donut might explain this constant temperature difference. It is thought that heat generated by LVDT during the plate tests dissipated more quickly in the plate. On the other hand uneven dissipation of heat under the portion of the plate where the sensors

were glued might have caused a temperature gradient, which would induce non-homogenous thermal strains. This factor should be considered when comparing the outputs of the two sensors caused by temperature changes to base plates. During all of the tests the displacements measured by the potentiometer closely followed the temperature fluctuations, which should justify the robustness of the sensor and sensitivity of the sensor to temperature variations in long-term.

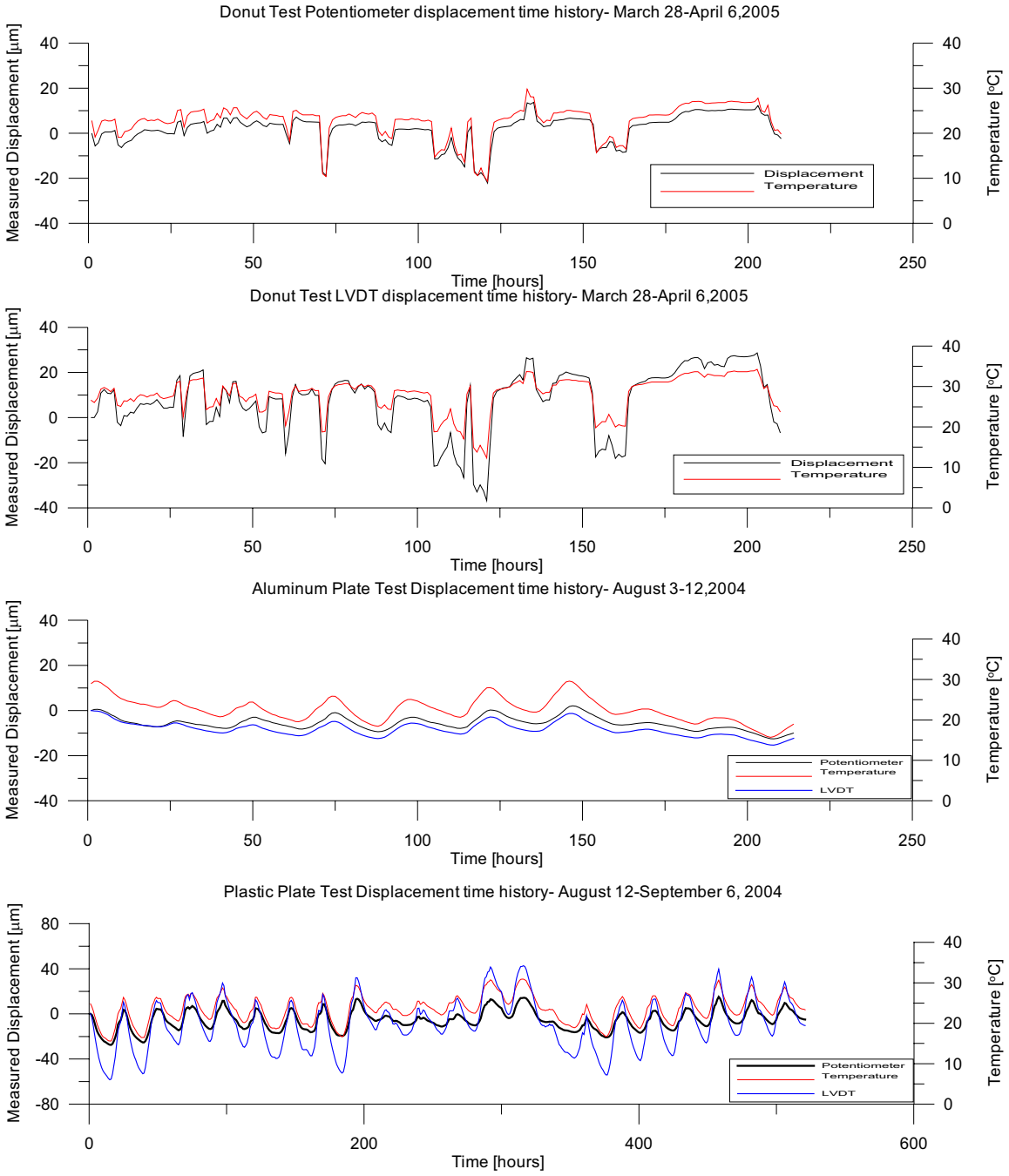


**Figure 3.7: Sensor displacements with temperature variation during the plate and donut tests**

### *3.3.1.2 Comparison of sensor response with theoretical displacement*

Plates and donuts used in the long-term tests were subjected to cyclic expansion/contraction that resulted from temperature variations in the test environment. Magnitude of expansion or contraction depends on the temperature changes, coefficient of

thermal expansion as well as the length of the material between sensor and its target. Thermal strain in a homogenous initially unstressed material with minimized body forces can be assumed to be uniform and given by Equation 1.

$$\Delta L/L = \alpha * \Delta T \qquad (1)$$

where $\alpha$ is the linear thermal expansion coefficient and $\Delta T$ is the temperature change. Thermal expansion coefficient of plastic donut and plate used in the tests are 198 μm/m/$^{o}$C (110 μin/in/$^{0}$F) and that of aluminum is 24 μm/m/$^{o}$C (13 μin/in/$^{0}$F).

As seen from Equation (1), displacement is also a function of the length, which might pose a challenge in the plate tests since the point of fixity of the sensor on the plates cannot be determined accurately. See Petrina (2004) for a detailed discussion of the comparison of full and partial gluing as well as "hot glue" vs epoxy. In the scope of this study, this length will be simply assumed to be the gap between the sensor body and its target. This fixity problem was eliminated during the donut test since the expandable material was placed between the body and the target so that the sensors could directly measure the changes in the length of that material.

Figure 3.8 shows the relationship between theoretical displacements and the displacements measured by the potentiometer, which correspond to the expansion and contraction of the plates and the donut. It is readily seen from the figures that the displacement measured on the aluminum plate (middle) is much less than those measured on the plastic plate (bottom) and the donut (top) as was expected because of its smaller thermal expansion coefficient, $\alpha$. The range of the displacements with respect to the initial position of the sensor is 2 to –12 μm (79 to –472 μin) during the aluminum plate test whereas it is 15 to –27 μm (590 to –1063 μin) during the plastic plate tests and -22 to 13 μm (-866 to 512 μin) in the donut test.

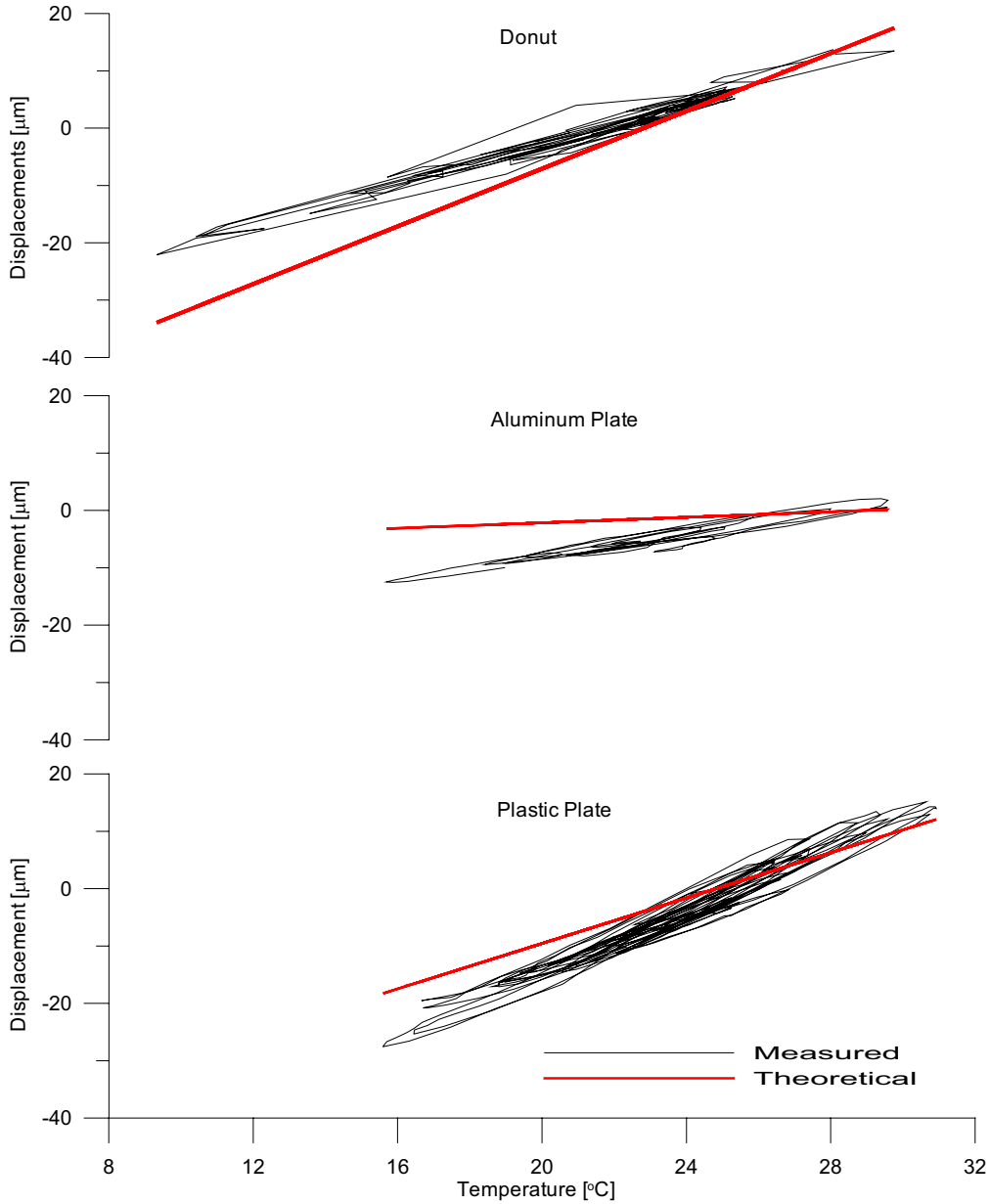


**Figure 3.8: Comparison of measured and calculated potentiometer sensor displacements induced by cyclically varying temperatures**

The best relationship between measured and theoretical displacements should ideally be a linear relationship. But there are various factors that might cause the measured displacements deflect away from the theoretical displacements. Most important of those is the uncertainty of the fixed length on the plates, L, which must be assumed in Equation 1. Other factors that can affect the mismatch might be the accuracy of the sensor or the non-uniform strains on the plate

or donut. In order to assess the accuracy of the potentiometer, the displacements measured by the potentiometer will be compared to those measured simultaneously by LVDT in the following section.

#### *3.3.1.3 Comparison of performance of Potentiometer to LVDT in the plate and donut tests*

Figure 3.9 provides a comparison between potentiometer and LVDT during the plate and donut tests. Except for the aluminum plate test, the displacements detected by the potentiometer are apparently smaller than the displacements measured by LVDT. Hysteretic loops for the LVDT are smaller than for the potentiometer.

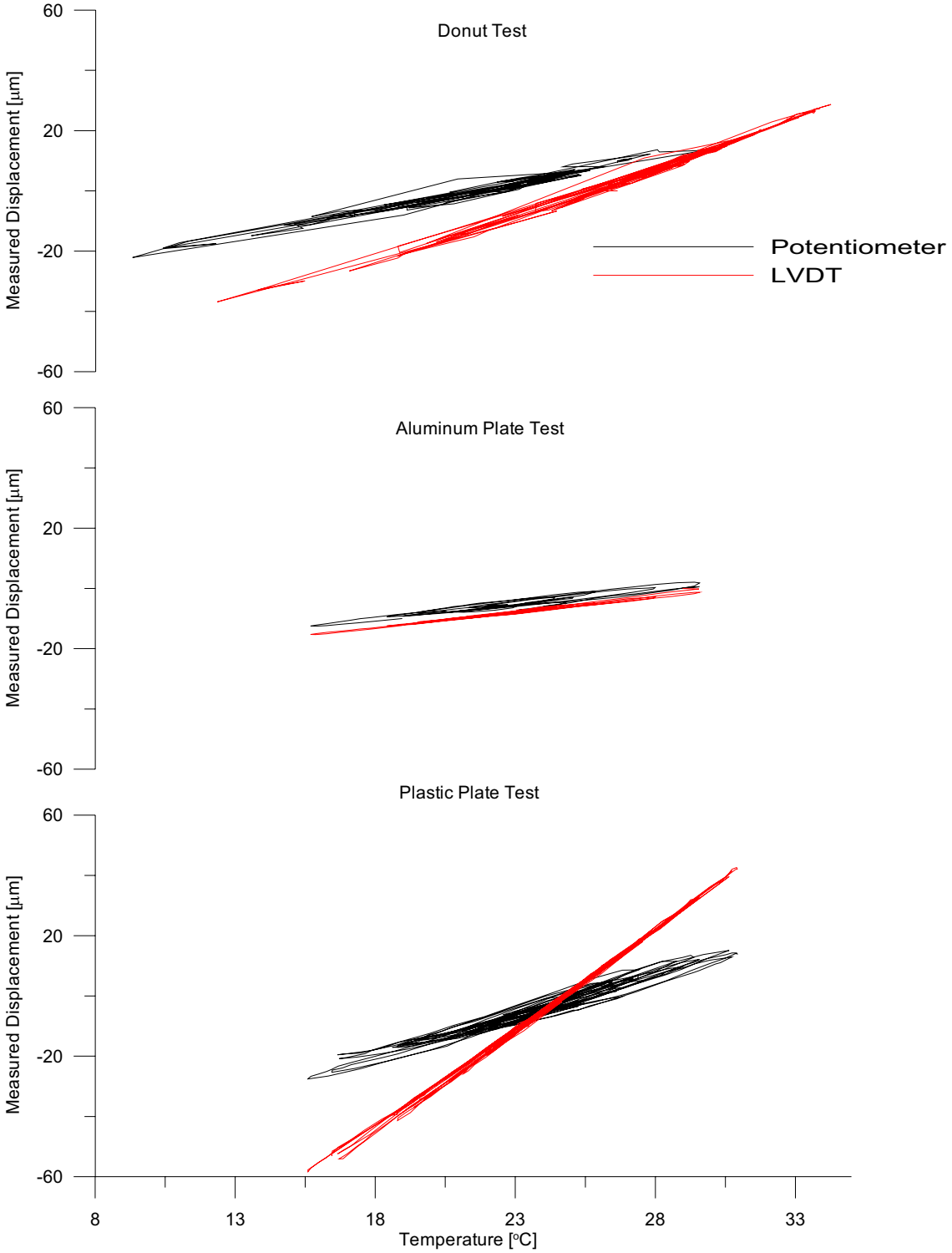


**Figure 3.9: Comparison of LVDT and potentiometer displacements induced by cyclically varying temperatures**

Hysteretic bandwidth is a function of the accuracy of the sensors as well as how the plate or donut material behaves linearly with respect to cyclic temperature variations. A statistical measure of the goodness of the data is defined by the following variables in Table 3-3: $\sigma_1$ is equal to the residual mean over the difference between the two extreme values of the measured cumulative displacements, whereas $\sigma_2$ is equal to the standard deviation of the measured cumulative displacements (with respect to the regression line), divided by the difference between the two extreme values of the measured cumulative displacements. R is the regression coefficient. These statistical measures are defined graphically in Figure 3.10.

$$\sigma_1 = [\text{Mean of Residuals}]/[\Delta H] \qquad (2)$$

$$\sigma_2 = [\text{Standard Deviation of the Residuals}]/[\Delta H] \qquad (3)$$

**Table 3-3: Some statistical measures of plate and donut tests**

| Test Description | Test Duration | LVDT | | | POTENTIOMETER | | |
|---|---|---|---|---|---|---|---|
| | | $\sigma_1$ | $\sigma_2$ | $R^2$ | $\sigma_1$ | $\sigma_2$ | $R^2$ |
| Aluminum plate | 8/03/04-8/12/2004 | 0.023 | 0.015 | 0.989 | 0.065 | 0.051 | 0.908 |
| Plastic plate | 8/14/04-9/6/2004 | 0.008 | 0.006 | 0.998 | 0.034 | 0.025 | 0.962 |
| Donut Test | 3/28/05-4/6/2005 | 0.014 | 0.012 | 0.991 | 0.023 | 0.019 | 0.973 |

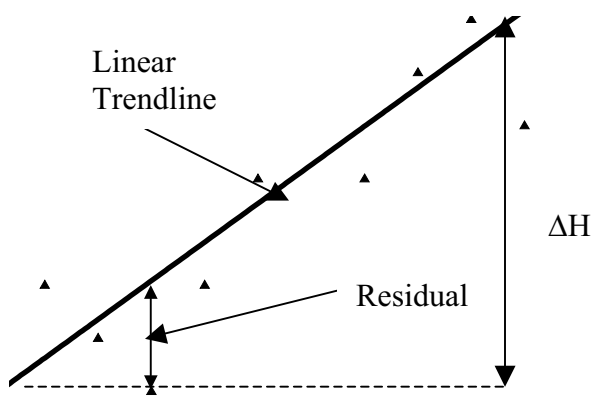


**Figure 3.10: Residual, largest cumulative displacements on a sketch**

Comparison of donut response with the plastic and aluminum plate responses for each sensor is shown in Table 3-3. For the aluminum and plastic plate test comparison (top and second row in Table 3-3) both $\sigma_1$ and $\sigma_2$ are larger for the aluminum plate. In other words the aluminum plate data are more spread out around their trend line per unit of measured cumulative displacement than are the plastic plate, which is obvious from Figure 3.8. On the other hand, the donut test, which most precisely controls L, shows lower $\sigma$'s than the aluminum plate tests. Scatter coefficients, $\sigma_1$ and $\sigma_2$, are smallest for the potentiometer from donut test but not for the LVDT. In terms of sensor-to-sensor comparison, those coefficients, which are measures of hysterisis and goodness of the data around the trend-line, are always greater for the potentiometer than the LVDT.

In addition to the different hysteretic behavior of the sensors, the magnitudes of the displacements also differ. Considering that average material temperatures are greater around LVDT due to the heat generation by LVDT, as discussed in the previous sections, displacements were normalized by temperature variations in order to compare the sensor outputs. This normalization procedure will be also helpful when comparing the response of the potentiometer to LVDT in the donut test since temperatures, as shown in Figure 3.7, are different during the entire test due to excess heat generated by LVDT. The differences between consecutive sensor readings were divided by the corresponding relative temperature readings when temperature changes were greater than 0.5 $^{o}$C. Setting a threshold temperature difference eliminates small, irregular responses of the sensors. The summary of the results is shown in Table 3-4.

**Table 3-4: Normalized displacements of the sensors from plate and donut tests**

| | Aluminum Plate [μm/°C] | Plastic Plate [μm/°C] | Donut Test [μm/°C] |
|---|---|---|---|
| **Potentiometer Expansion/Contraction** | 0.98/-1.03 | 2.62/-2.66 | 1.56/-1.64 |
| **LVDT Expansion/Contraction** | 1.00/-1.00 | 6.69/-6.54 | 3.04/-2.86 |

The potentiometer is less sensitive per unit temperature change than the LVDT for the plastic plate and donut tests. Similar response of the two sensors during the aluminum plate tests might just be a coincidence as a combination of different factors affecting the measurements such as non-uniform strains under the sensors caused by temperature gradient, uncertainty of the fixed length of the plate under the sensors etc. For the plastic plate and donut tests, the potentiometer measured approximately half the displacements of the LVDT per unit temperature changes.

The dynamic range of the potentiometer was set approximately to be 0.4 mm (0.016 in) of the string cable with an off-set of roughly 1 mm (0.039 in) away from the sensor body. Non-linearity of the response and cable itself at this working range, as shown in Figure 3.11, more likely caused the potentiometer to detect the displacements inaccurately. As discussed in the previous sections, resolution requirements govern the working range, which is denoted by (b) in the sketch on the right in Figure 3.11. The smaller the working range, the greater is the resolution. Range (b) is the maximum available range that meets resolution of typical daily crack displacements. So this range cannot be extended to capture sensor output in its more linear ranges. But if this working range was shifted to the region where sensor output is more linear by increasing the offset (denoted by range (a)), this problem could have been eliminated partly. However, the default offset is the maximum available that could be utilized, and inducing an

additional offset for the sensor caused other problems when the potentiometer is tested with the wireless data acquisition system.

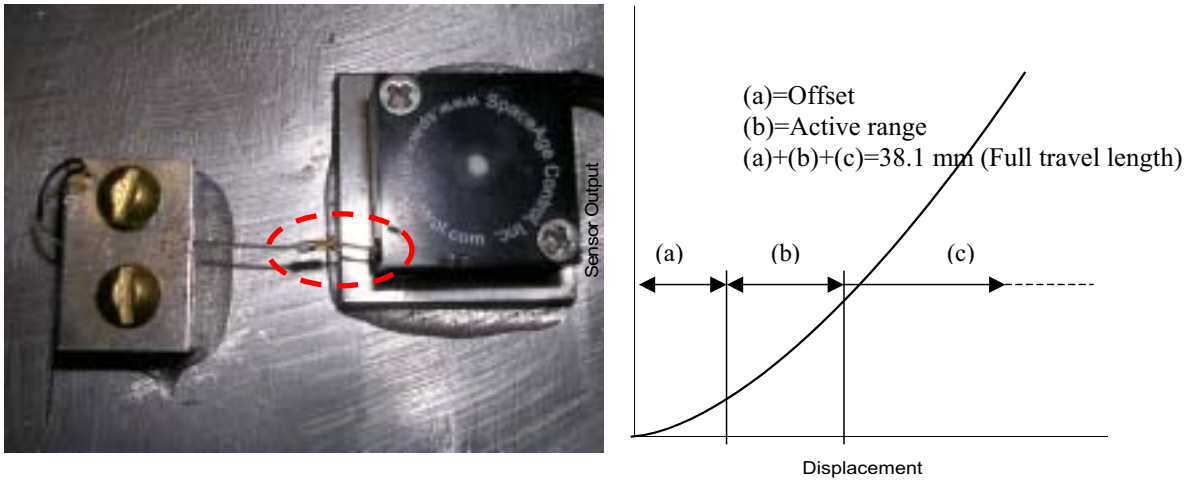


**Figure 3.11: A potentiometer displacement sensor used in qualification tests showing the irregularities in the cable**

### *3.3.1.4 Discussion of the results*

*Cable Tension on Application*

Non-contact sensing devices such as ultrasonic, radar or LVDT and eddy current proximity sensors do not mechanically affect the application. However potentiometer cable tension imparts a load on the application. Magnitude of tension varies between 0.3-0.5 and 1.0-1.2 N for low and high-tension potentiometers respectively. But only creep of the material under the tension of the cable might affect the long-term measurements of thermal strain. However, when yield strength of the PE-UHMW (20-25 Mpa) is compared to the stress imparted by the tension in the cable on a circular surface of 15 $mm^2$ (0.023 sq.in) (about 1 N/ 15 $mm^2$ = 0.07 Mpa), this effect can be assumed to be negligible.

*Noise Level*

Noisy output is one of the major challenges induced by either the sensor itself or the data acquisition system. Averaging every 1000 samples collected hourly eliminates noise effect in long-term measurements. Nevertheless, it is important to report the noise level in output in various test conditions. Figures A1-2 in Appendix-A show the noise level of the potentiometer during plate test and donut tests. Sampling method is burst type and sampling rate is 1000 HZ. The noise level is around 20 μm (787 μin) whereas the noise in LVDT output is just 0.1-0.3 μm (3.9-11.8 μin).

One of the possible sources of extremely high levels of noise might be the signal-to-noise ratio, which might be enhanced by increasing the excitation voltage. The effects of higher excitation voltages will be described in the following section where the transient response of the potentiometer is analyzed. Another reason for the high noise might be the unstable power supplied by SOMAT data acquisition system. So another power supply was used to excite the potentiometer in order to see if the problem arises from power provided by SOMAT. The results are presented in Figures A3-4 in Appendix-A. The magnitude of noise level in this case is 14-16 μm (551-630 μin), which is not significantly different than the noise measured by SOMAT power supply. Noise level obtained by the wired system (SOMAT) is also compared to that obtained by the wireless system, which will be presented in the proceeding sections.

*Relative expansion/contraction*

The effect of relative expansion and contraction of the base plate or donut with respect to the sensor materials such as the LVDT core and potentiometer string cable is demonstrated in Appendix D. As shown in Appendix D figures and tables, statistical measures of scatter in the output of the LVDT and potentiometer did not change significantly but the slope of the

hsyteresis loop deviated from the theoretical expansion/contraction line, which addresses the possible error in calculating the theoretical thermal expansion/contraction due to unknown fixity length.

### 3.3.2 Transient Response

#### *3.3.2.1 Combination of Potentiometer and the other sensors*

Figure 3.12 compares time histories of responses of potentiometer and eddy current sensors to dynamic drop ball impacts on the device shown in Figure 3.4. Spikes represent the each impact, with the magnitude of the response being the difference between the top of the spike and the position of the sensor at rest (middle of the thick, noise line).

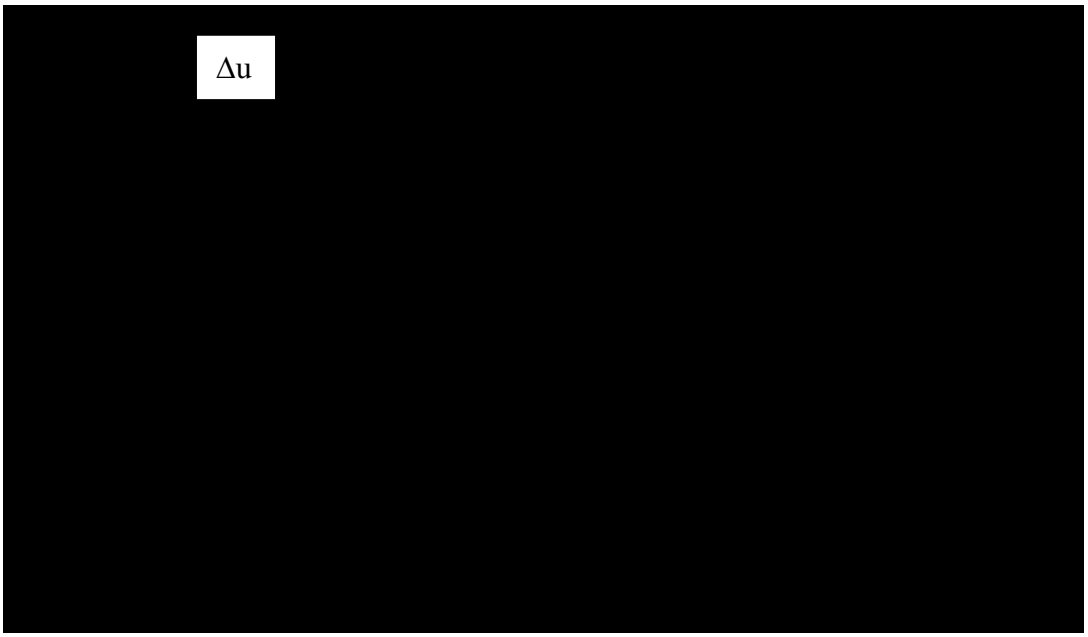


**Figure 3.12: Comparison of potentiometer and Kaman (eddy current) sensors to dynamic events produced by the same drop weight impacts**

Figure 3.13 is the comparison plots of dynamic impact displacements measured by high and low tension potentiometers compared to the benchmark LVDT and eddy current sensors. These comparisons were obtained with five pairs of sensors, where each pair responded to the

same impact to assess the relative responses of the various sensors. There is more scatter in the comparisons between potentiometer and benchmark sensors than for the comparison of the two benchmark sensors.

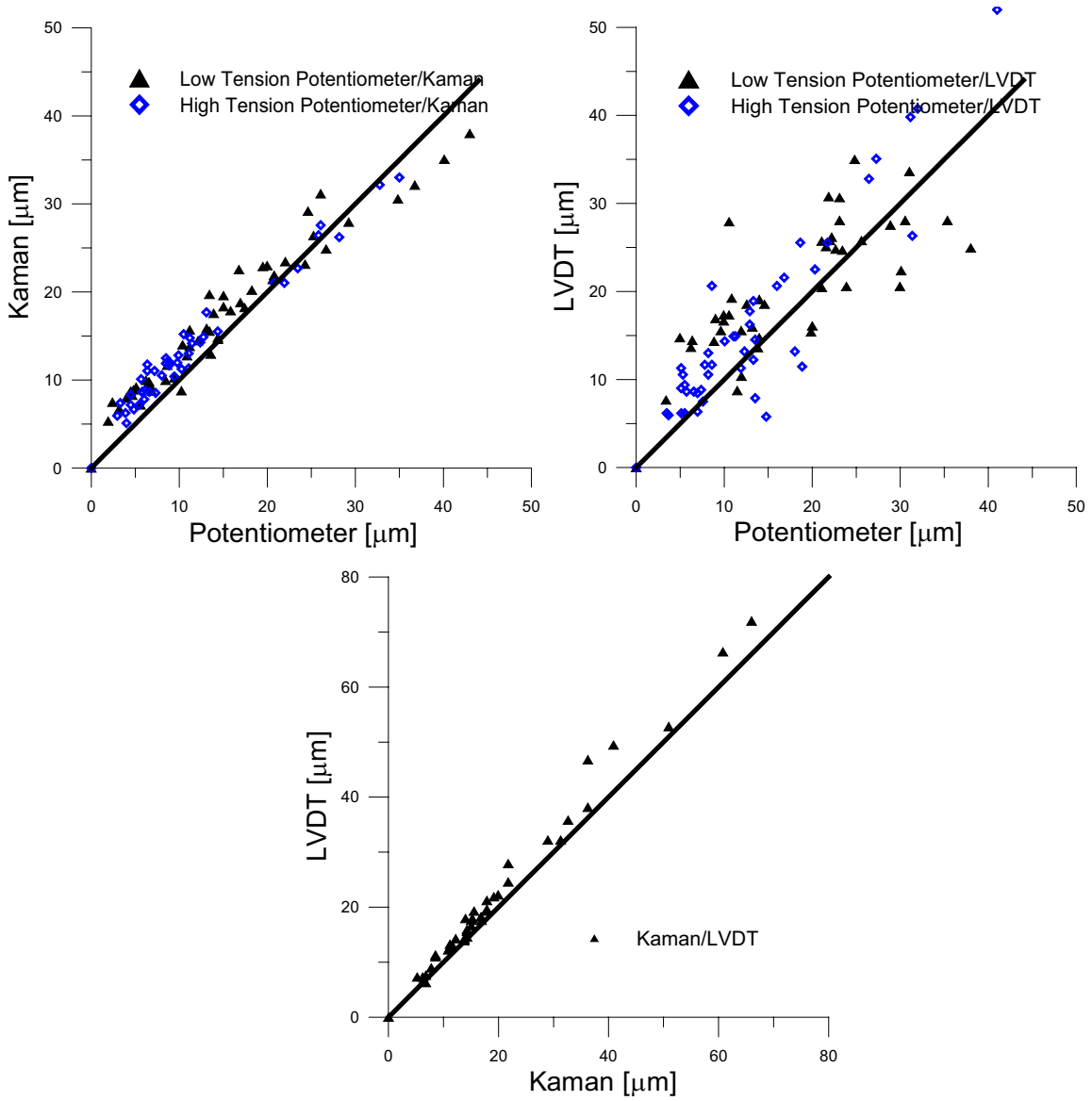


**Figure 3.13: Comparison of various sensors to the same impact produced by the laboratory device**

These dynamic displacements are large compared to blast events. There are no displacements imposed in the dynamic laboratory test that are smaller than 2 μm (79 μin). Past research indicates that crack displacements from typical blast induced ground motions range

between 2 to 12 μm (79 to 472 μin), (McKenna, 2002). The laboratory events were produced with the smallest drop weights possible. The magnitude of the impacts could not be adjusted in order to generate smaller displacements because of the high compliance of the material between the blocks. The smallest displacement that could be produced was around 2 μm (79 μin). In addition to the difficulty of generating smaller displacements, noise levels varying in between 3-5 μm (118-197 μin) obscured displacements in that range. This level of noise is significantly high and might prevent the measurements of crack displacements induced by small blast events.

As discussed in Section 3.2.2.1, the test mechanism produced displacements that varied slightly along the face of the aluminum block due to lack of horizontal restraint, eccentric loading and some irregularities of the thin rubber sheet. Considering these uncertainties inherent to this test, one-to-one comparison of sensor outputs in terms of magnitudes will not be analyzed in detail. Rather than the magnitudes, waveforms of the sensor response might make more sense for comparison purposes.

Figure 3.14 and Figure 3.15 compare the detailed time histories of the drop ball events with low and high-tension potentiometers and the Kaman eddy current sensor. As seen in these response waveforms, displacement waveforms measured by the potentiometer are identical to those measured by Kaman. It is apparent from response waveforms that neither the stiffness of the spring nor the vibrations in the string cable had any significant influence on the response of the potentiometer at the frequency of the input motion. Range of frequencies of dynamic test displacements are 10 to 100 Hz whereas those measured from blast induced ground vibrations are 10 to 30 Hz. This test was repeated with other sensor combinations such as LVDT and the two types of potentiometer and Kaman-LVDT. The results from those tests along with

frequency content and detailed time histories of the impact loading are presented in Figures B6-29 in Appendix-B.

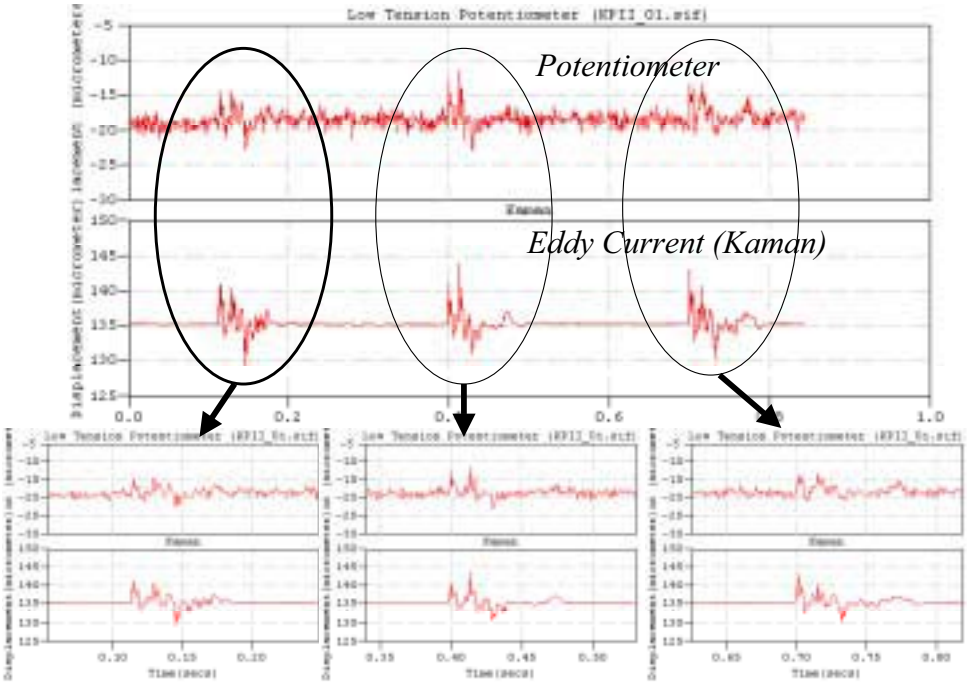


**Figure 3.14: Responses of low-tension potentiometer and eddy current sensor to the same three impacts**

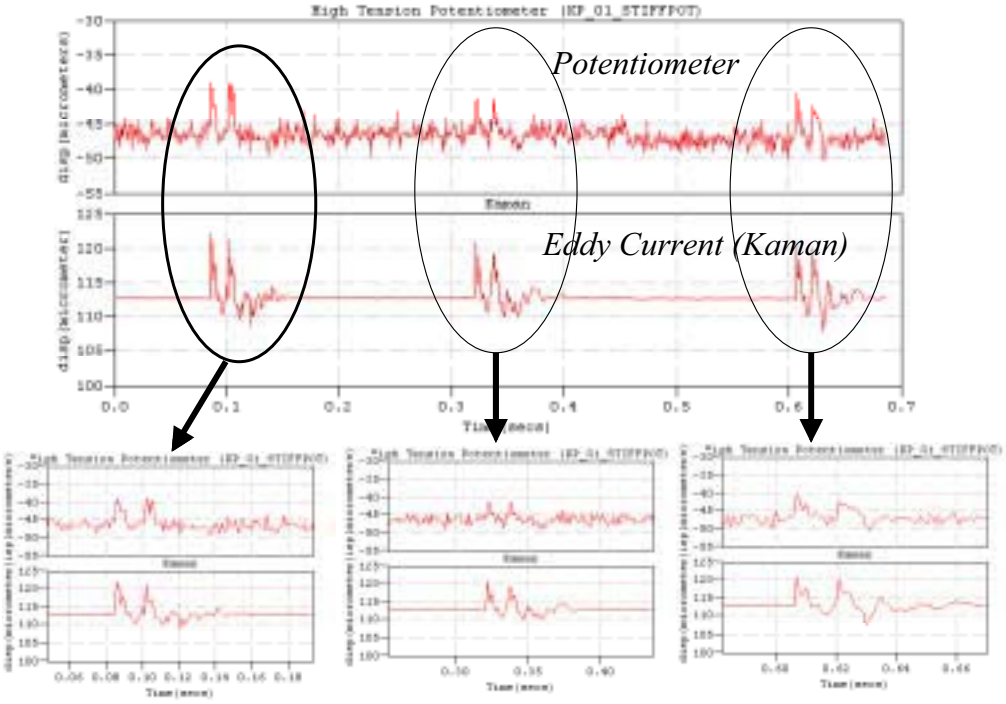


**Figure 3.15: Same comparisons as in Figure 3.14 only with high-tension potentiometer**

#### *3.3.2.2 Discussion of the results*

*Frequency Response*

Cables on these sensors have fundamental frequencies that may respond themselves. Vibrations of the string cable could produce additional response if the potentiometer were to measure a very high frequency motion. While such an additional response would be rare, it is possible. The natural frequency of the potentiometer string cable alone is found to be 414 and 585 Hz (SpaceAgeControl, 2005) for low-tension and high-tension potentiometers respectively. Since neither the dynamic test nor the real blast events involve frequencies that high, additional relative motion or vibration in the string cable is unlikely.

Another feature of the potentiometer that might affect its output due to dynamic loading is the contact force from the tension in the cable. However, the large momentum of the motion, which is proportional to the mass of the moving object (mass of the structure in the field or upper aluminum block in the dynamic test), can easily overcome the tension imparted by the cable.

Above considerations have little influence upon the dynamic response of the potentiometers, as shown by comparison with other sensors. Figure 3.16 compares the responses of the potentiometer and LVDT sensors to the same impact loading during the dynamic test. As shown, both response patterns and magnitudes of both sensors are remarkably similar except for polarity, which generates output with opposite signs. Frequency content of the responses is compared in Figure 3.16 by an FFT analysis. As shown, there are two dominant frequencies of the response; 8 and 35 Hz for both sensors.

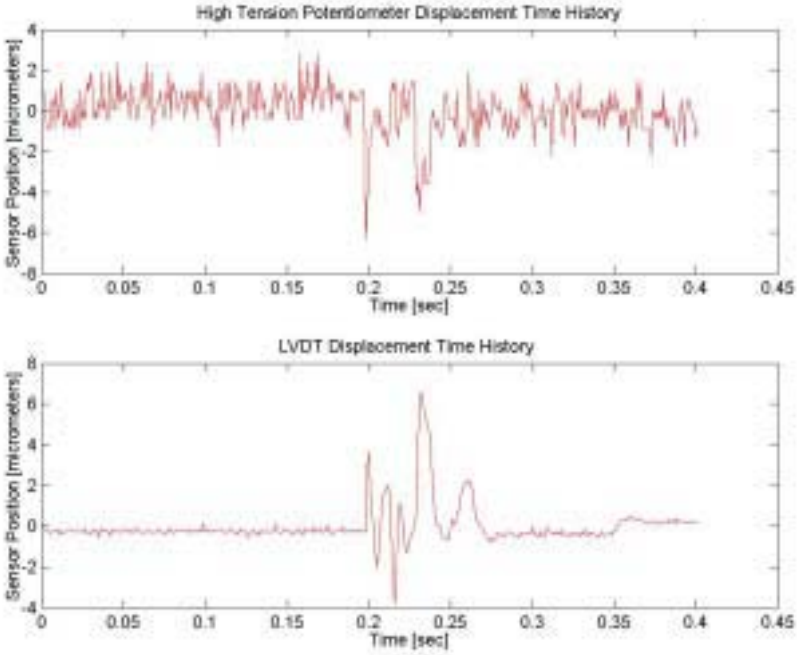


**Figure 3.16: Responses of high-tension potentiometer (top) and LVDT sensors to the same impact displacement (bottom)**

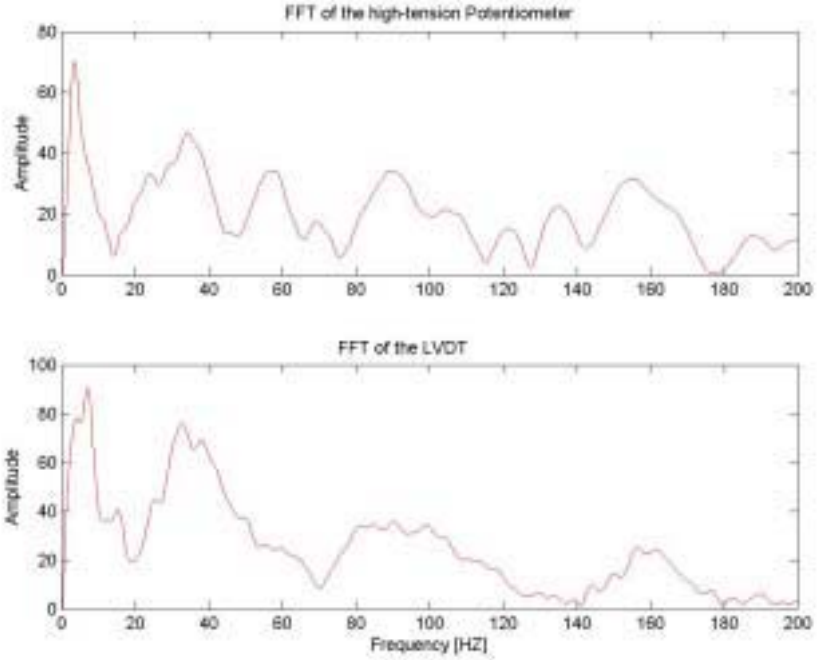


**Figure 3.17: FFT analysis of the response of the high-tension potentiometer (top) and LVDT (bottom) to impact loading shown in the previous figure.**

*Noise Level*

In addition to the frequency response effects above discussed, noisy output of the potentiometer might be another source of error that would obscure response to blast events. Such hidden-response occurred from March to June 2005, while the potentiometers were installed in the test house. Figure 3.18 shows the potentiometer and LVDT displacement time histories recorded during one of those blast events. Crack displacement induced by those ground motions were not captured by the potentiometers due to the noise which obscured the potentiometer output. However the LVDT connected to the same data acquisition system in the house measured 2-10 μm (79-394 μin) of crack displacements.

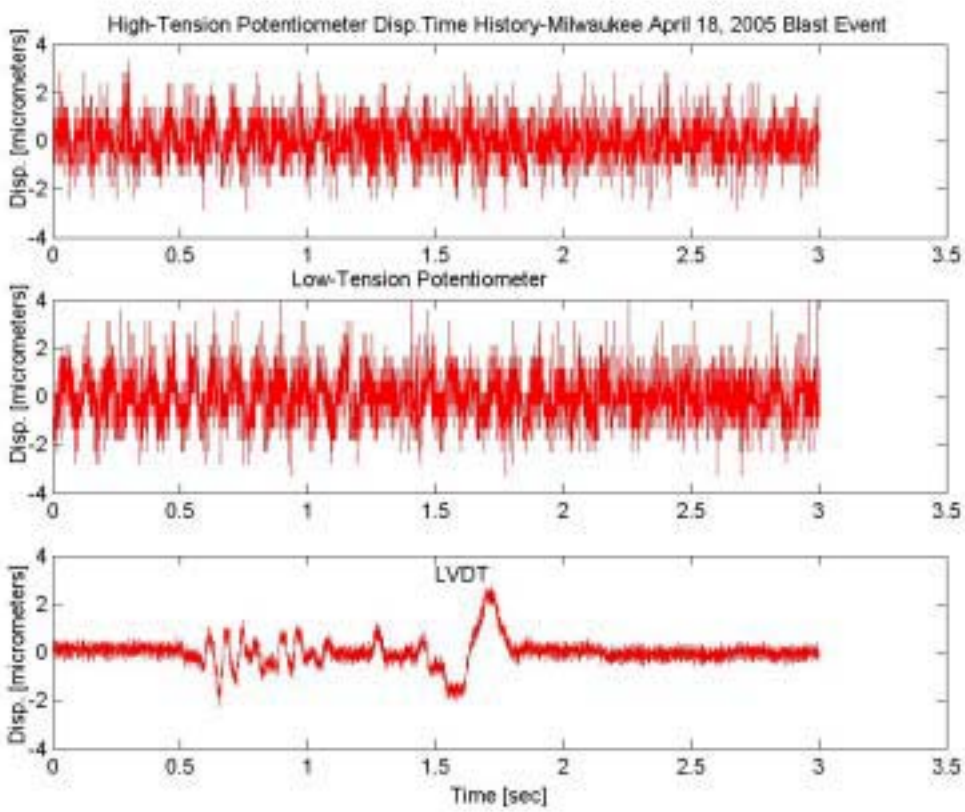


**Figure 3.18: Potentiometers and LVDT displacement time history recorded during a blast event at the Milwaukee test house**

Potentiometer peak-to-peak noise during the dynamic laboratory testing was 3-5 μm (118-197 μin), whereas the noise in the other sensor outputs was always smaller than 1 micrometer. Figures B1-5 in Appendix-B compare the output of the tests with potentiometer and LVDT or eddy current sensor pairs. The noise level in the potentiometer is apparent in each test and obscures the smaller displacements.

This laboratory test provides ideal conditions for the potentiometer output acquired by a wired system in terms of the noise level. Shorter wires relative to the field conditions and higher excitation voltage are the two major factors that affect the noise level. Different excitation voltages with varying sampling rates were set up in order to analyze the effect of those factors in the noise level of the potentiometer. In laboratory tests, the excitation voltage was 2.5 and 30 Volts whereas only 30 Volts excitation was used in the field. The results are shown in Figures A1-8 in Appendix-A and summarized in Table 3-5. Excitation of the potentiometer with 2.5 volts yields 20 micrometers of peak-to-peak noise, which proves that the lower excitation voltage deteriorates signal-to-noise ratio and thus increases the noise level. However, it should be noted that ground loops and longer wires associated with the field test might have also contributed to the noise level.

Results from the field test (bottom row) show that the noise is about 4-6 μm (157-236 μin). On the other hand, the noise was 3-5 μm (118-197 μin) with the same acquisition system and the excitation voltage in the laboratory, which shows that short wires reduce the noise, but only slightly. Sampling rate does not have any significant effect on the noise level of the potentiometer output. 10 Hz and 1000 Hz sampling rate yielded approximately same level of noise. (Figures A-5 and A-6 in Appendix-A)

**Table 3-5: Summary of the peak-to-peak noise level with varying excitation voltages, sampling rates and monitoring equipment**

| *TEST DESCRIPTION* | *PEAK-TO-PEAK NOISE LEVEL [μm]* |
|---|---|
| SOMAT/Internal Power (2.5V)/1000 HZ | 18-22 |
| SOMAT/External Power (2.5V)/1000 HZ | 14-16 |
| SOMAT/Internal Power (2.5V)/10 HZ | 18-22 |
| SOMAT/External Power (2.5V)/10 HZ | 14-16 |
| EDAQ[1]/External Power (30V)/1000 HZ | 3-5 |
| EDAQ[2]/External Power (30V)/1000 HZ | 4-6 |

[1]From dynamic test output
[2]From Milwaukee test house outputs

Most importantly use of the potentiometers with the wireless system will reduce noise level since it eliminates the wires that introduce the noise to the sensor output. As shown in Figure 3.19, when output is captured with the wireless system then with the wired system potentiometer output is far less noisy. In this comparison output was measured at a sample rate of 10 samples per second, which is the highest frequency that the wireless system can measure at present.

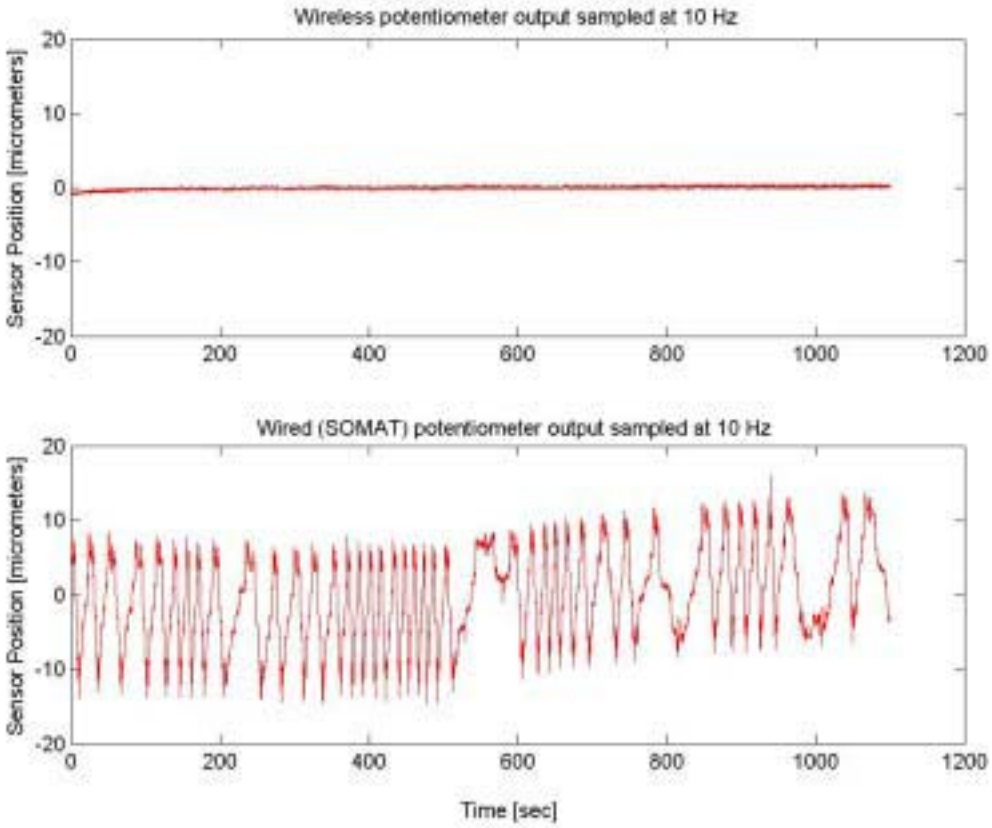


**Figure 3.19: Potentiometer output measured by wireless (top) and wired SOMAT (bottom) system at 10 Hz**

Figures C1-12 in Appendix C demonstrate the effectiveness of filtering the crack displacement time histories measured by potentiometers and LVDT. These responses are those of the same ceiling crack to blast events on 18 April and 5 May 2005. As seen in the FFTs of the potentiometer response, there is too much scatter in the frequency profile and it is impossible to differentiate the dominant frequency of the actual motion from the electrical noise in the output. LVDT response shown in Figure C5 and C11 in Appendix C indicate that the dominant frequency of the displacement is less than 10 Hz. Therefore, potentiometer response is filtered by eliminating the components of the motion whose frequency higher than 50 Hz. Unfortunately the filtered response of the potentiometer output in Appendix C apparently

reveals the fact that dominant frequency of noisy output coincides with the possible dominant frequency of the actual displacements, which makes the filtering option useless.

## 3.4 Conclusion

The following observations summarize the performance of the potentiometers for measuring long-term environmental changes and transient dynamic loadings:

- Responses to long-term, cyclical changes in displacement are linear.
- Hysteresis is sufficiently small to allow tracking of changes in displacements as small as 0.1 μm (3.94 μin). Hysteretic bandwidth is approximately the same for potentiometer and LVDT in the donut test whereas LVDT hysteretic bandwidth is approximately 50 % smaller in the plate tests.
- Drift is no greater than that of the LVDT or eddy current sensors.
- Response to transient displacements greater than 2 μm (78.7 μin) at frequencies between 10 to 100 Hz in general matches that of eddy current and LVDT sensors.
- Response to transient displacements is less than that of LVDT and eddy current sensors for especially displacements smaller than 15 μm (591 μin). The average ratio of potentiometer displacement to eddy current and LVDT sensors are 0.7 at this range of displacements.
- Response to long-term changes was observed to be less than that of LVDT in the plastic plate and donut tests. The average ratio of potentiometer displacement to LVDT is measured to be 0.4 in the plastic plate test, 0.5 in the donut test, and approximately same in the aluminum plate test (refer to Table 3-4 for calculation of these ratios). The same ratios with the relative temperature corrections shown in

Appendix-D Table D- 2 are 0.4 in the plastic plate test, 0.5 in the donut test and 0.7 in the aluminum plate test.

- Potentiometer output noise is only 0.5 μm (19.7 μin) peak to peak when operated with the wireless system and some 10-15 μm (394-591 μin) peak to peak when operated as a part of the wired system at the same excitation level.

Potentiometer displacement sensors with their very low power consumption, no warm up time and excitation voltage flexibility are suitable for the wireless sensor network described in previous chapter. MDA300 sensorboard provides only 2.5, 3.3 and 5.0 volts of excitation voltage, which eliminates the usage of LVDT and eddy current sensors that have been used many years in crack monitoring. As compared to these sensors, power consumption of the potentiometer is considerably smaller and requires no warm up time, which are some crucial requirements with the wireless system relying on just two AA batteries.

# CHAPTER 4

# 4 CONCLUSION

This thesis introduces a new wireless system to measure micrometer changes in crack width. Such measurements have been conducted with a wired system for some 6 years under at Northwestern University's Infrastructure Technological Institute (ITI) under the Autonomous Crack Measurement (ACM) program. ACM systems measure crack width changes from environmental factors (long-term) such as temperature, humidity and wind effects as well those from blast induced ground vibrations (dynamic). Measurement of long-term and dynamic crack response yields a good understanding of crack response in terms of the dominant feature of the crack displacement driving force.

The wireless system is designed to execute all the tasks that the wired system was capable of doing and replace it eventually. The advantages of the wireless system, as described in the relevant chapters, are mainly low cost, quick and easy installation, adaptability to variety of applications, and most importantly avoidance of intrusive and high cost of wiring. Presently the wireless system successfully measures long-term response but requires more research and development to measure dynamic crack response.

Two different case studies performed with the wireless system are presented along with discussion and introduction of wireless communication basics. Each case study was executed with the same hardware but differently designed communication protocols. Major improvements

included increasing total battery lifetime, which is crucial for wireless system relying on just two AA batteries, and a more robust communication. The first application involved a single-hop configuration in a test house to measure long-term changes in the crack width during a period of blasting. The network consisted of one remote node (sensorboard, radio module and outboard sensor) and a base station (serial gateway, radio module and external serial communicator). This system is capable of sensing and acquiring the crack displacements at predetermined intervals with a battery lifetime of some 25 to 50 days.

The second application is a multi-hop configuration placed on a roof top to measure long-term expansion and contraction of an aluminum plate and a plastic donut. The network consisted of several remote nodes (sensorboard, radio module and outboard sensor) and a base station (stargate gateway and a radio module). This system is capable of multi-hop communication in which remote nodes can form their own coverage area and thus extend the distance of coverage. Battery lifetime is expected to be about a year with reporting intervals of 3 times per hour.

In addition to the prolonged battery lifetime, this new multi-hop software protocol (Xmesh) improves the data transmission efficiency and long-term robustness of wireless communication. The remote nodes and the base station were deployed on the roof of ITI building where they were exposed to intense microwave and electro-magnetic interference, but performed well. Two of the remote nodes with the outboard displacement transducers attached to them measured the expansion and contraction of an aluminum plate and a plastic donut as well as temperature, humidity and battery voltage. A third remote node located next to the base station measured only temperature, humidity and battery voltage.

Both field tests conducted with the wireless system proved that this new system could measure long-term crack response, which is referred as a Level-I surveillance in ACM projects. Crack response measured wirelessly was compared to that obtained by the wired system. Measurement of dynamic response, or Level-II surveillance requires more research and development. It is necessary to provide a triggering mechanism that does not consume power as well as to control the sampling frequency once the system is triggered.

This thesis also includes the analysis for qualification of the potentiometer, as an ACM displacement transducer. This sensor was chosen to be the outboard displacement sensor for the wireless sensor network due to its low power consumption (0.5 mA) and no warm up time. Qualification of the potentiometer involved a series of field and laboratory tests to analyze the potentiometer response to cyclic temperature variations (long-term) and impact loading (dynamic). Assessed were the linearity, accuracy and long-term robustness of the potentiometer. The output of the potentiometer was also compared to that of the benchmark sensors (LVDT and eddy current sensor) where simultaneously subjected to the same environment. The potentiometer, as a contact sensing device, senses slightly lower magnitude than the other benchmark sensors. In summary the following specific observations can be made at the comparative performance of the potentiometer;

- Responses to long-term, cyclical changes in displacement are linear.
- Hysteresis is sufficiently small to allow tracking of changes in displacements as small as 0.1 μm (3.94 μin). Hysteretic bandwidth is approximately the same for potentiometer and LVDT in the donut test whereas LVDT hysteretic bandwidth is approximately 50 % smaller in the plate tests.
- Drift is no greater than that of the LVDT or eddy current sensors.

- Response to transient displacements greater than 2 μm (78.7 μin) at frequencies between 10 to 100 Hz in general matches that of eddy current and LVDT sensors.
- Response to transient displacements is less than that of LVDT and eddy current sensors for especially displacements smaller than 15 μm (591 μin). The average ratio of potentiometer displacement to eddy current and LVDT sensors are 0.7 at this range of displacements.
- Response to long-term changes was observed to be less than that of LVDT in the plastic plate and donut tests. The average ratios of potentiometer displacement to LVDT are 0.4 in the plastic plate test, 0.5 in the donut test, and approximately same in the aluminum plate test (refer to Table 3-4 for calculation of these ratios). The same ratios with the relative temperature corrections shown in Appendix-D Table D- 2 are 0.4 in the plastic plate test, 0.5 in the donut test and 0.7 in the aluminum plate test.
- Potentiometer output noise is only 0.5 μm (19.7 μin) peak to peak when operated with the wireless system and some 10-15 μm (394-591 μin) peak to peak when operated as a part of the wired system at the same excitation level.

# References


Culler, D.E. (2002) "Mica: A wireless platform for deeply embedded networks." *IEEE Micro*, 22(6), p 12-24

Crossbow Technology Incorporation (2005) "Wireless Sensor Networks Getting Started Guide and http://xbow.com/"

Dowding, C.H. and Siebert D. (2000) "Control of Construction Vibrations with an Autonomous Crack Comparometer." Conference on Explosives and Blasting Technique in Munich, Germany

Glaser, S.D. (2004) "Some real world applications of wireless sensor nodes." *Proceedings of SPIE - The International Society for Optical Engineering*, 5391 344-355

Lewis P., Madden S., Gay D., Polastre J., Szewczyk R., Woo A.,Brewer E., and Culler D., (2004) "The emerging of networking abstractions and techniques in TinyOS." First Symposium on Network Systems Design and Implementation

Louis, M. (2001) "Field authentication of autonomous crack comparameter." M.S. thesis, Northwestern University, Evanston, IL

McKenna, L. (2001) "Comparison of Measured Crack Response in Diverse Structures to Dynamic Events and Weather Phenomena." M.S. thesis, Northwestern University, Evanston, IL

Petrina, M.B. (2004) "Standardization of Automated Crack Monitoring Apparatus for Long-Term Commercial Applications." M.S thesis, Northwestern University, Evanston, IL

SpaceAgeControl Inc. (2005) "http://www.spaceagecontrol.com/index.htm"

TinyOS (2005) "http://www.tinyos.net/"

## A. Appendix NOISE LEVEL IN POTENTIOMETER OUTPUT

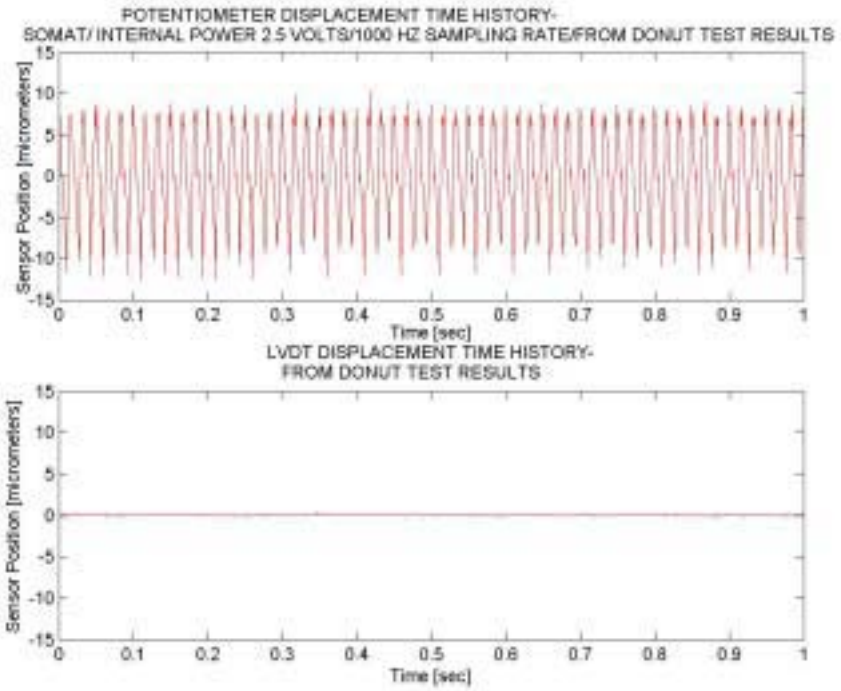


**Figure A- 1 Noise level in the potentiometer and LVDT output during the donut tests**

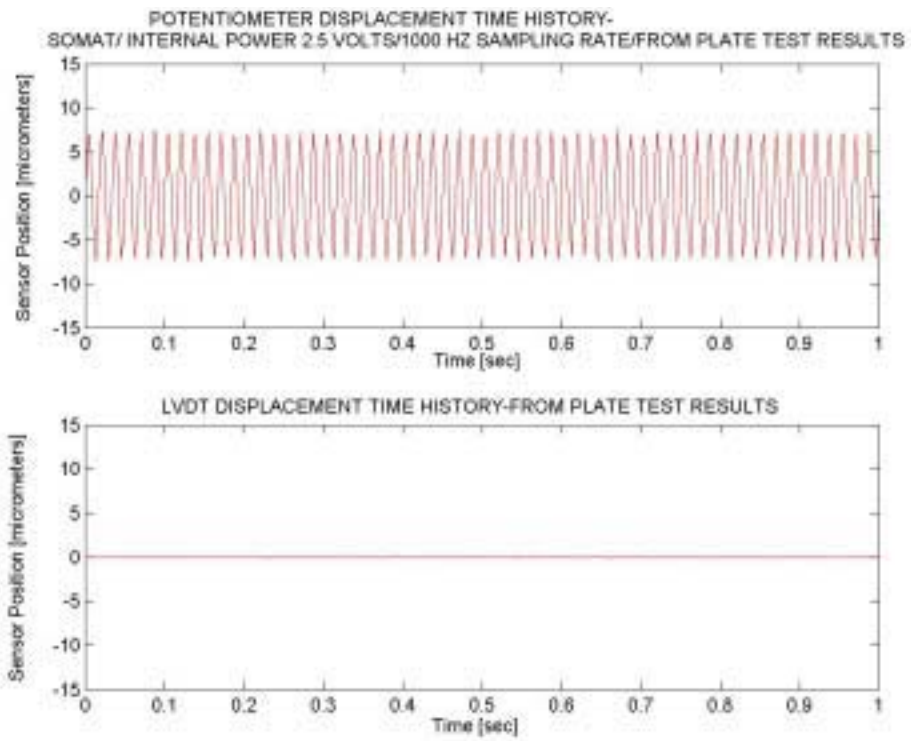


**Figure A- 2 Noise level in the potentiometer and LVDT output during the plate test**

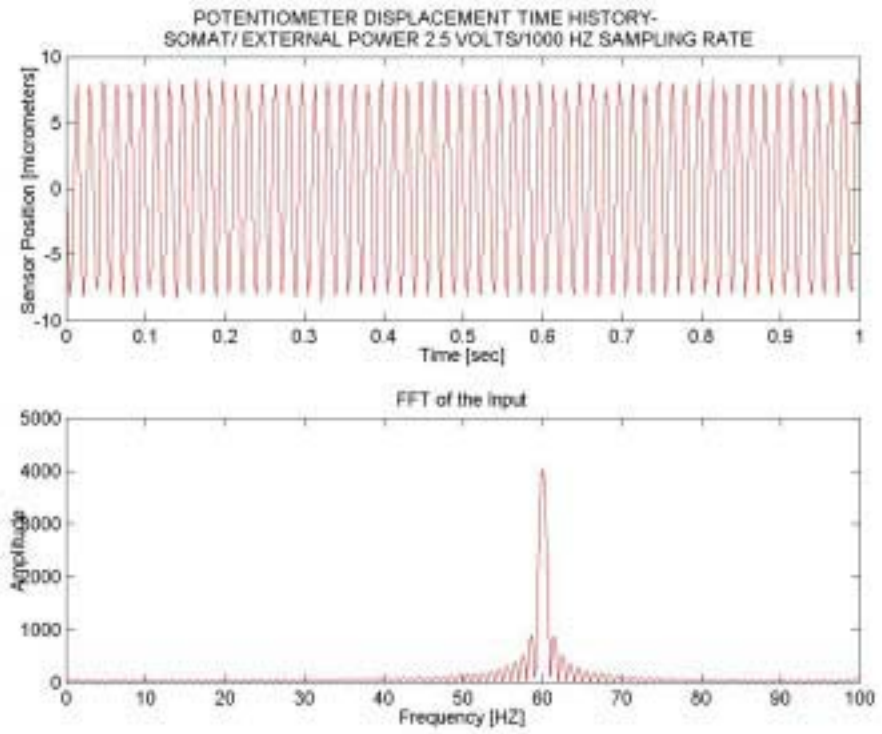


**Figure A- 3 Noise level and frequency content of noise with SOMAT and external power supply (1000 HZ sampling)**

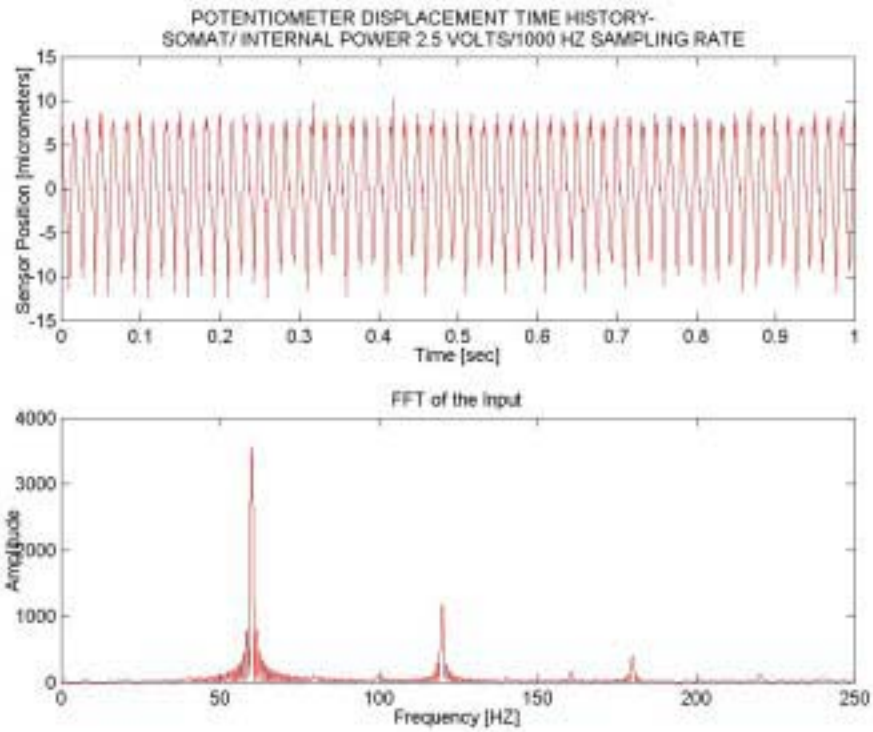


**Figure A- 4 Noise level and frequency content of noise with SOMAT and internal power supply (1000 HZ sampling)**

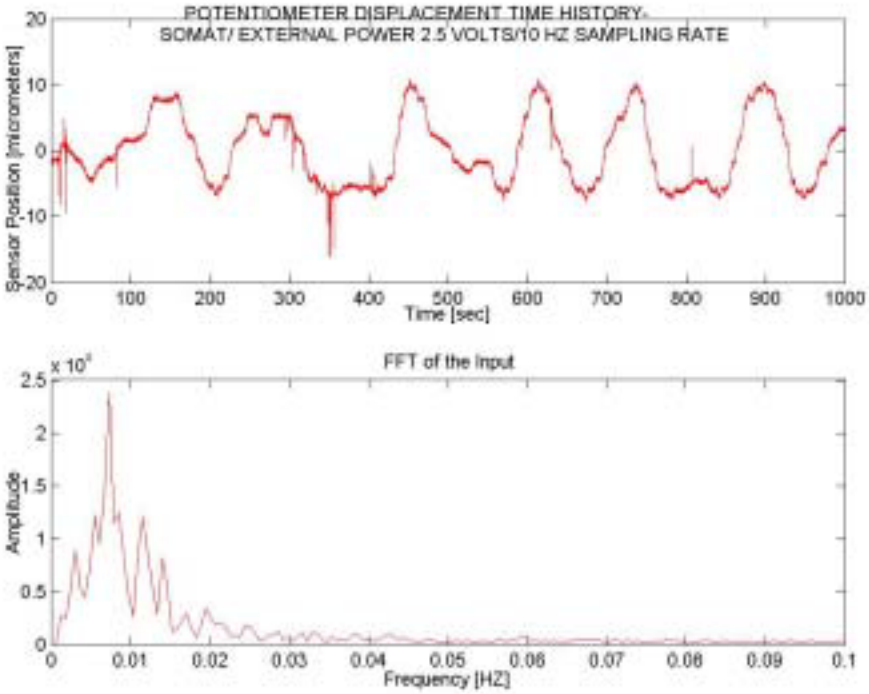


**Figure A- 5 Noise level and frequency content of noise with SOMAT and external power supply (10 HZ sampling)**

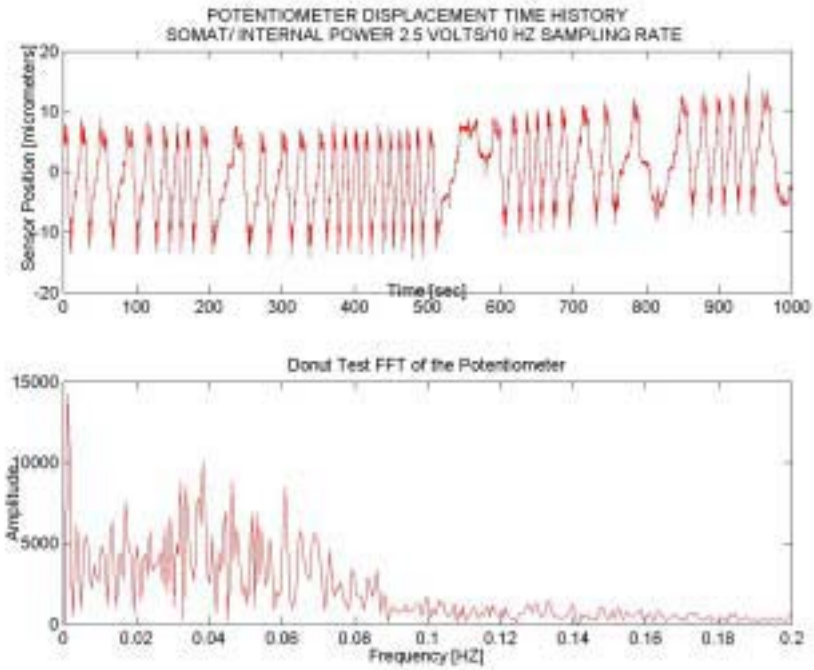


**Figure A- 6 Noise level and frequency content of noise with SOMAT and internal power supply (10 HZ sampling)**

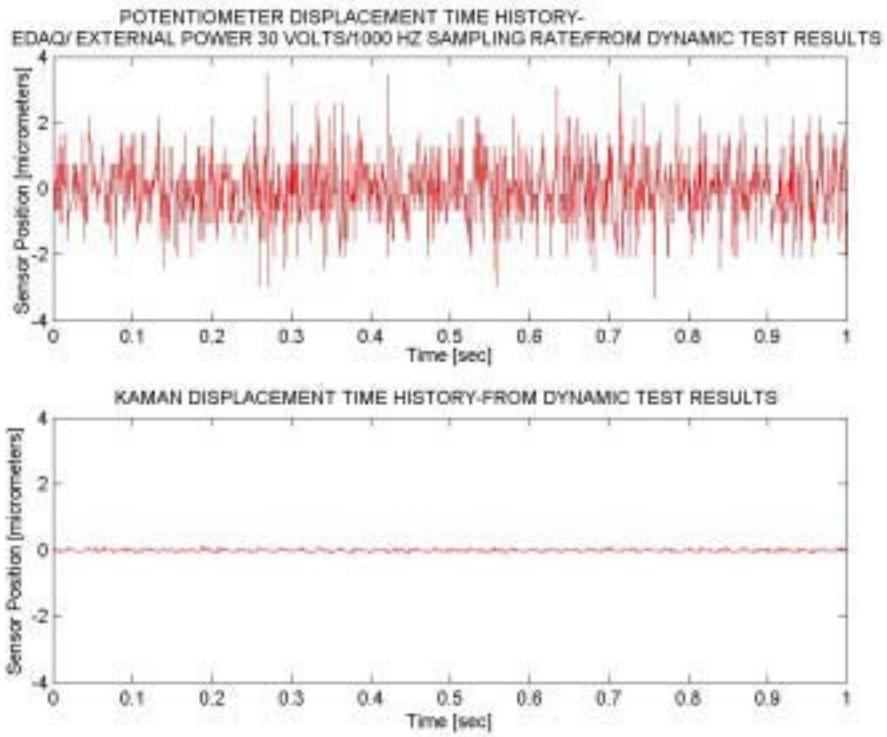


**Figure A- 7 Noise level during the dynamic test (1000 HZ sampling)**

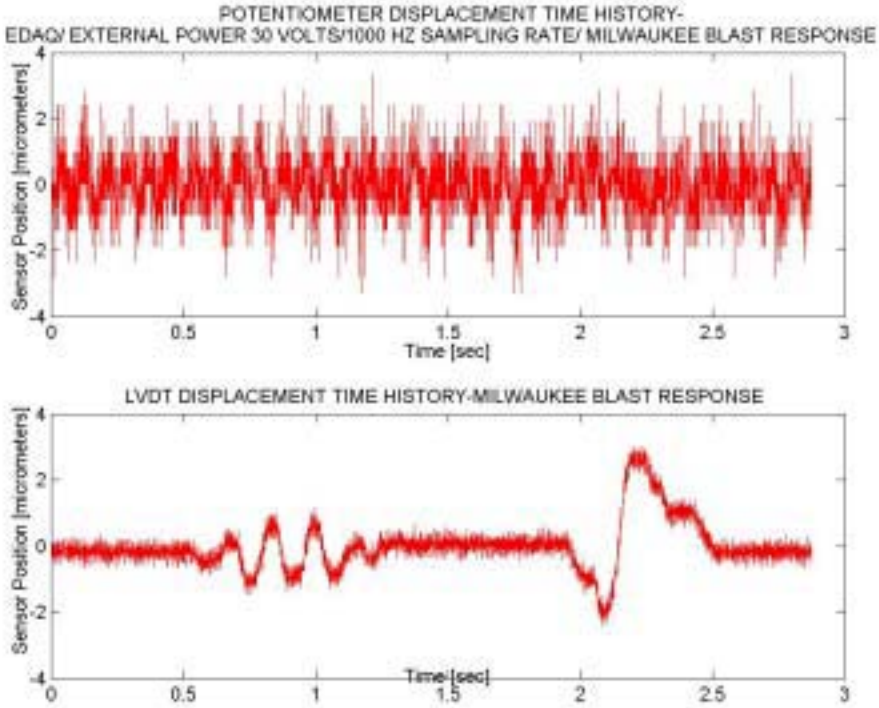


**Figure A- 8 Noise level during the field test (1000 HZ sampling)**

**B. Appendix** DYNAMIC TEST-IMPACT DISPLACEMENT TIME HISTORIES AND FFT ANALYSIS

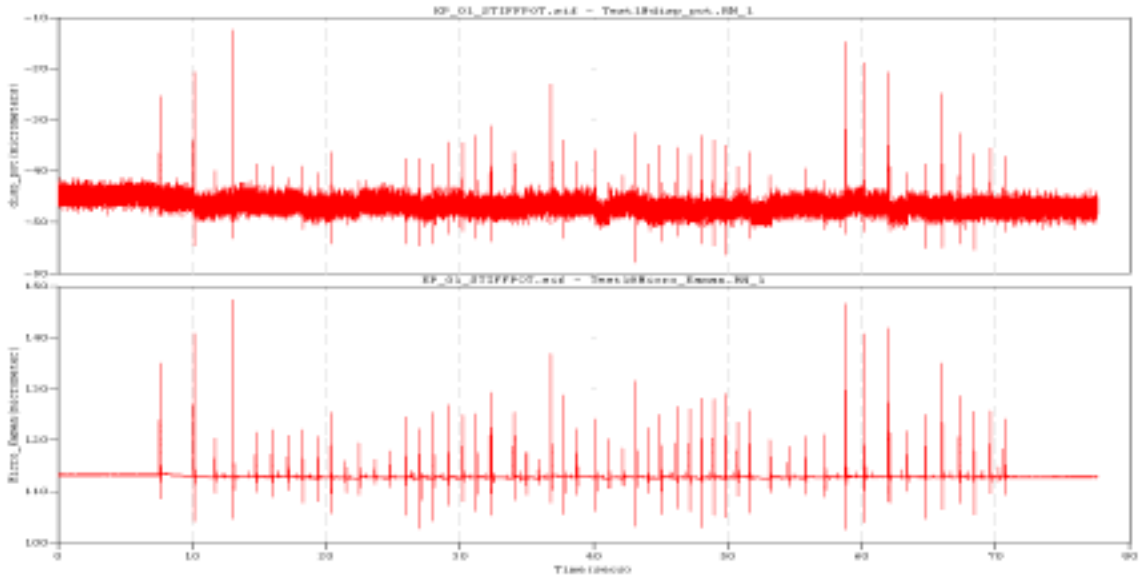

**Figure B- 1: Dynamic test impact displacements of high-tension potentiometer (top) and Kaman (bottom)**

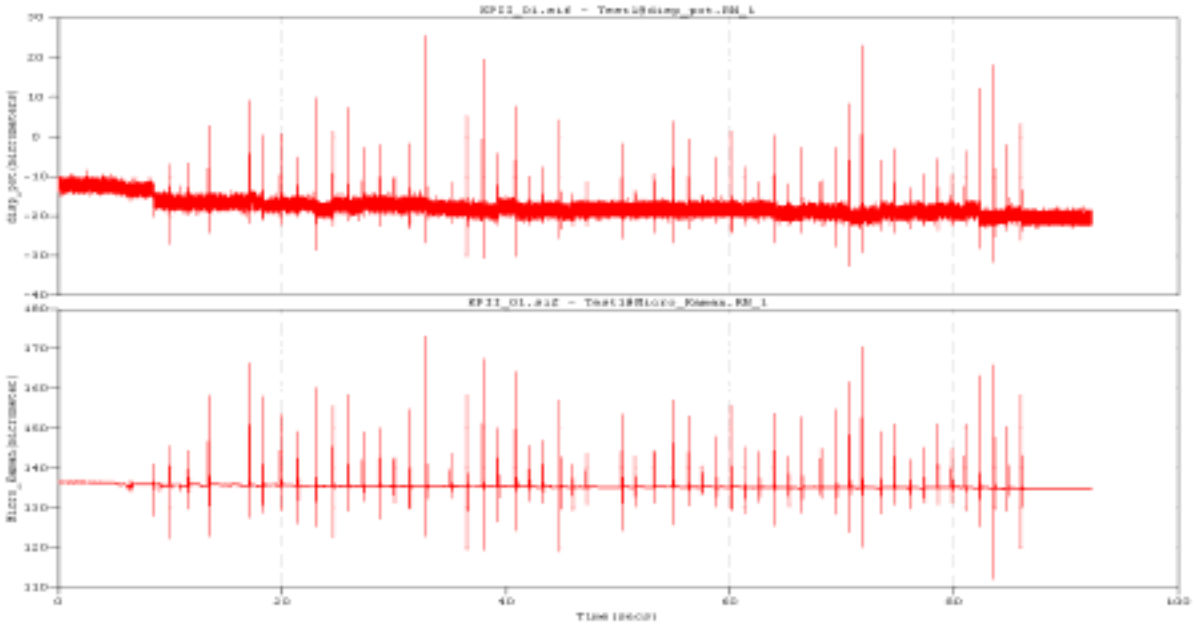

**Figure B- 2: Dynamic test impact displacements of low-tension potentiometer (top) and Kaman (bottom)**

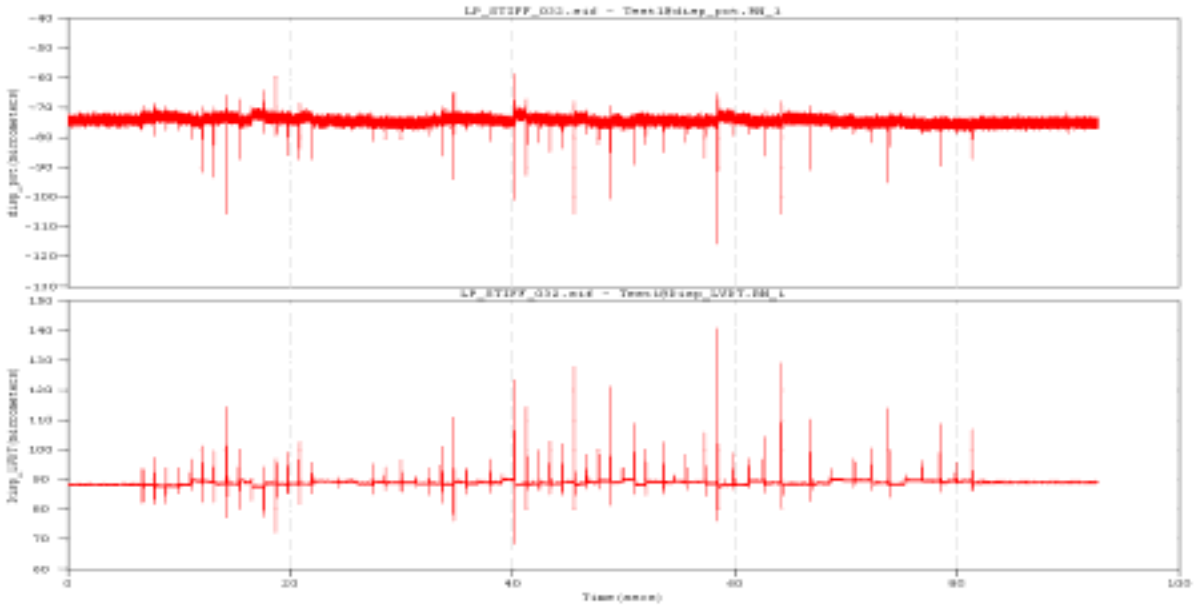

**Figure B- 3: Dynamic test impact displacements of high-tension potentiometer (top) and LVDT (bottom)**

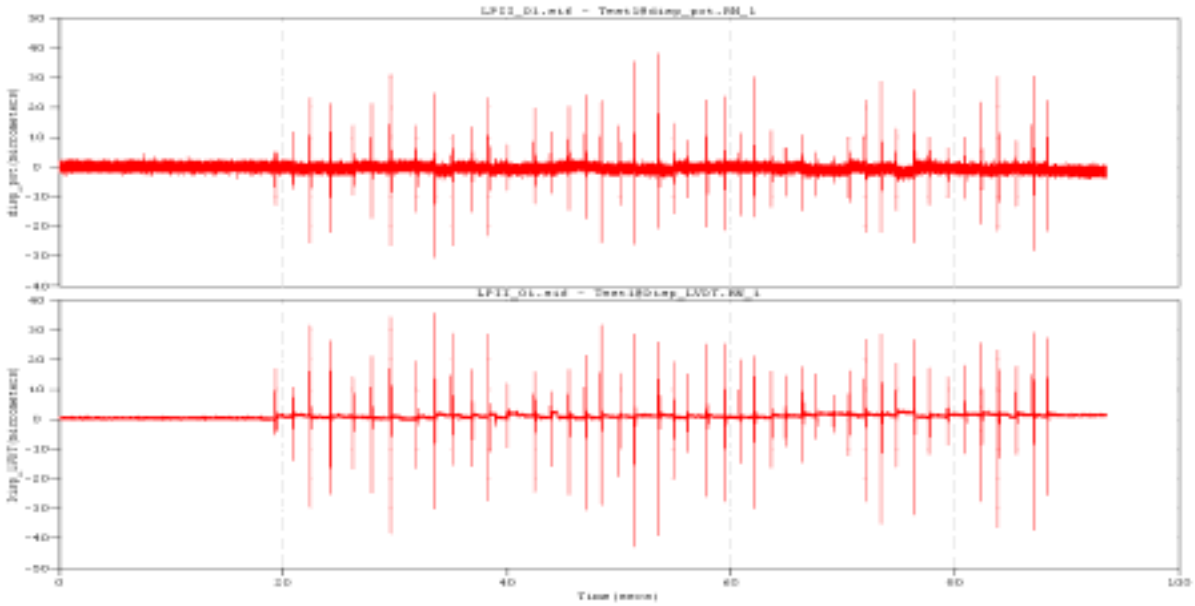

**Figure B- 4: Dynamic test impact displacements of low-tension potentiometer (top) and LVDT (bottom)**

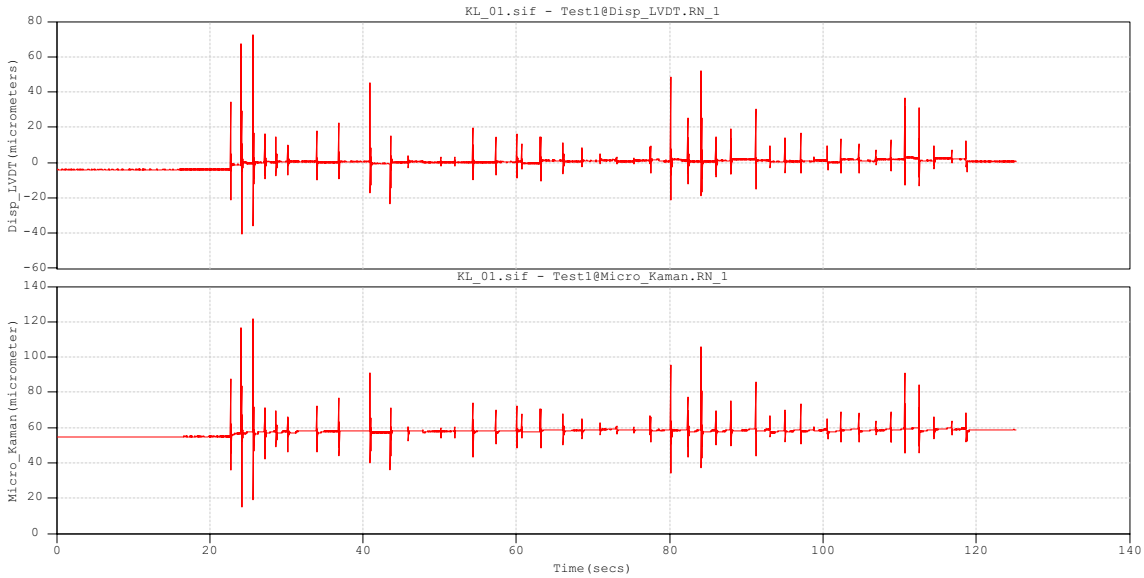


**Figure B- 5: Dynamic test impact displacements of LVDT (top) and Kaman (bottom)**

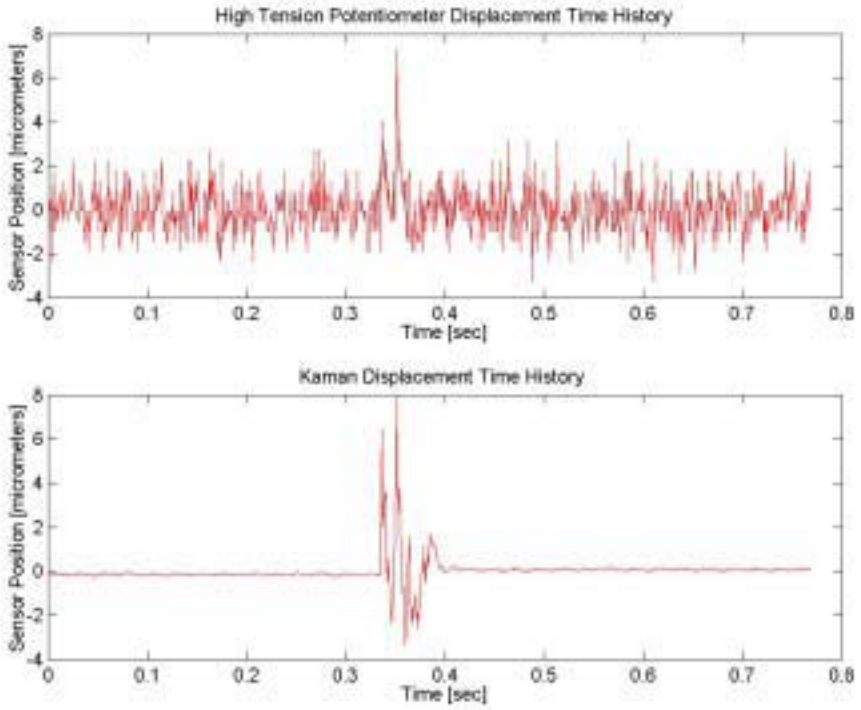


**Figure B- 6: One impact loading from dynamic test with high-tension potentiometer and Kaman**

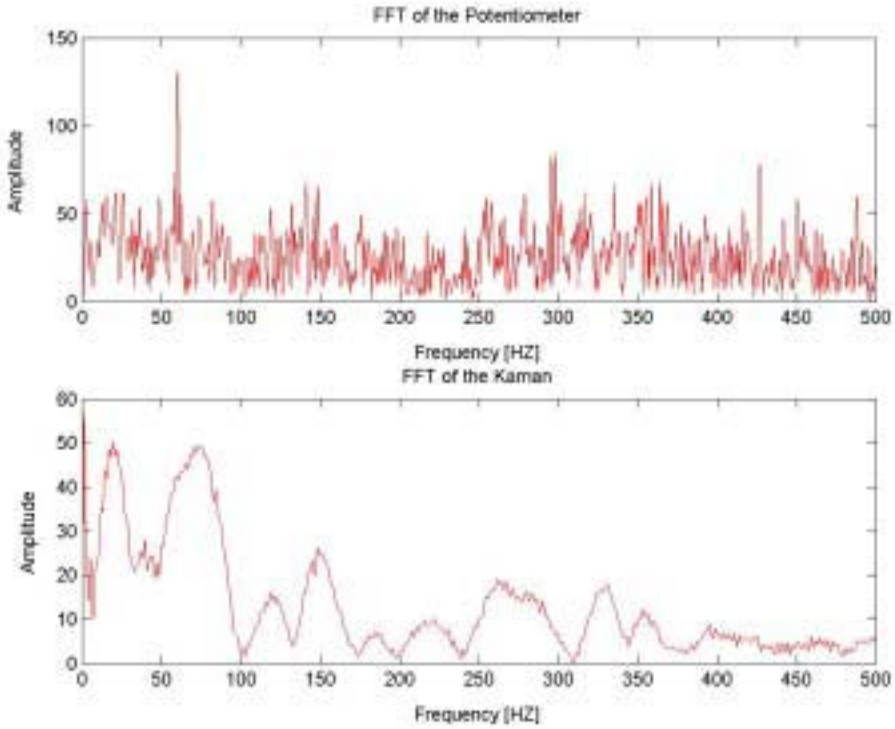


**Figure B- 7: FFT of the impact loading. High-tension potentiometer (top) and Kaman (bottom)**

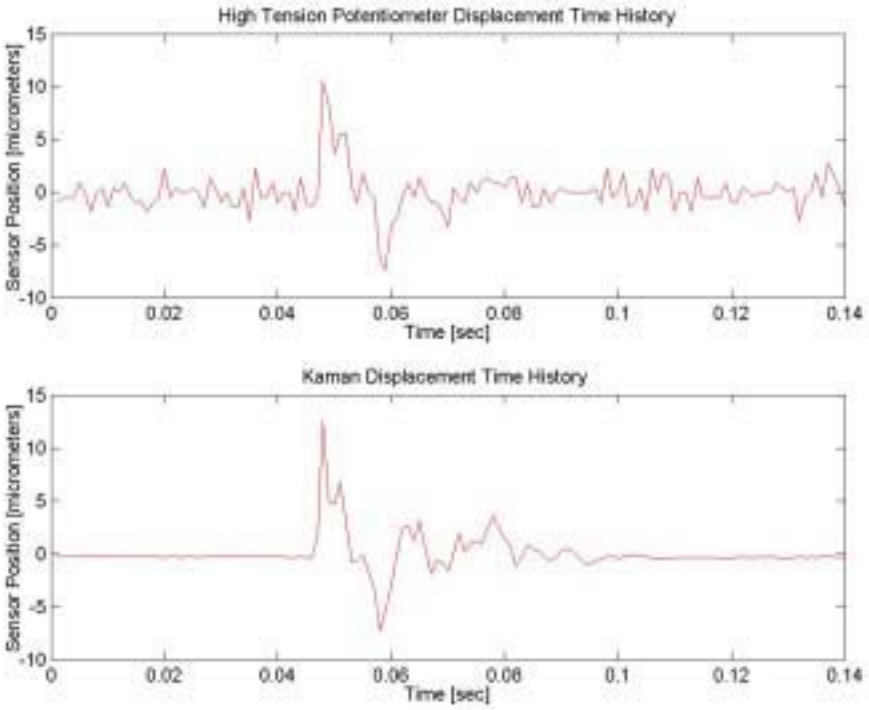


**Figure B- 8: One impact loading from dynamic test with high-tension potentiometer and Kaman**

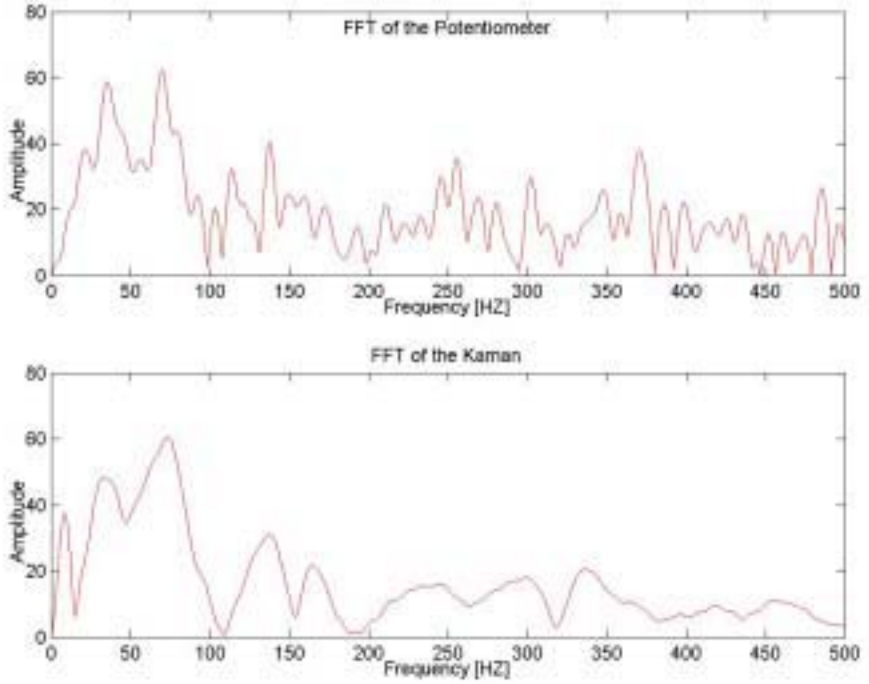


**Figure B- 9: FFT of the impact loading. High-tension potentiometer (top) and Kaman (bottom)**

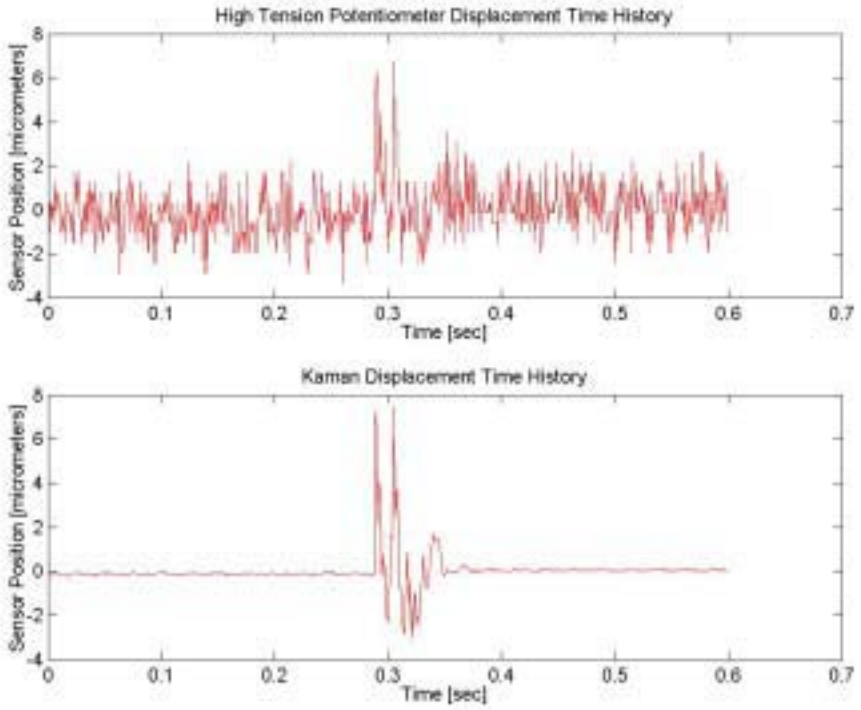


**Figure B- 10: One impact loading from dynamic test with high-tension potentiometer and Kaman**

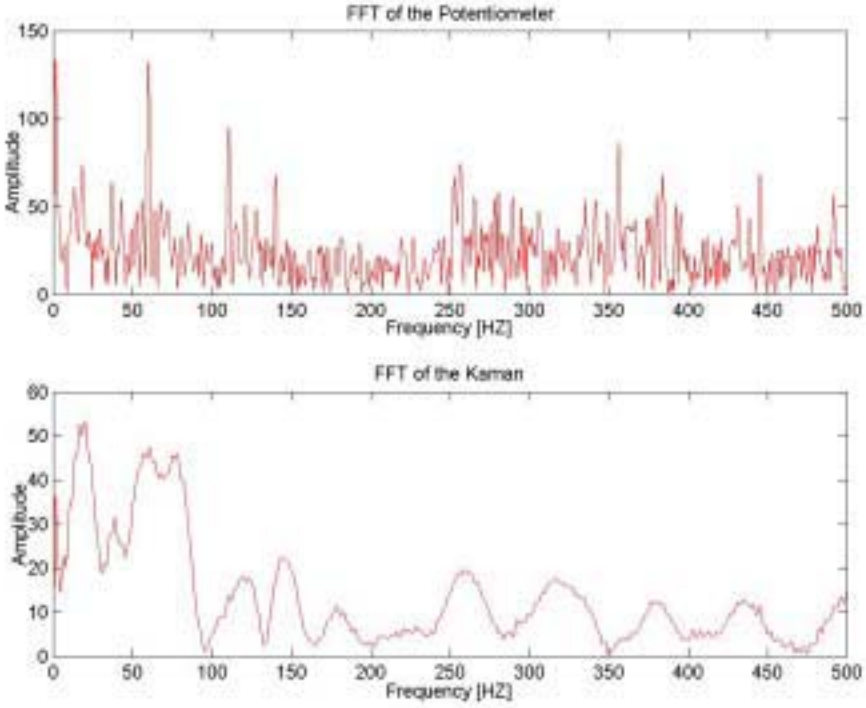


**Figure B- 11: FFT of the impact loading. High-tension potentiometer (top) and Kaman (bottom)**

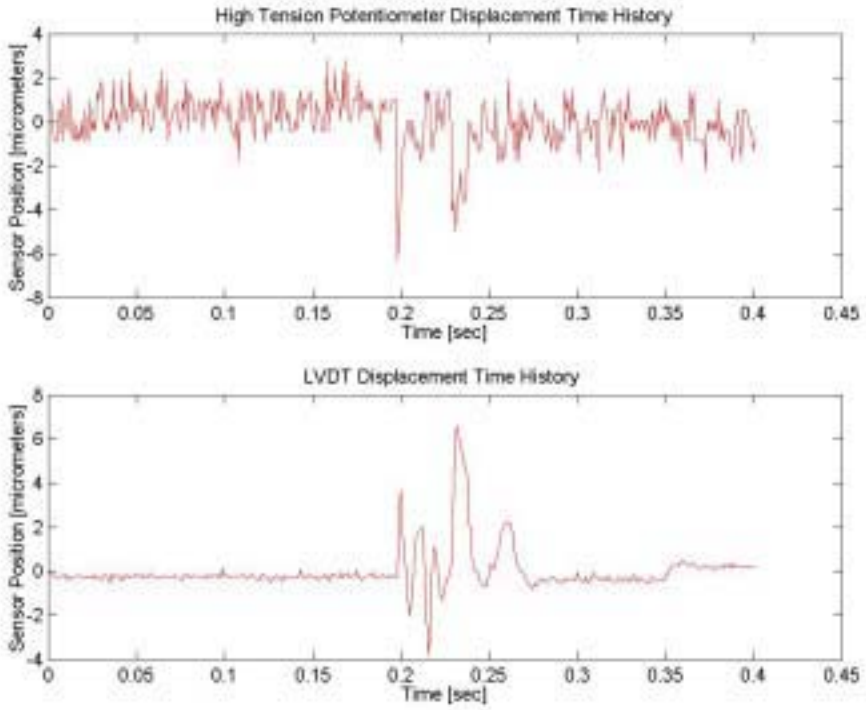


**Figure B- 12: One impact loading from dynamic test with high-tension potentiometer and LVDT**

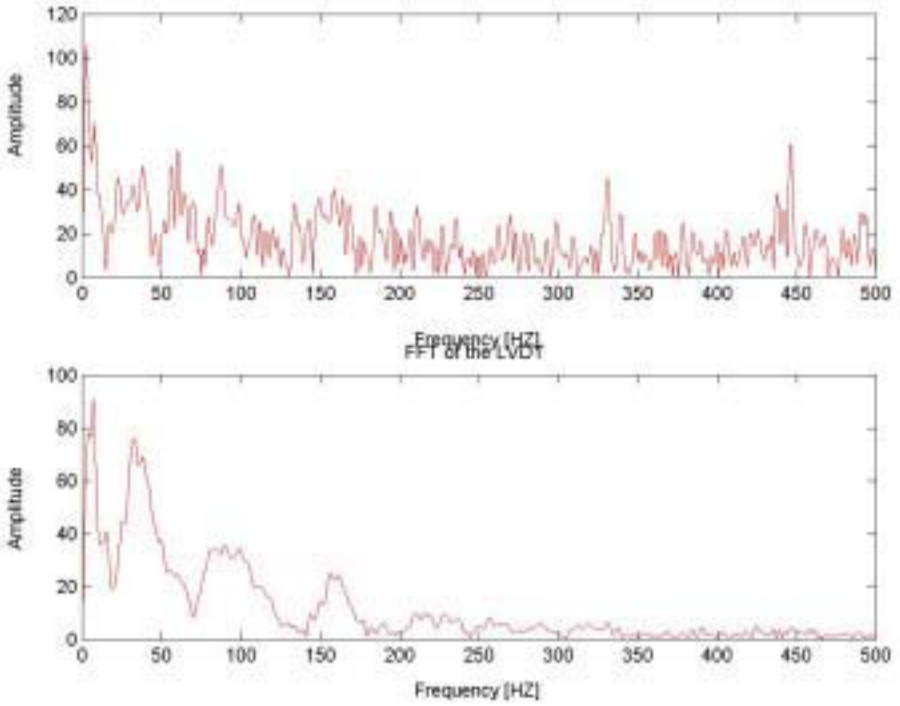


**Figure B- 13: FFT of the impact loading. High-tension potentiometer (top) and LVDT (bottom)**

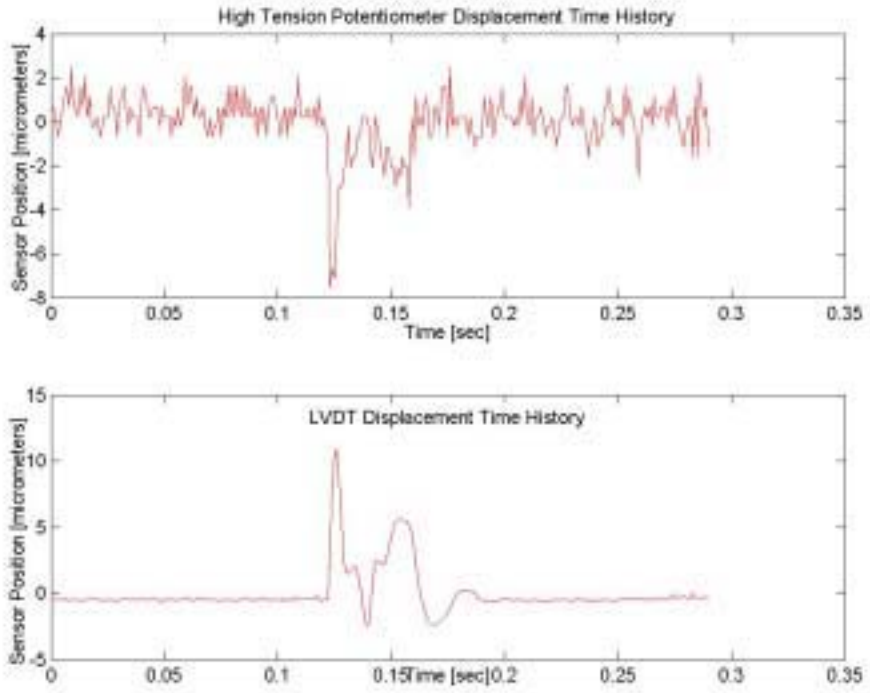


**Figure B- 14: One impact loading from dynamic test with high-tension potentiometer and LVDT**

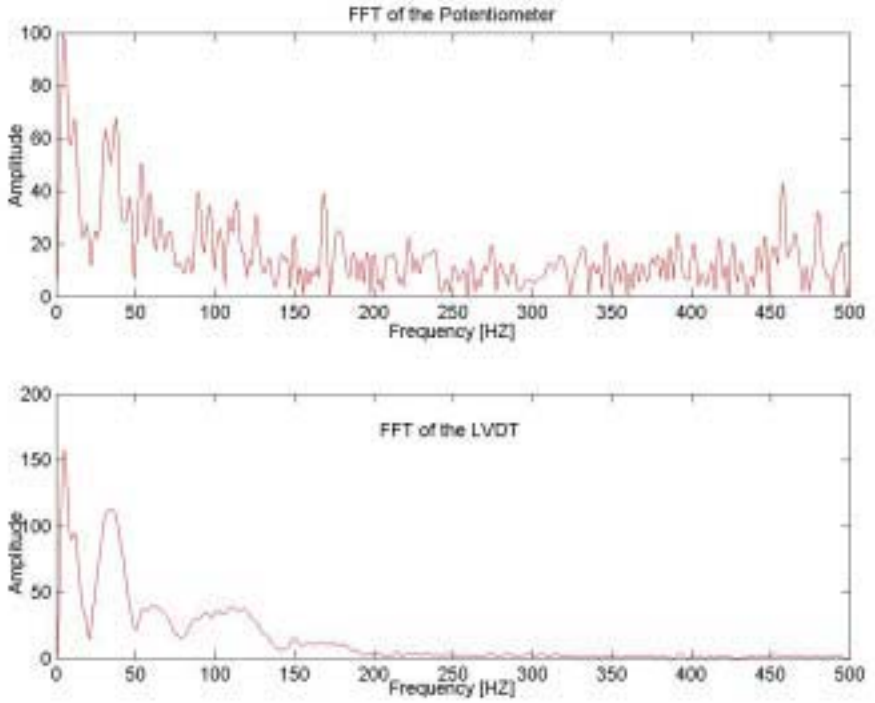


**Figure B- 15: FFT of the impact loading. High-tension potentiometer (top) and LVDT (bottom)**

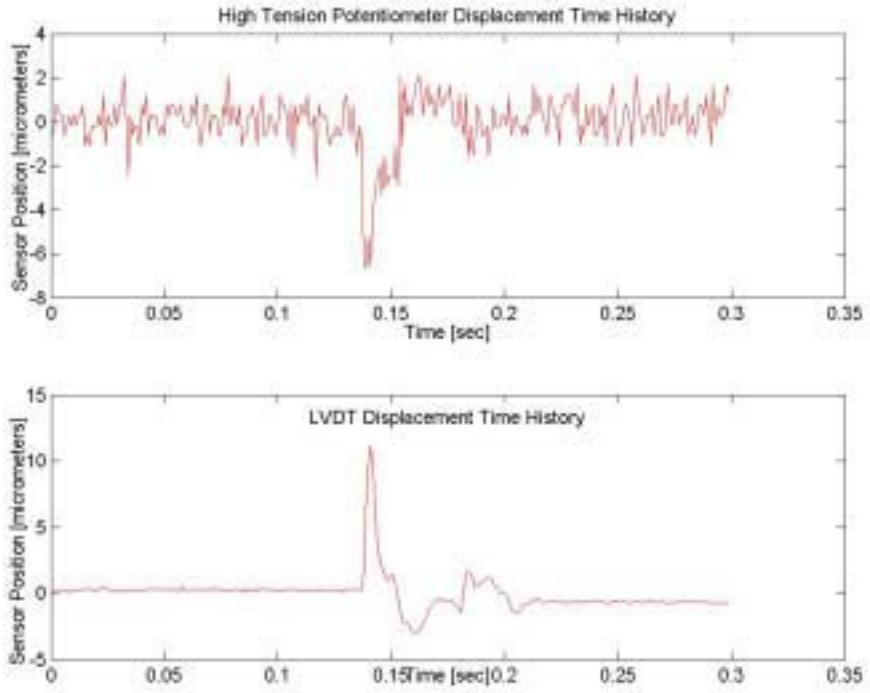


**Figure B- 16: One impact loading from dynamic test with high-tension potentiometer and LVDT**

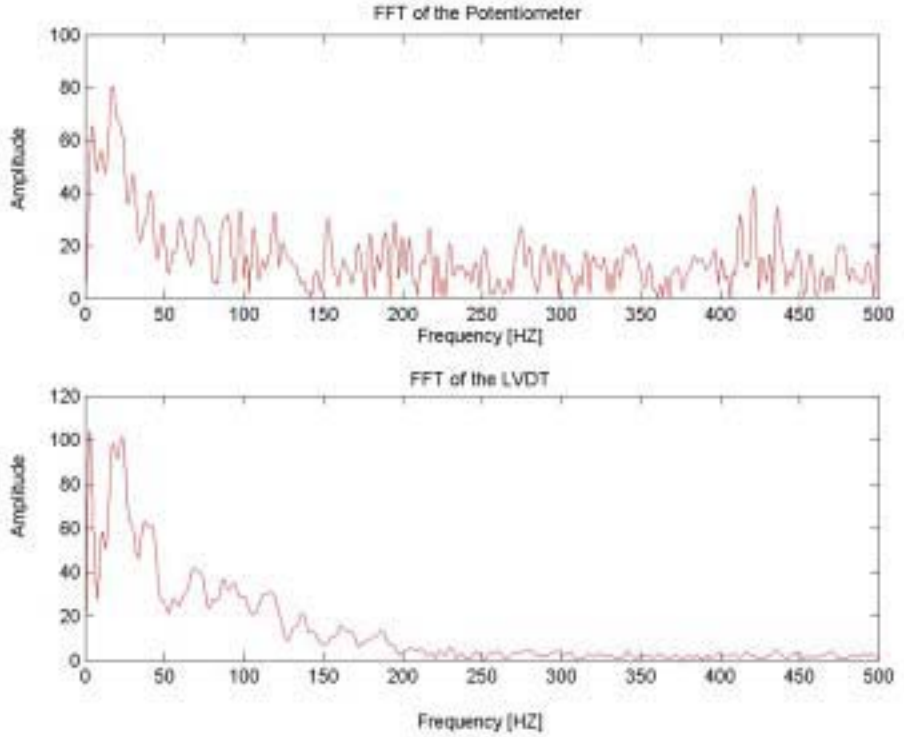


**Figure B- 17: FFT of the impact loading. High-tension potentiometer (top) and LVDT (bottom)**

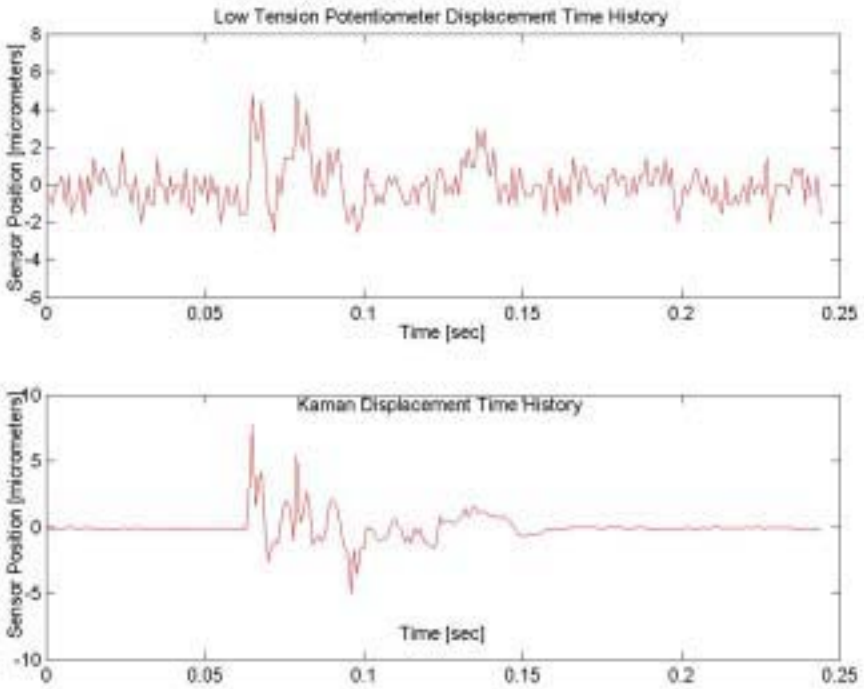


**Figure B- 18: One impact loading from dynamic test with low-tension potentiometer and Kaman**

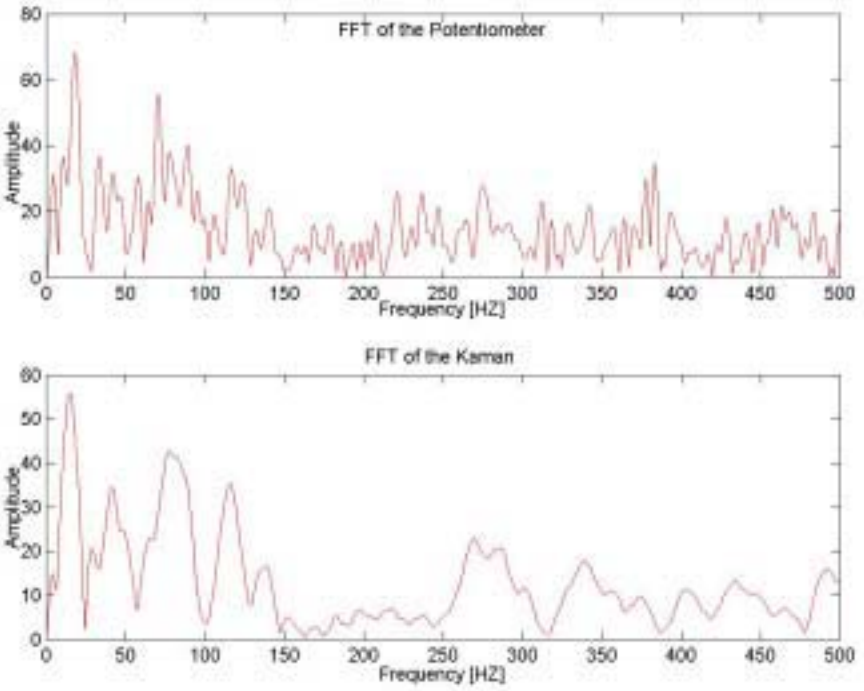


**Figure B- 19: FFT of the impact loading. Low-tension potentiometer (top) and Kaman (bottom)**

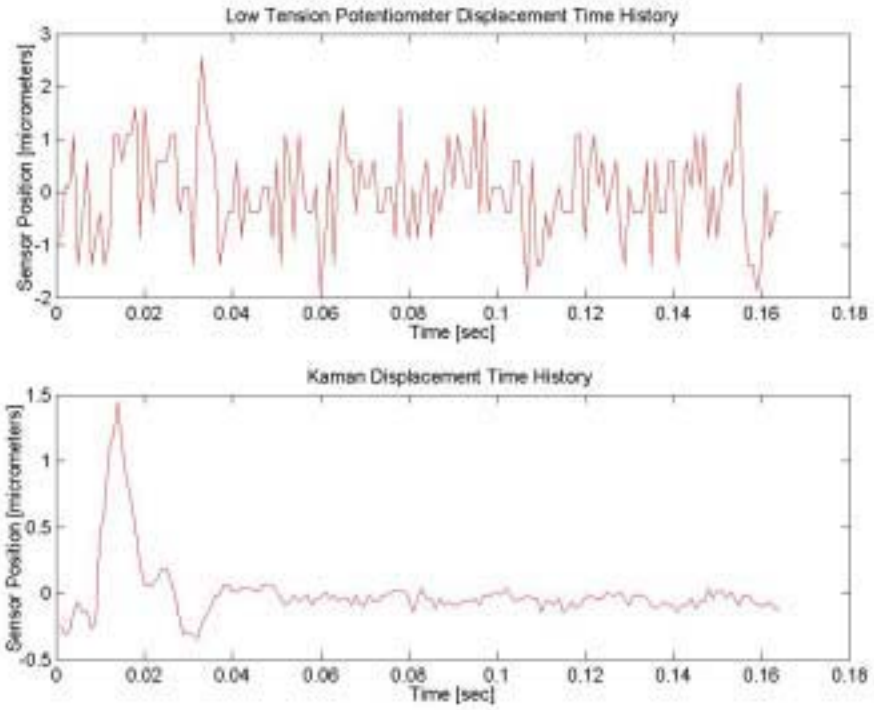


**Figure B- 20: One impact loading from dynamic test with low-tension potentiometer and Kaman**

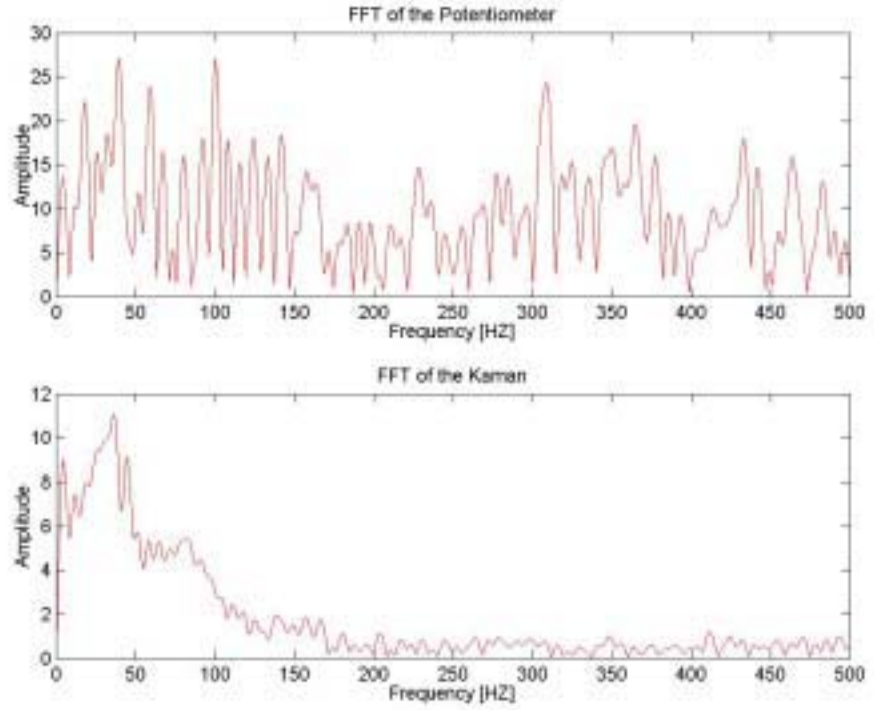


**Figure B- 21: FFT of the impact loading. Low-tension potentiometer (top) and Kaman (bottom)**

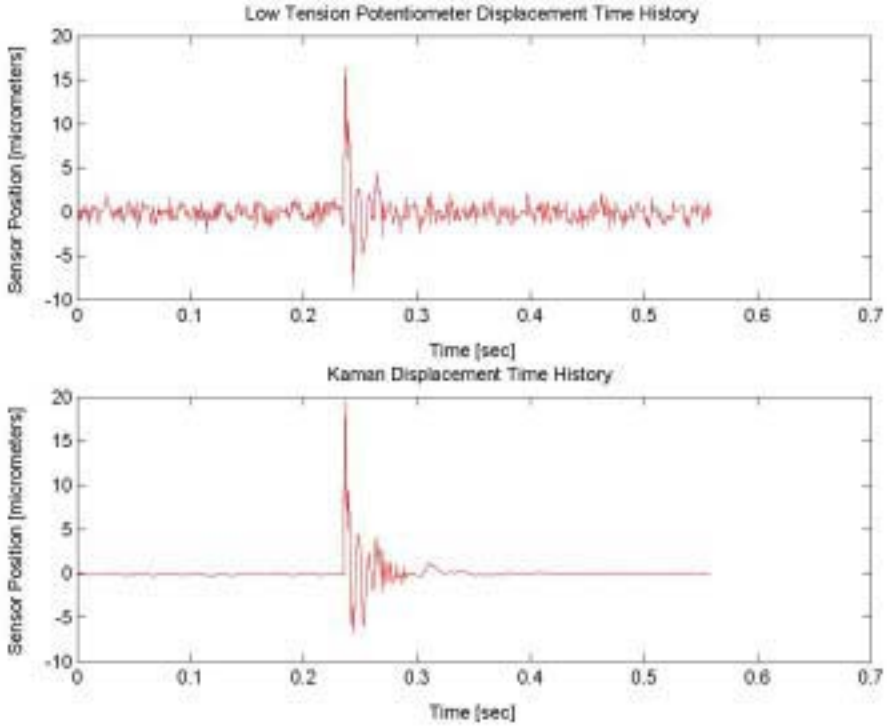


**Figure B- 22: One impact loading from dynamic test with low-tension potentiometer and Kaman**

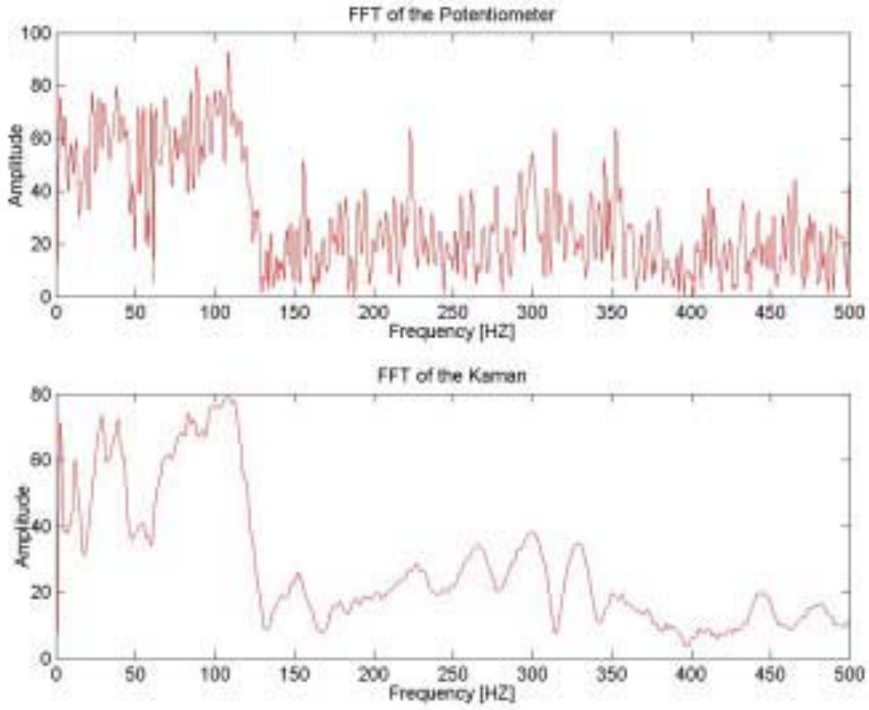


**Figure B- 23: FFT of the impact loading. Low-tension potentiometer (top) and Kaman (bottom)**

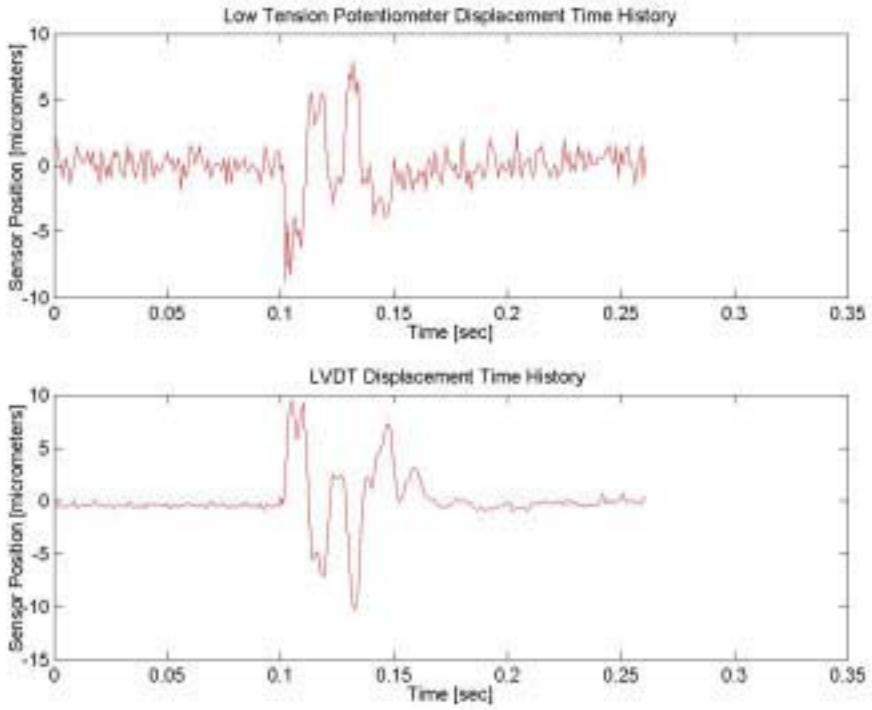


**Figure B- 24: One impact loading from dynamic test with low-tension potentiometer and LVDT**

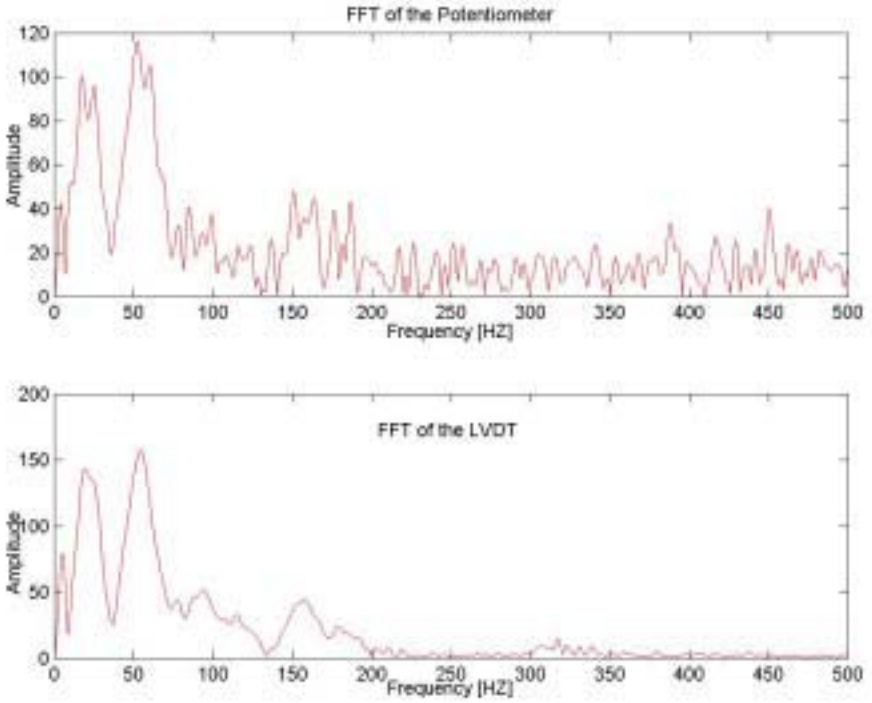


**Figure B- 25: FFT of the impact loading. Low-tension potentiometer (top) and LVDT (bottom)**

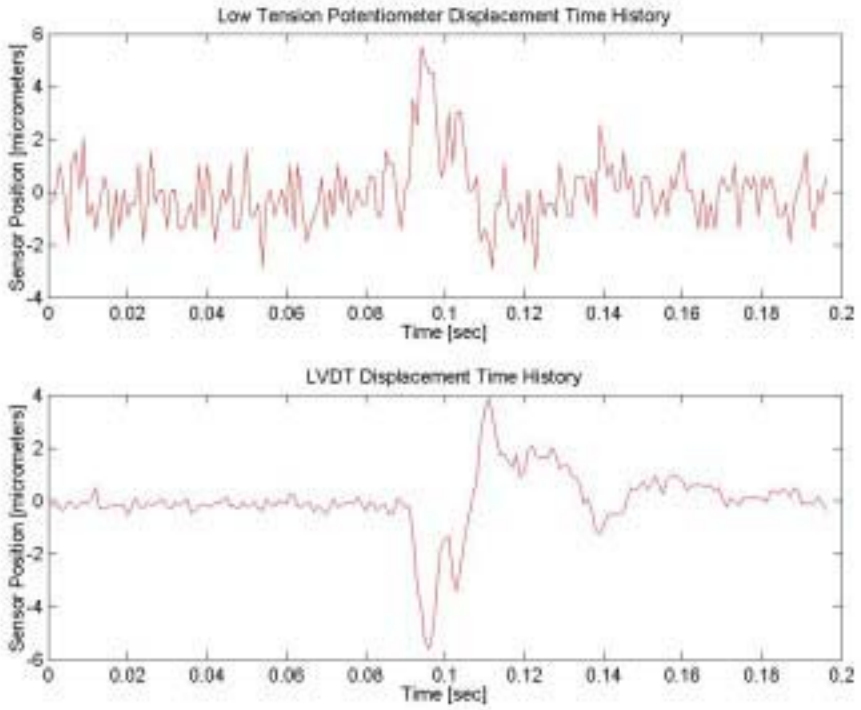


**Figure B- 26: One impact loading from dynamic test with low-tension potentiometer and LVDT**

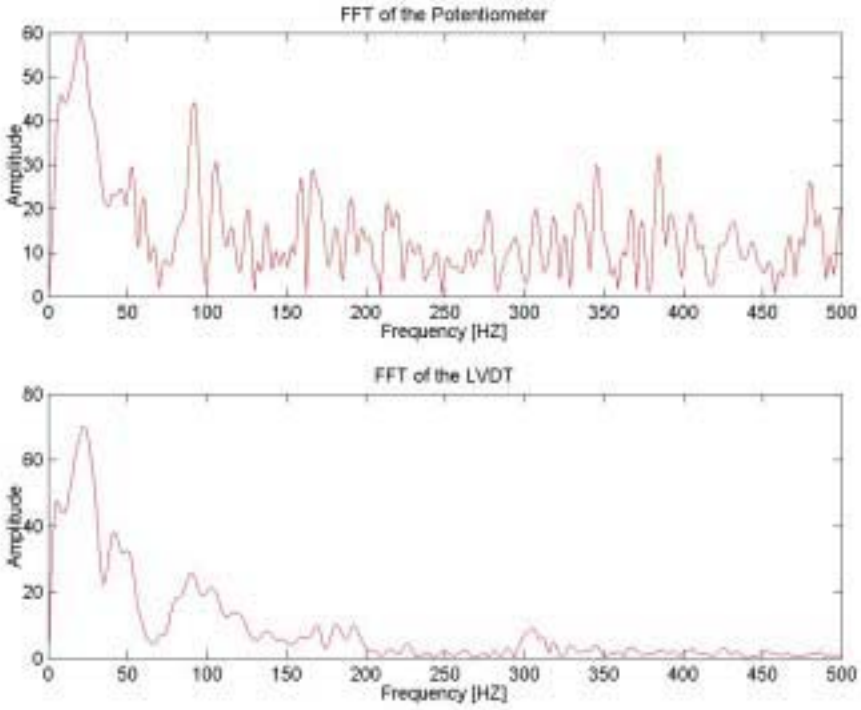


**Figure B- 27: FFT of the impact loading. Low-tension potentiometer (top) and LVDT (bottom)**

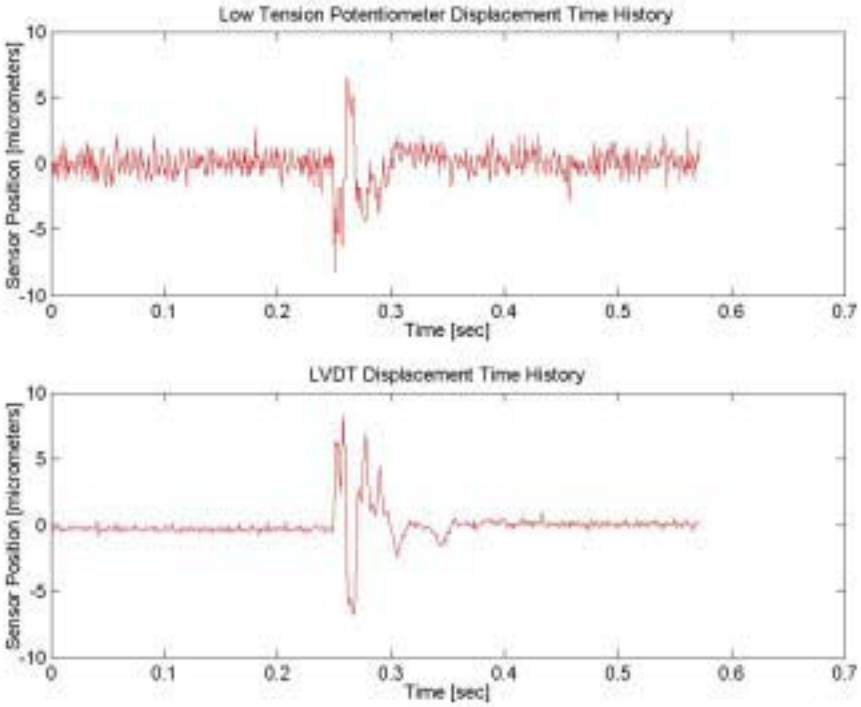


**Figure B- 28: One impact loading from dynamic test with low-tension potentiometer and LVDT**

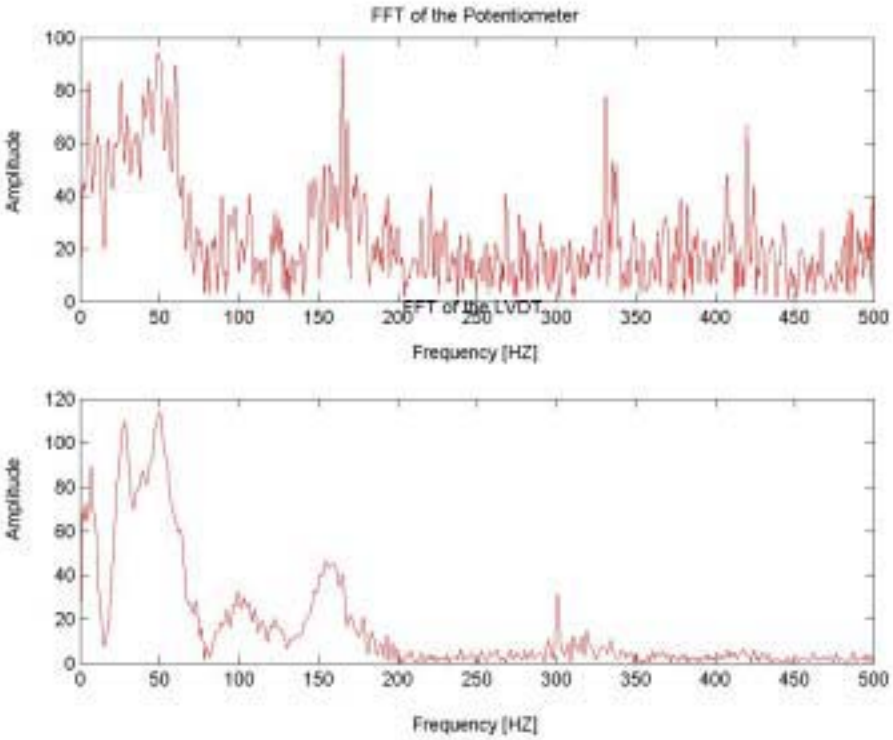


**Figure B- 29: FFT of the impact loading. Low-tension potentiometer (top) and LVDT (bottom)**

**C. Appendix** COMPARISON OF BLAST INDUCED CRACK RESPONSES MEASURED BY POTENTIOMETER AND LVDT

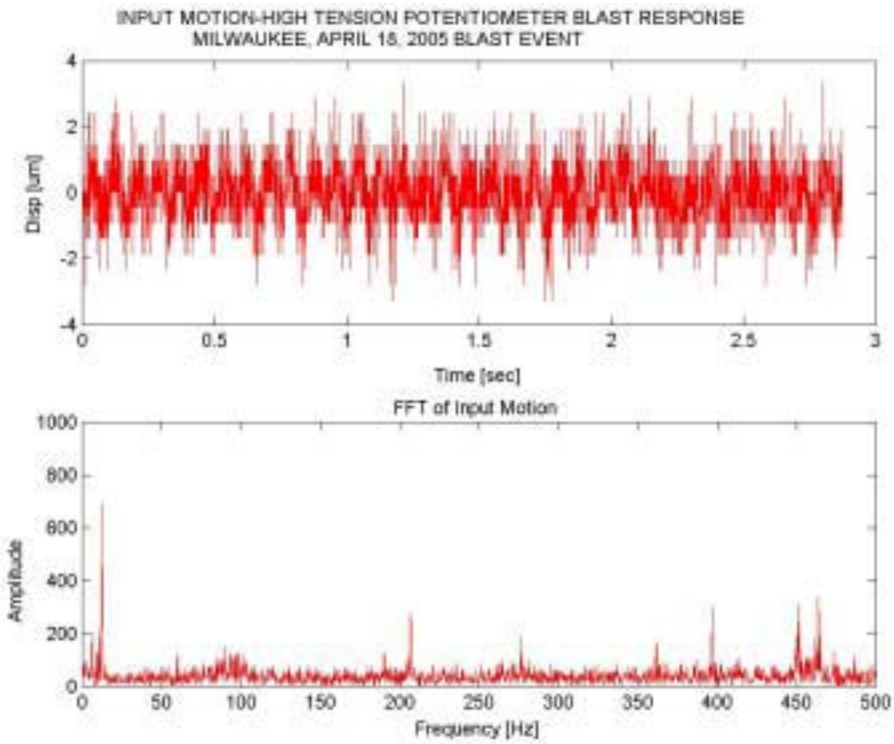


**Figure C- 1: Displacement time history and FFT of the high-tension potentiometer response to blast event (April 18, 2005)**

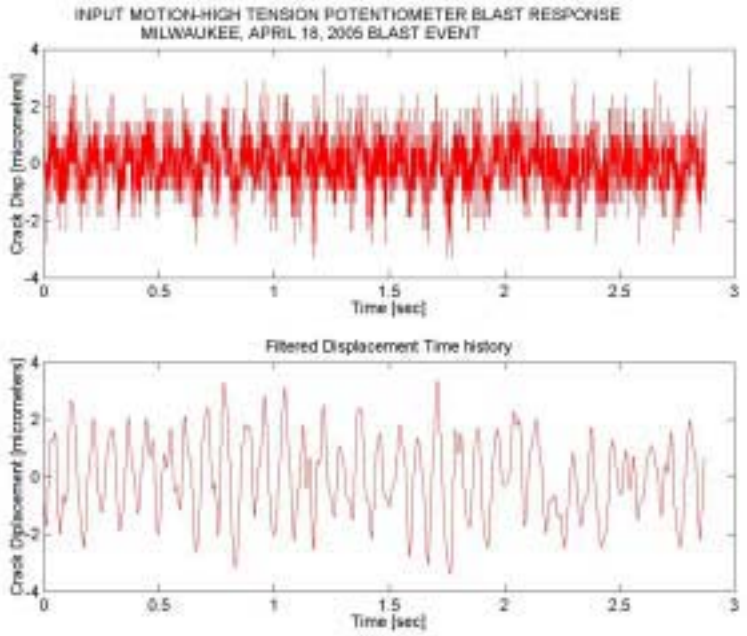


**Figure C- 2: Original displacement time history (top) and filtered displacement time history of high tension potentiometer**

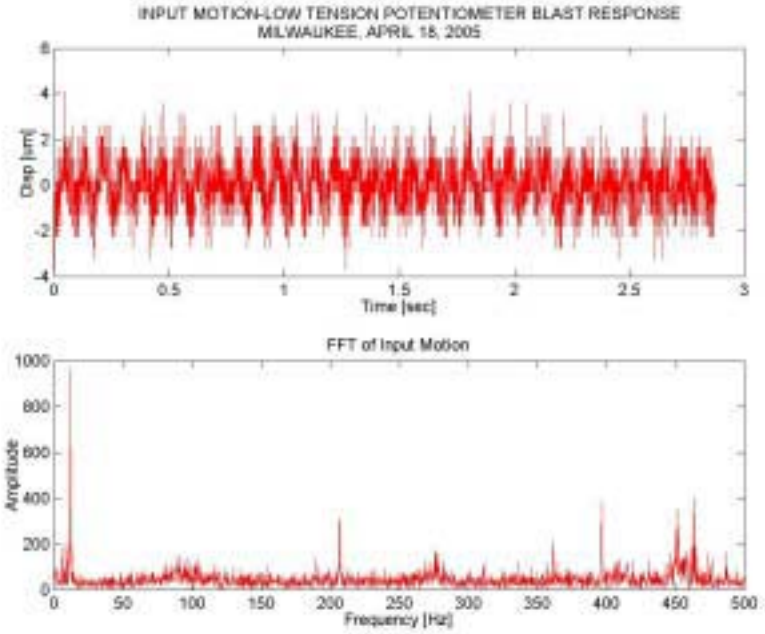


**Figure C- 3: Displacement time history and FFT of the low-tension potentiometer response to blast event (April 18, 2005)**

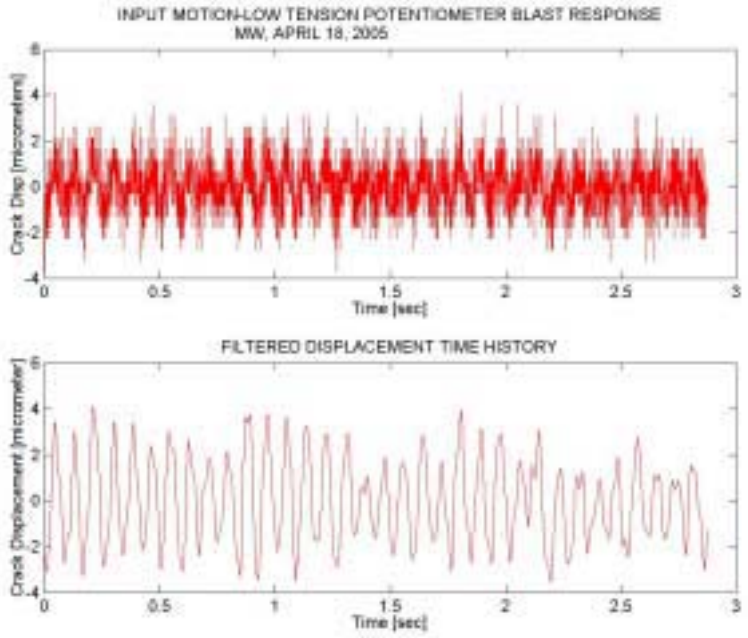


**Figure C- 4: Displacement time history and FFT of the low-tension potentiometer response to blast event (April 18, 2005)**

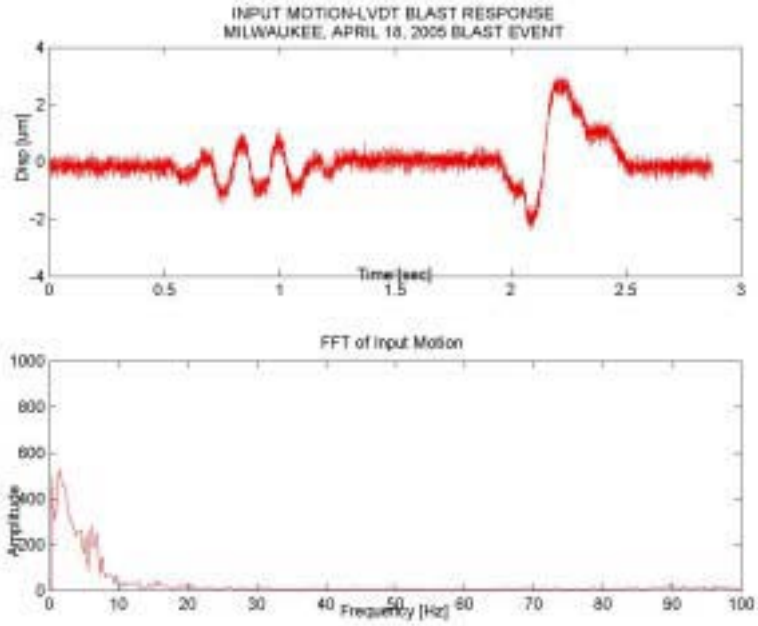


**Figure C- 5: Displacement time history and FFT of the LVDT response to blast event (April 18, 2005)**

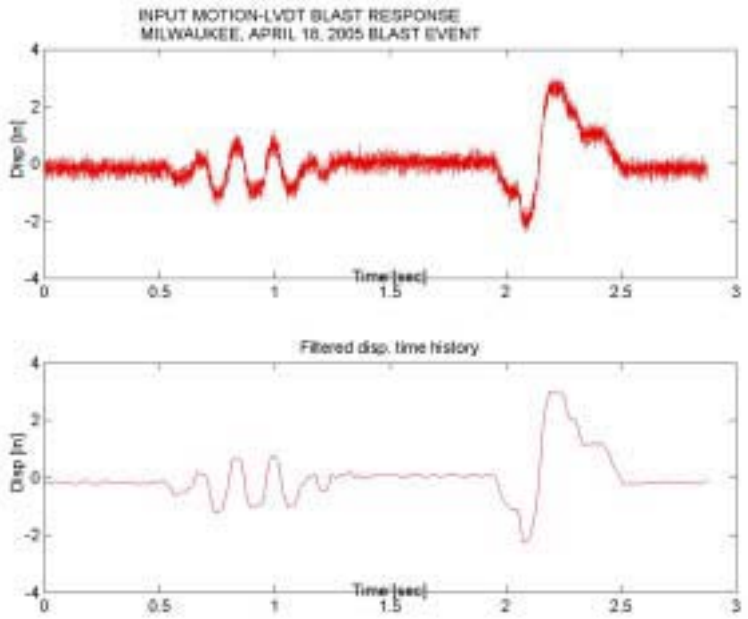


**Figure C- 6: Original displacement time history (top) and filtered displacement time history of LVDT**

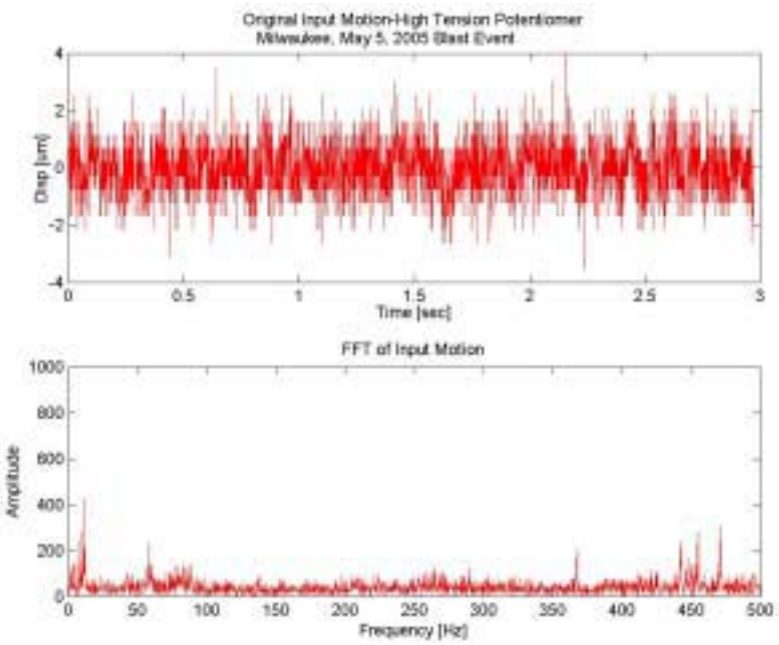


**Figure C- 7: Displacement time history and FFT of the high-tension potentiometer response to blast event (May 5, 2005)**

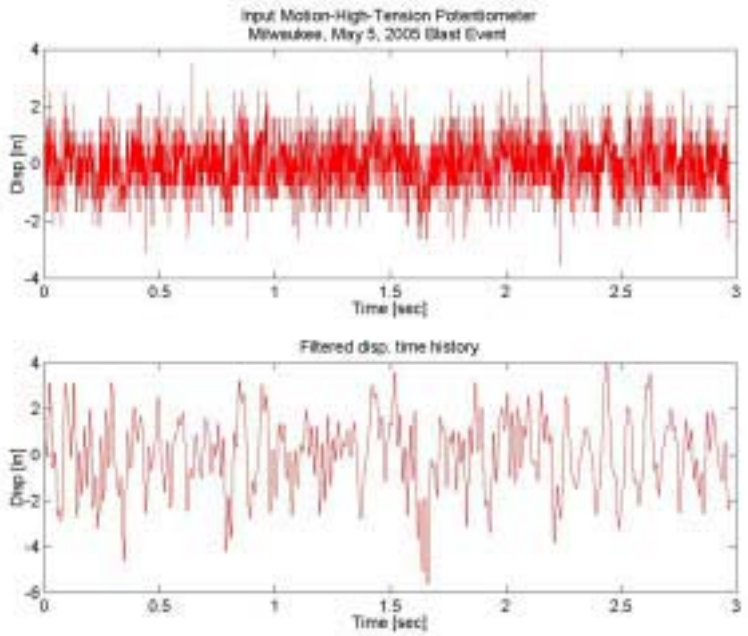


**Figure C- 8: Original displacement time history (top) and filtered displacement time history of high-tension potentiometer**

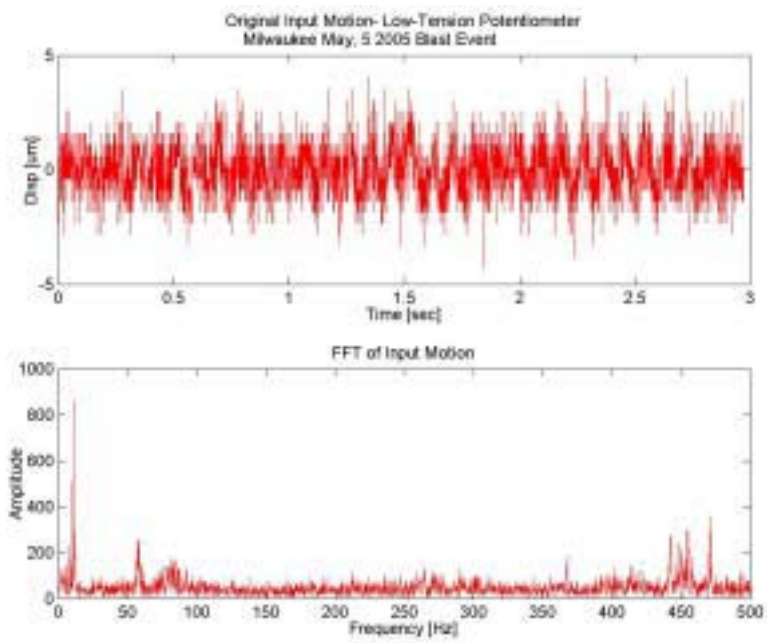


**Figure C- 9: Displacement time history and FFT of the low-tension potentiometer response to blast event (May 5, 2005)**

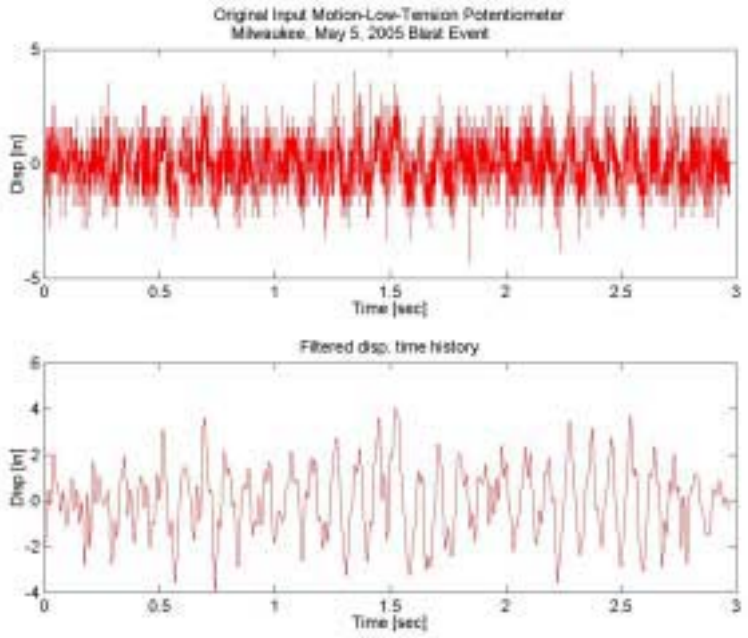


**Figure C- 10: Original displacement time history (top) and filtered displacement time history of low-tension potentiometer**

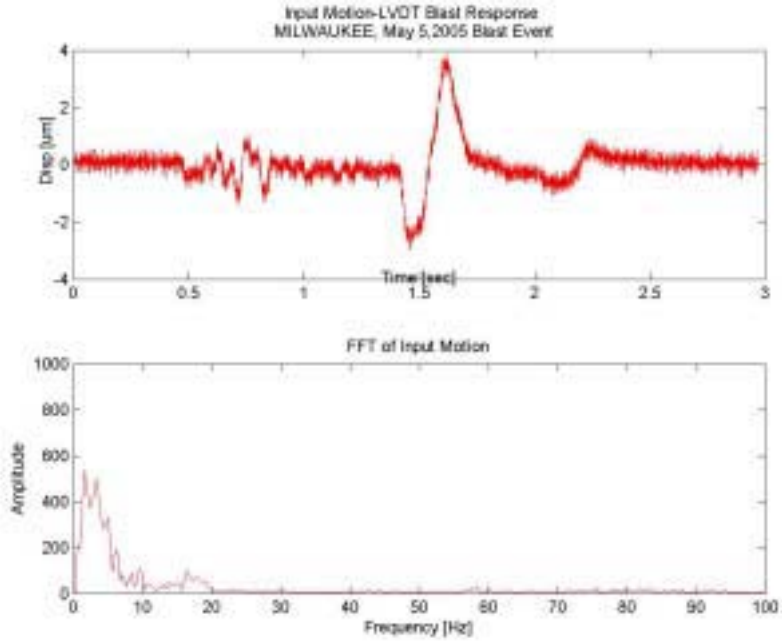


**Figure C- 11: Displacement time history and FFT of the LVDT response to blast event (May 5, 2005)**

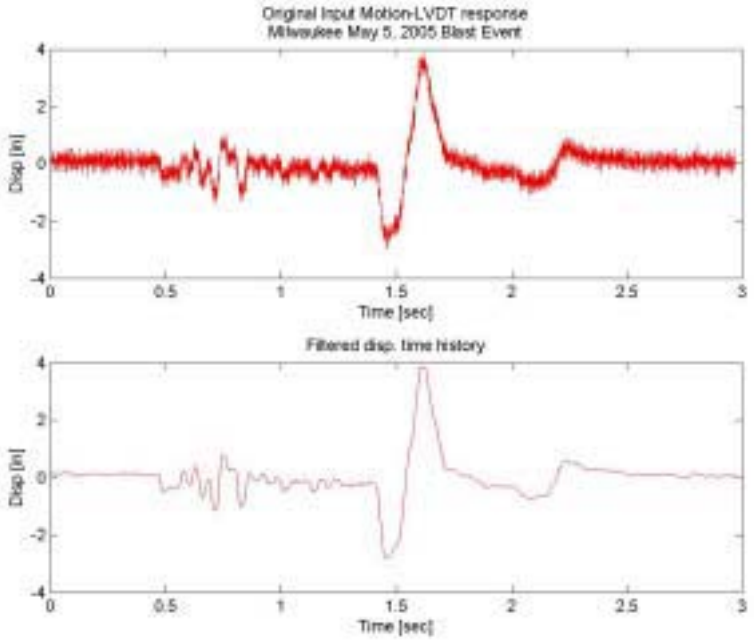


**Figure C- 12: Original displacement time history (top) and filtered displacement time history of LVDT**

**D. Appendix** RELATIVE TEMPERATURE CORRECTIONS IN PLATE AND DONUT TESTS

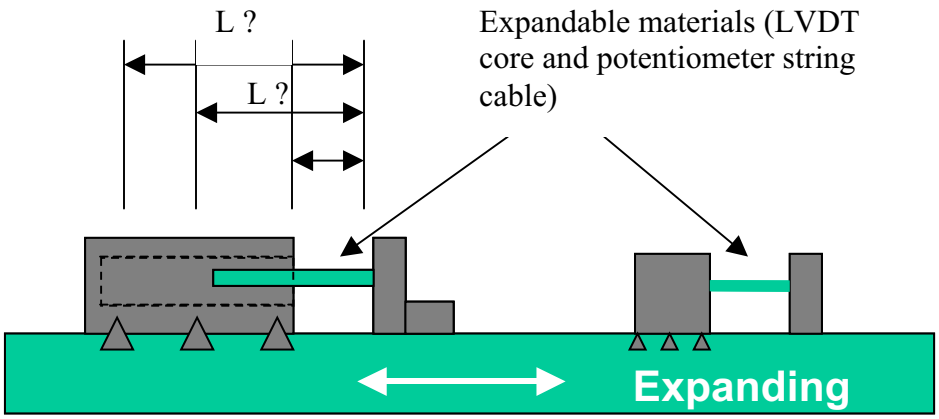


**Figure D- 1: Schematic of the plate test showing the importance of fixity length of the sensor to the plate and relative expansion/contraction**

$\Delta d_{measured} = \Delta d_{plate/donut} - \Delta d_{core/cable}$

$\Delta d_{plate/donut} \sim \alpha * \Delta T * L$

where $\alpha$ is the coefficient of linear thermal expansion, L is the fixity length shown in the above sketch, and $\Delta T$ is temperature changes.

In order to compare pure plate/donut expansion or contraction, expansion/contraction of the core or the string cable is added to the measured values. In this case, core length of LVDT and the potentiometer string cable is 38.1 mm (1.5 in) and 10 mm (0.04 in). Thermal expansion coefficient of core and string cable is taken to be 19 and 17.28 μm/m/$^{o}$C respectively.

$(\Delta d_{measured} + \Delta d_{core/cable})$ vs. $(\Delta d_{plate/donut})$

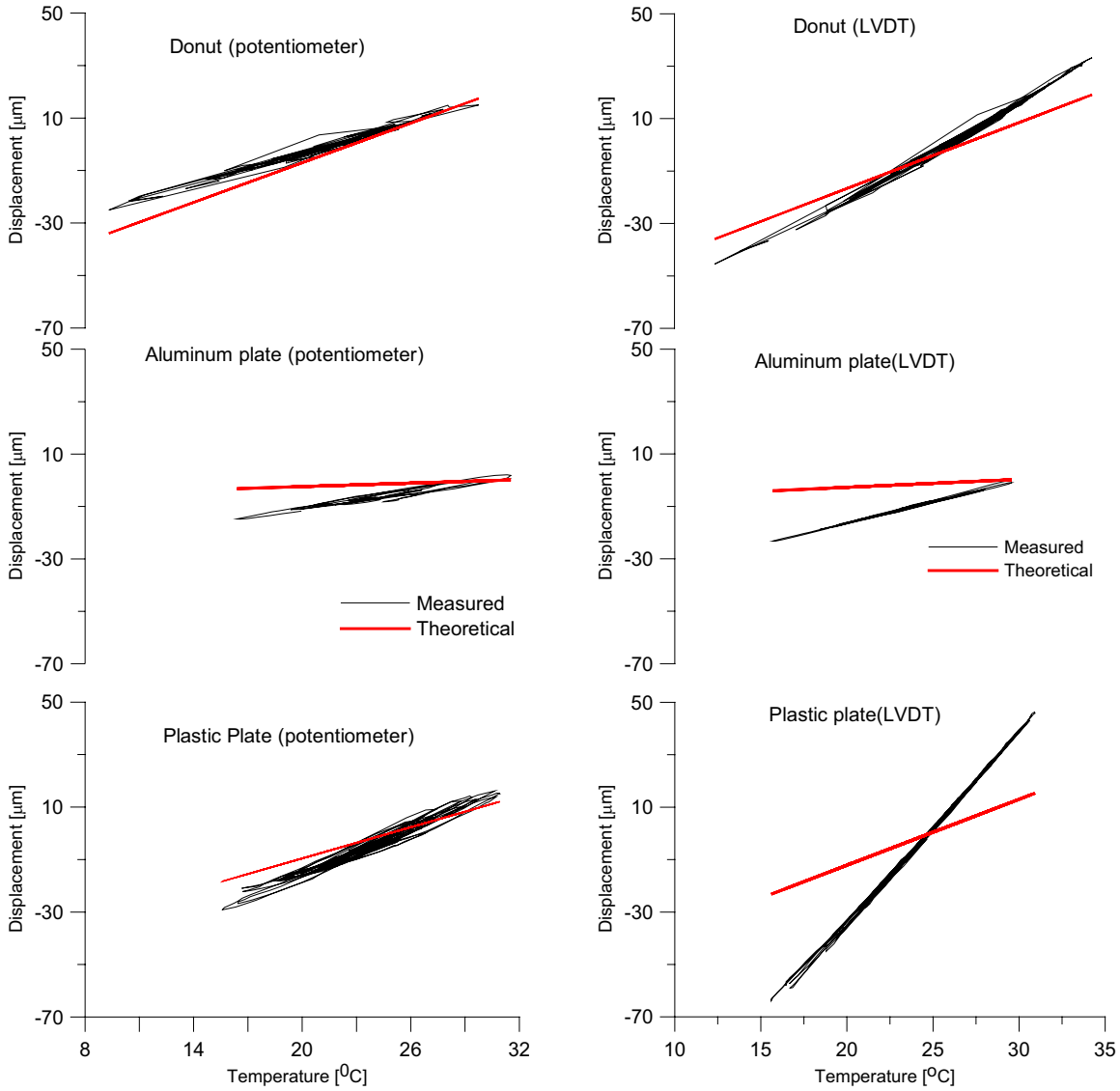


**Figure D- 2: Comparison of temperature corrected potentiometer and LVDT response to cyclically changing temperature variations**

Statistical measures of the scatter according to the corrected results are also given in Table D- 1.

**Table D- 1: Statistical measures of plate and donut tests with the corrected results**

| Test Description | Test Duration | LVDT | | | POTENTIOMETER | | |
|---|---|---|---|---|---|---|---|
| | | $\sigma_1$ | $\sigma_2$ | $R^2$ | $\sigma_1$ | $\sigma_2$ | $R^2$ |
| **Aluminum plate** | 8/03/04-8/12/2004 | 0.012 | 0.009 | 0.99 | 0.044 | 0.035 | 0.94 |
| **Plastic plate** | 8/14/04-9/6/2004 | 0.007 | 0.005 | 0.99 | 0.032 | 0.023 | 0.962 |
| **Donut Test** | 3/28/05-4/6/2005 | 0.012 | 0.010 | 0.99 | 0.020 | 0.017 | 0.98 |

Same normalization procedure described in Chapter 3 also applied to the corrected results and results are shown in Table D- 2.

**Table D- 2: Temperature normalized displacements from plate and donut tests with corrected results**

| | **Aluminum Plate [μm/$^o$C]** | **Plastic Plate [μm/$^o$C]** | **Donut Test [μm/$^o$C]** |
|---|---|---|---|
| **Potentiometer Expansion/Contraction** | 1.17/-1.18 | 2.83/-2.79 | 1.71/-1.81 |
| **LVDT Expansion/Contraction** | 1.57/-1.63 | 7.29/-7.14 | 3.61/-3.44 |